Titre: Title:	Compensation Tables for the Correction of Geometric and Volumetric Errors in Five-Axis Machine Tools from Indirect Calibration Data
Auteur: Author:	Sareh Esmaeili Marzdashti
Date:	2021
Type:	Mémoire ou thèse / Dissertation or Thesis
Référence: Citation:	Esmaeili Marzdashti, S. (2021). Compensation Tables for the Correction of Geometric and Volumetric Errors in Five-Axis Machine Tools from Indirect Calibration Data [Thèse de doctorat, Polytechnique Montréal]. PolyPublie. https://publications.polymtl.ca/6575/

URL de PolyPublie: PolyPublie URL:	https://publications.polymtl.ca/6575/
Directeurs de recherche: Advisors:	J. R. René Mayer
Programme: Program:	Génie mécanique

POLYTECHNIQUE MONTRÉAL

affiliée à l'Université de Montréal

Compensation tables for the correction of geometric and volumetric errors in five-axis machine tools from indirect calibration data

SAREH ESMAEILI MARZDASHTI

Département de génie mécanique

Thèse présentée en vue de l'obtention du diplôme de *Philosophie Doctor*

Génie mécanique

Avril 2021

POLYTECHNIQUE MONTRÉAL

affiliée à l'Université de Montréal

Cette thèse intitulée :

Compensation tables for the correction of geometric and volumetric errors in five-axis machine tools from indirect calibration data

présentée par **Sareh ESMAEILI MARZDASHTI**

en vue de l'obtention du diplôme de *Philosophie Doctor*

a été dûment acceptée par le jury d'examen constitué de :

Luc Baron, président
René Mayer, membre et directeur de recherche
Maxime Raison, membre
Soichi Ibaraki, membre externe

DEDICATION

Never my heart never deprived of knowledge

Few secrets were not divulged

For seventy-two years I pondered day and night

Only to know that I know nothing

(Omar Khayyam)

ACKNOWLEDGEMENTS

Foremost, I would like to express my special gratitude to my tremendous supervisor and research director, Professor René Mayer, for his continuous caring, patience, motivation, enthusiasm, and immense knowledge, which have deeply inspired me. It was a great privilege and honour to research under his guidance. Without his persistent help, this dissertation would not be possible.

I sincerely appreciate my thesis committee, Professors Luc Baron, Maxime Raison, Soichi Ibaraki and Samuel Jean Bassetto for their time and effort, insightful comments, and acceptance to participate in the jury.

I wish to extend my special thanks to Drs. Robert Schmitt and Martin Peterek for giving me the excellent opportunity to do part of the project and the experimental test in Machine Tool Laboratory WZl and also the researchers Philippe Dahlem and Mark Sanders for their help, feedback, cooperation and of course friendship.

I am also grateful to the NSERC Canadian Network for Research and Innovation in Machining Technology (CANRIMT) for funding this Ph.D. research and our industrial partners, Drs. Serafettin Engin and Rachid Guiassa for clarifying current issues in the industry and for their support, valuable feedback, and cooperation.

I take this opportunity to thank all of my colleagues and teammates at École Polytechnique, especially Najma Alami-Mchichi, Anna Los, Heidarali Hashemiboroujeni, Saeid Sepahi, Babak Beglarzadeh, Kanglin Xing, Gabriel Bernard, Ngoc Huy Vu, Rosalie Laure Woulache for their support and friendship during all these years. Besides, the high assistance in doing the experimental test provided by Guy Gironne and Vincent Mayer, CNC technicians at Virtual Manufacturing Research Laboratory (LRFV) in Polytechnique Montréal, is greatly appreciated.

I also want to express my special thanks to my family for their endless support and for always believing in me. Words cannot express how grateful I am to my father, mother, and brothers.

Last but not least, I thank my steadfast husband, Adel Nazari, for his always support and his enduring love and my little son Mehrad who was just 17 months when I had started my Ph.D. His smile has been absolutely a good reason for me to stand firm in the difficult path of doing research.

RÉSUMÉ

Les erreurs volumétriques et géométriques des machines-outils sont dues aux imperfections dans le procédé de construction, à l'usure et à des facteurs environnementaux. La compensation d'erreur logicielle est une alternative à la correction physique qui permet de réduire les erreurs systématiques et d'augmenter la précision lors de l'usinage de pièces. Une méthode de compensation logicielle courante consiste en l'utilisation de tables de compensation CNC définissables par l'utilisateur. La table de compensation des machines-outils à trois axes est populaire pour compenser les erreurs volumétriques de mouvement de translation de la pointe de l'outil où le maillage 3D utilise l'espace articulaire mécanique comme entrée et sortie. Les valeurs de compensation requises à chaque nœud du maillage sont optimisées sur la base des modèles de paramètres d'erreur géométrique de la machine. L'efficacité de la compensation est mesuré à l'aide d'un test de barre à billes 3D le long des méridiens d'un espace hémisphérique. Les résultats montrent une amélioration de plus de 82% de la non-sphéricité de la trajectoire de l'outil relativement à l'espace de travail. Pour les machines-outils à cinq axes, l'utilisation de tables de compensation complexes a été explorée. Ces tables complexes peuvent être combinés à l'aide de multiplication et de sommation. Dans un modèle préliminaire, 25 pseudo tables, 5 tables par axe, sont combinées à l'aide de sommations et remplis pour les deux modèles d'erreur. Toutes les fonctions de table sont simulées par des polynômes de troisième degré. Le système d'équations est linéarisé en générant la jacobienne des coefficients de la table. Les erreurs géométriques et volumétriques sont comparées avant et après compensation avec une compensation d'erreur plus de 63%. Un autre modèle de compensation d'erreur basé sur une table de compensation, inspiré du calcul de la jacobienne et de la jacobienne inverse, est proposée. Cette méthode permet de faire ressortir une variété de termes trigonométriques qui sont utilisés pour peupler les tables de compensation. Ce schéma augmente la compensation d'au moins 32% sur le modèle à base polynomiale. Le dernier schéma de compensation basé sur une table de compensation qui a été étudié utilise un modèle variationnel direct et inverse linéarisé exact représentant la relation entre les paramètres d'erreur et les corrections nécessaires à la compensation. Pour la machine-outil testée, 40 tableaux ont été créés dans le contrôleur Siemens 840D pour compenser 13 paramètres d'erreur. Une compensation de 79% des erreurs volumétriques est obtenue. Les normes des erreurs

volumétriques estimées moyennes sont réduites de 44 µm avant compensation à 9 µm après compensation.

ABSTRACT

Machine tool volumetric and geometric errors occur during to initial construction imperfections, and subsequent wear and tear and environmental factors. Software error compensation is an alternative to physical correction to reduce systematic errors and achieve more accurate machined parts. A practical software compensation method is the use of CNC user definable look up tables.

Three axis machine tools lookup table are common for the purpose of tool tip translational volumetric error compensation. The 3D mesh grid uses the mechanical joint space as input and output. The required compensation values at each mesh grid node are optimised based on one of two machine geometric error parameter models. The compensation effectiveness is tested using a 3D ball-bar test along meridians of a hemispherical space. The results show an improvement over 82% of the out-of-sphericity of the tool trajectory relative to the workpiece frame.

For five-axis machine tools the use of complex compensation tables is studied. Such complex tables can be combined using multiplication and summation functionalities. In a preliminary model, 25 pseudo tables, 5 tables per axis, are combined by summation functionality and populated for the two error models. All table functions are simulated by polynomials of degree three. The system of equations is linearized by generating the sensitive Jacobian of the table coefficients. The geometric and volumetric errors before and after compensation are compared showing an error compensation of over 63%.

Another table-based error compensation model is proposed which is inspired by the Jacobian and the inverse Jacobian of command which leads to variety of trigonometric terms to populate the tables. This scheme increases the compensation by at least 32% over the polynomial based model.

The last table-based compensation scheme studied implements an exact linearized forward and inverse variational model representing the relationship between the error parameters and the command corrections required for compensation. For the tested machine tool, 40 tables were created in the Siemens controller 840D for compensating 13 error parameters. Compensation of 79% of the volumetric errors is achieved. The mean estimated volumetric error norms are reduced from 44 µm before compensation to 9 µm after compensation.

TABLE OF CONTENTS

LIST OF TABLES

LIST OF FIGURES

CHAPTER 1 INTRODUCTION

Machine tool error compensation becomes more important not only due to producing more complicated parts with tighter tolerances but also to automate the process of keeping a machine at its best accuracy potential. To maintain the maximum possible accuracy of the machine tools under production mechanical maintenance such as applying overhaul, repairing parts and assemblies might be useful especially when the errors are large. However, there are some software methods by which small errors of micrometers can be compensated without mechanical correction which are generally time and resource consuming. Since the machine is an open kinematic chain, its geometric errors affect the relative movement of the tool to the workpiece. Hence, by correcting this relative movement, the influence of the geometric errors on the tool tip can be reduced.

Among different software methods, using lookup tables is attractive because it is more practical for the user to have the command correction automatically done in comparison with G-code compensation in which the user modifies the G-code program. However, generating the complex tables or modifying the control parameters requires a deep understanding of the errors, machine tool kinematics and joint correction. To generate complex tables, a precise model of geometric parameters and the optimization method is used. There is a lack of knowledge of producing such complex tables which can mimic the behaviour of kinematic-based error compensation in which the controller uses the tables to assign compensation value to every machine tool command. This thesis aims to propose strategies and techniques to answer the following main research questions:

- How does table-based error compensation capability in the controller can improve machine tool accuracy?

The detailed questions relative to the main one are;

- Which criteria indicate machine tool error compensation?
- What is the relationship between the geometric errors and the command corrections required for volumetric error compensation?
- How to optimize and predict joint correction?
- Is the number of table entries important? If yes, How to optimize them?
- How to build compensation tables to mimic the kinematic-based error compensation?

- How many tables are required to fully compensate a set of errors in a machine tool?

1.1 Objectives

The main objective is to exploit the use of the capability of current indigenous software compensation tables in machine controllers and to explore solutions where shortfalls are identified. The specific objectives are defined as;

1. Correct translational errors using three-dimensional error compensation with optimized mesh grid.
2. Propose a simplified table-based error compensation model in which the summation functionality is participated to correct geometric and volumetric errors.
3. Introduce a more complex table-based error compensation model with multiplication and summation functionalities with trigonometric terms as the table functions to correct geometric and volumetric errors.
4. Identify a table-based error compensation model, which behaves close to kinematic-based error compensation to correct geometric and volumetric errors.

1.2 Hypothesis

A table-based error compensation model can be produced that behaves like kinematic-based error compensation.

The geometric and volumetric error compensation is dependent on the numbers of mesh grids built on the machine tool joint space.

The numbers of tables required for geometric and volumetric error compensation are dependent on the magnitude of different geometric errors.

Multiplication and summation functionalities may be required in generating table-based error compensation to correct different geometric errors.

1.3 Assumptions

- The machine is supposed to have rigid body behaviour resulting in neglecting error variation of one component while moving on the other component.
- The machine tool controller is supposed to track all the input data.
- Compensation algorithm is applied on repeatable errors.
- The geometric error parameters and volumetric errors obtained using a SAMBA calibration process are reliable.
- Although this project investigates the dynamic and thermal-induced deviations resulting in some geometrical and volumetric deviations, it does not directly involve the dynamic and thermal errors.

CHAPTER 2 THEORY AND LITERATURE REVIEW

2.1 Machine tool deviations

Hocken defined the error as “the difference between the actual response of a machine to a command issued according to the accepted protocol of that machine's operation and the response to that command anticipated by that protocol” (R. J. Hocken, 1980). A change in geometry of the components like the tool, spindle shaft, housing, frame and guideways, bearings, drives and fixtures leads to position and orientation error of the end-effector relative to the workpiece. The influence of machine imperfections on the machined part dimensions and geometry appears as the volumetric deviation. The overall machine imperfections may come from the interaction between several error sources like kinematic errors, thermal effects, machining forces, loads, contouring and servo errors. Hocken (R. J. Hocken, 1980) classified these discrepancies into two general classes as quasi-static errors and dynamic errors. By neglecting the influence of a machine’s particular operating conditions, the sources of quasi-static errors contain geometric deviations, the error induced by the forces and deadweight of the machine components and thermal errors. Those errors are almost constant or slowly vary in time. Dynamic error, the consequence of the machine’s dynamic behaviour and machining conditions during the cutting operation, is classified by Hocken into sub-categories, namely vibration of the machine structure, spindle error motions, tool deflection and servo control and contouring errors (R. J. Hocken, 1980) (Figure 2.1). Some major error sources are discussed in the following.

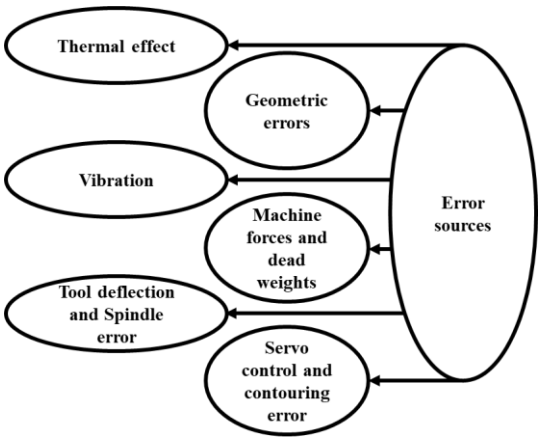

Figure 2.1. The overall effect of several error sources on a machine tool based on Hocken (R. J. Hocken, 1980).

2.1.1 Thermal deviation

The heat generated in a machine tool may lead to expanding the machine base and its components. The expansion coefficient varies depending on the temperature and thermal conductivity, resulting in machine element thermal distortion (Schwenke et al., 2008). Among various sources of errors, the thermal deviation has almost been a 40%-70% contributing factor of workpiece errors. Thermal induced errors contribute to the part-dimensional deviations in precision machining and cause a variation in the axes' actual position. Figure 2.2 illustrates a possible thermal error classification. The thermal error sources can be heat produced by drive equipment or high ambient temperature. However, the primary thermal source is produced by the cutting process (Haitao, Jianguo, & Jinhua, 2007). The others are room environment, the heat created by coolant systems, hydraulic oil, frame stabilizing, cutting fluid and lubricating oil. Electronic systems can also participate in this heat generation. Besides, the effect of people and solar radiation cannot be negligible (Attia & Kops, 1979; Haitao et al., 2007; J., 1990).

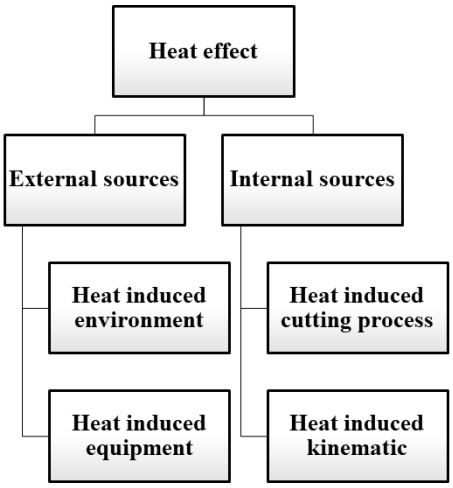

Figure 2.2. Thermal error classification based on (Attia & Kops, 1979; Haitao et al., 2007; J., 1990).

The temperature-induced deformation of components may directly impact precision machining. They can flow as convection, conduction or radiation depending on the thermal source. Heat can flow uniformly or non-uniformly in all components of the machine tool. The classifications

proposed by Allen (J.P. Allen, 1997) for the thermal errors are the position-independent thermal errors (PITE) and the position-dependent thermal errors (PDTE). In PITE, the errors can vary as a function of temperature and influence on the machine offsets independently from the axis positions and PDTE is the position and the temperature variation errors (J.P. Allen, 1997).

2.1.2 Load induced deviation

Because of the machine structure's limited static stiffness, components may be deformed by gravity or cutting load resulting from the cutting process. Gravity force is defined as a function of machine structural weight resulting in axis acceleration load. It mainly occurs because of the displacement of machine components and the workpiece's mass (Slocum, 1992). Ramesh et al. (R. Ramesh, 2000) proposed that despite the strain caused by cutting load, it is minimal in finish machining and can be neglected. However, due to the existence of large forces, this assumption cannot be considered in machining hardened steel materials. New research has been done on the load-induced error to reduce total discrepancies (Ratchev, Liu, Huang, & Becker, 2006).

2.1.3 Contouring and servo errors

The discrepancies may be caused by numerical control wherein the necessary calculations are computed, such as the trajectory interpolation and tool path generation. Servo controller may be the other reason for such errors in which the position and the speed of each axis are controlled in real-time. Contouring deviation is a function of feed rate and can arise by increasing the feed rate (Lavernhe, Tournier, & Lartigue, 2007).

2.1.4 Dynamic force induced errors and vibrations

Machine tool structure is subjected to dynamic effects producing discrepancies in the nominal tool path trajectory. Various factors can lead to this type of distortion, including vibrations of the components, inertial forces caused by acceleration or deceleration of the axes and forces variation resulting from the sudden change in cutting forces during the process (Jingxia Yuan, 1998).

The vibration effect is more detectable in the milling process because of the nature of periodically forced vibration. Schmitz et al. (Schmitz, Ziegert, Canning, & Zapata, 2008) have studied the impact of the spindle speed, teeth number of the tool, radial and axial depth of cut and cutter helix

angle on vibration in the milling process. Typically two types of vibration may be introduced namely forced vibration produced by external sources such as foundation, bearings or other components and self-excited vibration that occurs when the machine vibration is almost near the one or several natural frequencies of the structure (R. J. Hocken, 1980).

2.1.5 Geometric errors

Geometric errors may be the result of imperfect geometry and dimensions of machine components, its axes misalignments, errors of machine's measuring systems, and elastic deformation of parts. Assembly errors of machine structural components are directly affected by the errors in angles like squareness, horizontal and vertical parallelism errors, or the errors in length like improper offsets between components, wrong component dimensions, and linkage length. The weak surface straightness of the machine components may also produce a negative effect. Also, having inappropriate bearing pre-loads is the other reason for these errors (Schwenke et al., 2008). Thermal errors can lead to permanent errors in the machine tool's structure or load, and load variation may affect the spindle, holder, and tool's material properties.

Kinematic deviations lead to imprecise function resulting in one axis's error components being functions of other axes positions. In general, two classifications are proposed for the geometric errors, namely intra-axis errors or position-dependent geometric parameters (PDGEPs) and inter-axis errors or position-independent geometric parameters (PIGEPs) (Schultschik, 1977). The surface straightness of the guideways causes the first category. In contrast, the second one is caused by structural component misalignments such as out of squareness, angular offset, and rotary axes separation errors (Y A Mir, 2002). The volumetric error contains a functional point's overall deviations in a machine tool caused by intra- (error motion) and inter-axis (link error) errors (ISO/TR16907, 2015). The concepts of the volumetric error, inter- and intra-axis errors are illustrated in Figure 2.3.

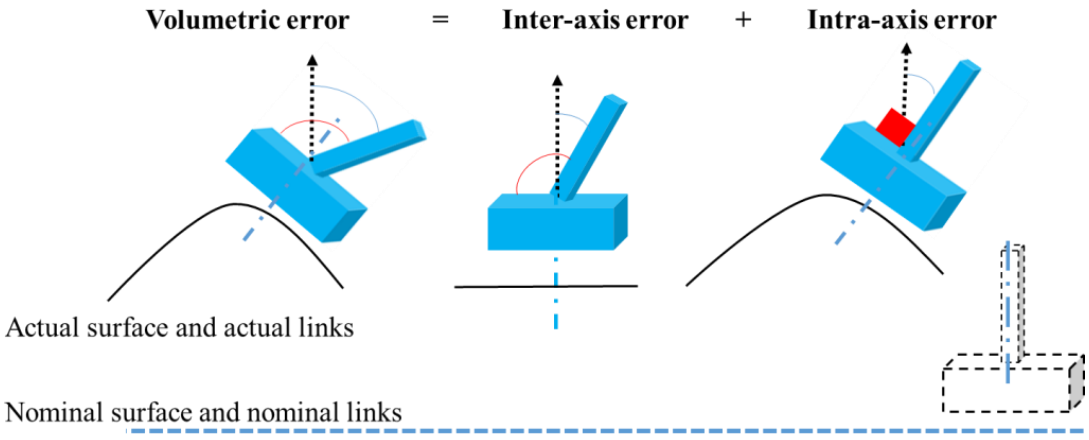

Figure 2.3. Exaggerated machine tool errors schematic.

2.1.5.1 Intra- and inter-axis errors

This section yields the main description of intra-axis and inter-axis errors for prismatic and rotary joints by which the machine tool error is modelled. Ideal prismatic joints provide straight movements along the linear axes. Thus, possible six motions are for linear axes, three translations along the X, Y, Z axes, and three rotations around them. Similarly, ideal rotary joints provide angular motions around the axis of rotation. Actual rotary joints are influenced by six deviations, including three translational error motions along the X, Y, Z axes and three angular error motions around them (ISO230-1, 2012). The errors are mapped in Figure 2.4 and the definitions are expressed in Table 2-1. The definitions are based on ISO 230-1 (ISO230-1, 2012).

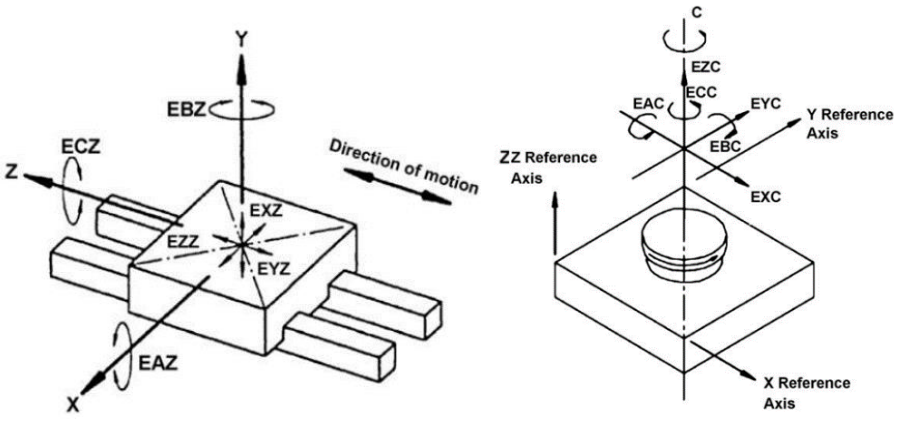

Figure 2.4. Linear and angular error motions of a linear and a rotary axis considering the movement respectively along Z- and C-axis (ISO230-1, 2012).

Table 2-1. Error definitions for a linear and a rotary axis(Z- and C-axis) (ISO230-1, 2012).

Axis	Error sign	Error definition
Z-axis	**EXZ**	Straightness error motion in X direction
	EYZ	Straightness error motion in Y direction
	EZZ	Linear positioning error motion in Z direction
	EAZ	Angular error motion around X-axis (Pitch)
	EBZ	Angular error motion around Y-axis (Yaw)
	ECZ	Angular error motion around Z-axis (Roll)
C-axis	**EXC**	Radial error motion of C in X direction (after rotation)
	EYC	Radial error motion of C in Y direction (after rotation)
	EZC	Axial error motion in of C direction (after rotation)
	EAC	Tilt error motion of C around X-axis (Pitch)
	EBC	Tilt error motion of C around Y-axis (Yaw)
	ECC	Angular positioning error motion around Z-axis (Roll)

Based on the inter-axis error description, which is an orientation and displacement of the actual axis from the nominal location for a linear or rotary joint, the relevant parameters are defined as the two orientation angle and one zero position error for the linear axis. The two orientation angles, and two position coordinates and a zero position of the axis are the parameters of the inter-axis errors for the rotary axis. Figure 2.5 illustrates these errors for the Z- and C-axis. The error definitions are also expressed in Table 2-2 (ISO230-1, 2012).

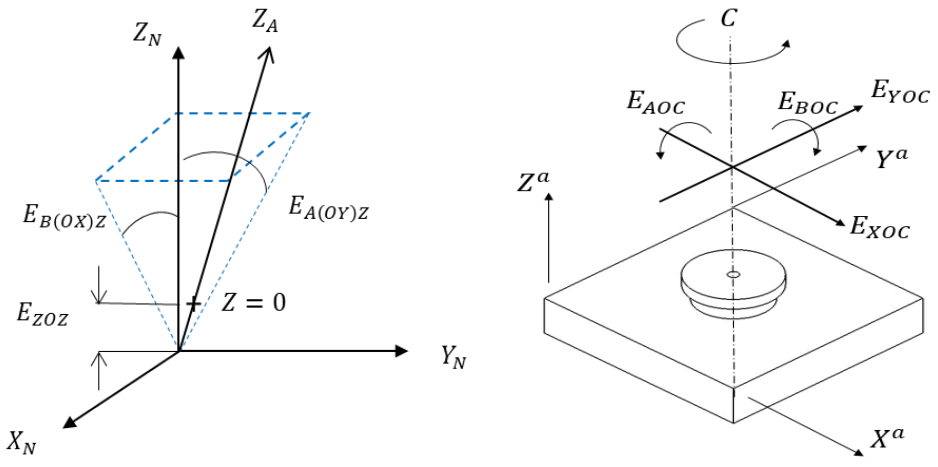

Figure 2.5. Inter-axis errors for linear Z-axis and rotary C-axis (ISO230-1, 2012).

Table 2-2. Error definitions of inter-axis errors for linear Z-axis and rotary C-axis (ISO230-1, 2012).

Axis	Error sign	Error definition
Z-axis	**EZOZ**	Zero position error of Z
	EA(OY)Z	Squareness error of Z related to Y
	EB(OX)Z	Squareness error of Z related to X
C-axis	**EXOC**	Position error of C in the direction of X
	EYOC	Position error of C in the direction of Y
	EA(OY)C	Orientation error of C in the direction of A (squareness of C to Y)
	EB(OX)C	Orientation error of C in the direction of B (squareness of C to X)
	ECOC	Zero position error of C

2.1.5.2 Actual machine tools with errors

Among various machine tools, five-axis machines are more popular because of providing the necessary movements and producing complicated parts. In general, five-axis machines have three prismatic and two rotary axes, which can be variously sequenced considering their specific application. Figure 2.6 illustrates the kinematic of two types of five-axis machine tools.

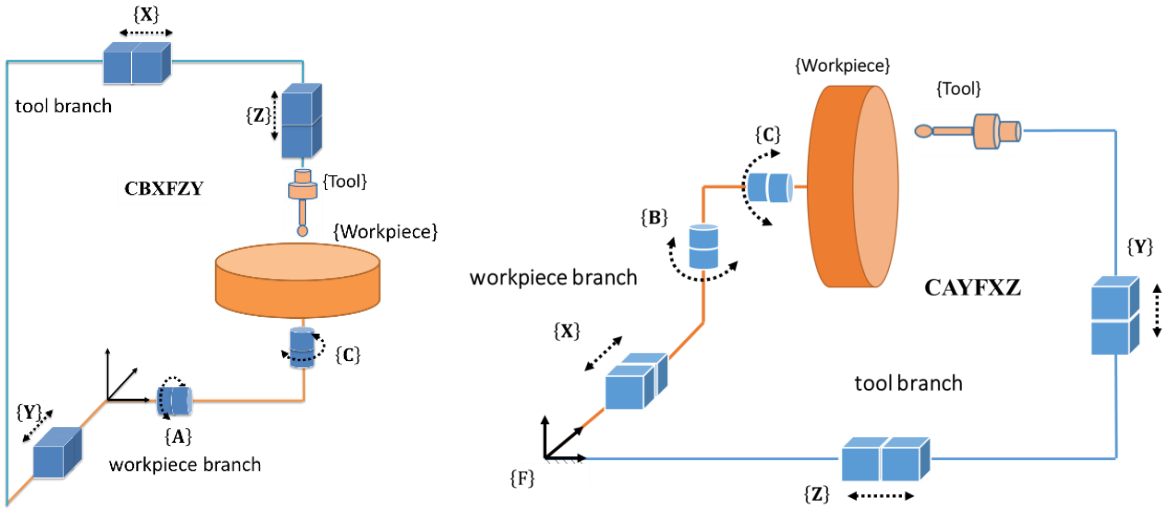

Figure 2.6. Kinematic of two five-axis machine tools with topologies of CBXFZY, CAYFXZ.

Everett et al. (Everett, 1988) propose a zero-order minimal model to explain the errors. They introduce N as the minimum essential number of properties for a kinematic chain from base to the end-effector frame obtained as,

$$N = 4R + 2P + 6 \quad (1)$$

where, R and P refer to the number of rotary and translation axes, respectively. The coefficient of P becomes two in this model because the prismatic joint is as a vector without a specific origin where the orientation of the actual axis is adjusted to the nominal one by two angle corrections. The first term's coefficient in Eq. (1) becomes four because the rotary axis is defined as a vector with a specific origin. Hence, to bring the actual axis to the nominal one, two angle corrections and two displacement corrections are needed. The third term in Eq. (1) is the tool orientation and displacement. In 1991, Mooring et al. (Mooring, 1991) proposed another equation close to the former model. The only difference between the two models is the third term in Eq. (1). The latest minimum model expresses that depending on the type of operation of the tool in machines, five degrees of freedom can be considered instead of six for the tool errors. So, the tool's orientation around its axis can be ignored, and the third term becomes 5 instead of 6 (Freeman, 2016).

Based on the first theory, there are 20 independent parameters for a five-axis machine. Thus, by considering 6 parameters for the workpiece branch and 6 parameters for the tool branch, 8 parameters remain which can refer to the link errors. However, this number is decreased to 7 in latest model (Zargarbashi & Mayer, 2009).

2.2 Error measurement

Typically, there are two methods for measuring the geometric errors called direct and indirect measurement. A suitable measuring technique is selected depending on the type of errors and the relevant parameters to be estimated.

Direct measurement refers to an approach resulting in analyzing the errors directly. It is an applicable method for measuring a single error of a specific axis in the machine tool without considering other axes errors. Direct measurement can be material-based and laser-based. The material-based method utilizes such artefacts as straightedges, line scales, step gauges, and multidimensional artefacts, which have been recently used (Weckenmann A, 2005). Laser-based measurement is a common approach to identify individual errors like positioning errors, straightness, and angular errors (Schwenke et al., 2008). This technique uses waves' interference in the laser to calculate the distance between the reference and measurement object. The Michelson

interferometer principle is splitting a monochromatic light source into two beams using a half-silvered mirror (Loughridge & Abramovitch, 2013). Li et al. (Z. Li, Yang, Fan, & Zhang, 2014) applied laser measurement to calculate 18 error parameters and the electronic level to measure three roll errors of the translational axes in a three-axis machine. Due to its high precision and long coherence length, it is an appropriate choice in characterizing the accuracy and the repeatability of the machine tools. However, the interferometer can be affected by environmental conditions like thermal, surrounding air, and relative humidity variation. Laser wavelength, which is considered as the reference, can vary by the surroundings (Castro, 2008). A precise initial setup is essential to avoid any misalignment between the laser beam and the measured axis. Figure 2.7 shows the measurement procedure by a laser with a retroreflector.

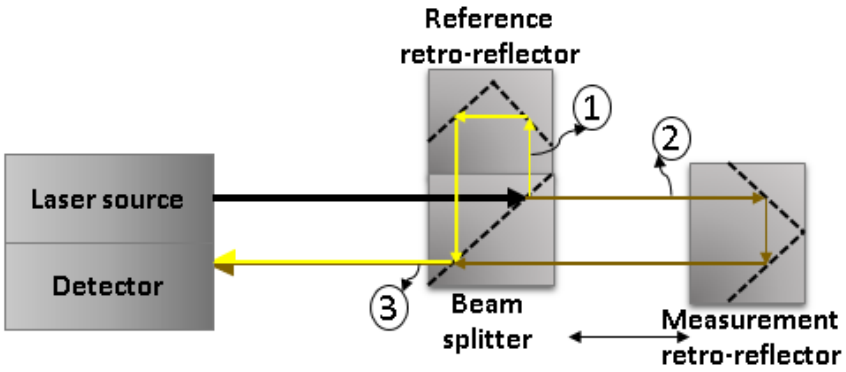

Figure 2.7. Laser interferometer measurement.

The indirect method relies on simultaneously measuring multiple positions or multiple axes in the machine tool's working volume. Some indirect tests are R-test (Bryan J, 1967; Hong, Ibaraki, & Oyama, 2012), ball-bar tests (Abbaszadeh-Mir, Mayer, Cloutier, & Fortin, 2002; Bryan, 1982a, 1982b; Kato, Masaomi., & Sato, 2013; M. Esmaeili & Mayer, 2020; Yang & Ding, 2016) and calibrated or non-calibrated artefacts. The indirect method can also use the advantages of the laser sequential diagonal measurement techniques demonstrated by Wang (C. Wang, 2000) and Liotto (Liotto & C.P., 1997) to calculate volumetric errors. This technique incorporated with Laser Doppler Displacement Meter (LDDM) allows finding positioning volumetric errors with a single

beam, single aperture, and a flat mirror as the target. LaserTRACER and laser trackers are laser interferometry methods to indirectly calibrate the machine tool. LaserTRACER measures the distances between the retro-reflector target installed at the tool tip and the reference sphere in the LaserTRACER. A linearized set of equations obtained from multiple setups measurements are then solved by a Gaussian fit (Härtig et al., 2009) to calculate machine geometric errors. The error motions of rotary axes can be also measured by LaserTRACER (Schwenke, Schmitt, Jatzkowski, & Warmann, 2009). Zha et al. (Zha, Wang, Li, & Chen, 2020) validated LaserTRACER calibration results with a conventional laser interferometer in a three-axis machine tool. The effect of the ambient temperature on LaserTRACER geometric errors estimation results was studied by Groos et al. (Groos et al., 2020). They concluded that in comparison with straightness and rotational errors, linear axes' positioning and squareness errors are more affected by the temperature variation. The principle of Laser trackers is using two angles and a distance resulting in measuring the spherical coordinate for each position. Using multiple setups during calibration increases the estimation results accuracy (Schwenke, Franke, & Hannaford, 2005).

Calibrated or non-calibrated artefacts such as one, two or three-dimensional ones are the other indirect calibration methods composing a plate and several balls variously distributed on the plate (Bringmann, Küng, & Knapp, 2005; G. X. Zhang & Zang, 1991). Those artefacts are probed in different positions and provide sufficient information while simultaneously moving linear and rotary axes (Bringmann et al., 2005). Bi et al. (Bi et al., 2015) probed a cubic element to identify geometric errors of the rotary axes in a five-axis machine. Measuring the linear displacement between the tool and the workpiece is carried out by radial test (R-test). This technique uses at least three linear displacement sensors installed on a precision artefact. The sensors read against a reference sphere and measure the displacements (Bryan J, 1967). Hong et al. (Hong et al., 2012) used R-test to measure three-dimensional trajectories and calculate the rotary axes motion errors. Yang and Ding (Yang & Ding, 2016) ran a ball-bar test with different setups on a five-axis machine tool. Afterwards, by establishing the differential motion matrices, they estimated position-independent geometric errors.

René Mayer (Mayer, 2012) proposed SAMBA (scale and master ball artefact) in which several master balls and a scale bar were probed. The software of the method contains the homogeneous transformation matrix (HTM) to estimate the error parameters. HTM is a four-by-four matrix used

in the indirect methods to model the erroneous kinematic of a machine. A rigidity assumption between the axes joints (prismatic or rotary joints) is considered (Srivastava, Veldhuis, & Elbestawlt, 1995). Bringmann and Knapp (Bringmann & Knapp, 2006) proposed an artefact calling chase the ball in which one master ball was probed by a strategy to measure the machine tool errors. Reconfigurable uncalibrated master ball artefact (RUMBA) has been introduced by René Mayer (Mayer, 2012). It contains several master balls which are probed during simultaneous movement of the axes. The differences between the methods containing the masterballs are the models' ability to estimate a certain number of error parameters. The artefact containing masterballs is subject to have a certain number of masterballs and an optimized measurement strategy done by Mchichi and Mayer (McHichi & Mayer, 2019). The error model concept has been introduced and used by some researchers while estimating the maximum possible machine error parameters (Abbaszadeh-Mir et al., 2002; Mayer, 2012; McHichi & Mayer, 2014; M. M. Rahman & Mayer, 2015). The error model is an optimized model of all possible errors in a machine tool in which the reliability of the model has been considered during error estimation. The reliability is determined by applying the SVD on the Jacobian of the error parameters (Abbaszadeh-Mir et al., 2002).

2.3 Concept of rigid and Non-rigid body behavior

Rigid-body and non-rigid body behavior are common techniques considered to model a machine tool while estimating the errors. According to the type of machine, one of them may be appropriate. In general, the rigid body approach relies on the independence of the prismatic axes' angular deviation from the relative position of the machine's other components. Non-rigid body modeling is applicable especially for heavy machine tools with cross-table configuration. Due to the possible deformation of the guideway, the impact of the machine tool components' relative position on the angular error of the linear motions cannot be neglected in this approach. So, every deviation in one axis is affected by the other axes. Hence, offset from the measuring point to the destination point must be considered. In 1992, Wang (S.M. Wang, 1992) presented non-rigid modeling to compensate the volumetric errors in any arbitrary multi-axis machine. The method is based on FEM wherein; by using a linear order shape function, precise interpolated values are achieved in sample points(S.M. Wang, 1992).

2.4 Error compensation

Compensation is an approach for eliminating errors or the effect of the errors by a virtual equal and opposite error. However, due to uncertainty in the mechanical chain, the errors cannot be entirely deleted. Error correction plays an essential role in the industry wherein to have an accurate part, the approximate costs significantly grow.

Error compensation can be done mechanically or numerically. Changing and repairing the parts, which generate the errors are the techniques for mechanically compensating the errors. Having been time and money consuming on one hand and having the necessity for calibration after mechanical compensation, on the other hand, motivated the industry to pay attention to the numerical approaches. Later approaches are helpful for minor deviations and enhance machine accuracy.

Nevertheless, the numerical correction may have its limitations. Due to considering the axes' additional movement to compensate the errors, which are nominally supposed to be fixed, the finished surface may not be obtained. Especially, if this movement is combined with the hysteresis, it may cause some discrepancies. Nonetheless, for the present generation of controllers, this can be neglected. In the following sub-sections, types of numerical correction are discussed.

2.4.1 First part inspection

It is a method whereby the first machined part is entirely inspected by an independent machine such as a coordinate measurement machine (CMM) and the errors are calculated. Then, the tool path is adjusted concerning the measured error. This approach has high reliability due to considering the effects of all error sources on the machined part. However, it is not very useful when there is flexible manufacturing (LO & HSIAO, 1998).

2.4.2 Probing after machining

This method is also called In-cycle inspection in some references. Predicting machine errors can be done after the part is machined and before moving it. After the part is machined, the process is stopped and the touch probe replaces the tool to measure it and the machine tool acts like a CMM in this case. Thus, the measuring is performed by the same set-up to increase the accuracy of the error prediction. The probe radius and probe pre-travel could hurt the estimation of the deviations.

However, by combining the HTM and the present method, the error approximation can be improved in vertical machining (M.-W. Cho, Seo, & Kwon, 2003; M. W. Cho & Seo, 2002).

2.4.3 G-code correction

“It involves modifying the original G-code offline to produce an ephemeral G-code.” (Givi & Mayer, 2014). Thus, the measurement is done by offline methods, then the HTM is constructed, and the new G-code is built concerning the corrections and finally, commands are up-to-date. It is a practical approach for volumetric error compensation to reduce the deviations. The compensability is claimed 90% (Givi & Mayer, 2014) for a five-axis machine tool under the test. This kind of compensation may be time-consuming while the production frequently varies.

2.4.4 On-line compensation

On-line or real-time compensation is a technique that deals with the actual values wherein the workpiece errors are measured during the actual machining process. It is then fed forward by writing them directly on the current position without any interruption to the process itself. Thus, reading and writing commands must be accessible in the NC. Although it offers an overall solution for absolute improvement in machining quality, it is not applicable in most machining operations, and due to lack of dedicated probes on the machine tool, most compensation studies are limited to identify thermal errors and partially cutting force-induced errors (Zhan-Qiang, Venuvinod, & Ostafiev, 1998). By installing temperature sensors in particular locations during the machining process, the thermally induced errors are measured. This approach's accuracy highly depends on carefully recognizing the optimal location of the sensors, such as thermocouples. Although, some trial-and-error processes may be necessary (Chen, Chang, Hung, Lee, & Wang, 2016). Figure 2.8 shows two setups for thermocouple for temperature distribution in two different machine tools. Due to the on-line compensation's random nature, the error model is usually approximated with the neural network. Generally, the neural network is an algorithm that consists of an input layer of neurons, hidden layers, and output layers (Prakash Vinoda, 2014). A simplified error model was proposed by Kang et al (Kang, Chang, Huang, Hsu, & Nieh, 2007), to optimize the process using the limited data.

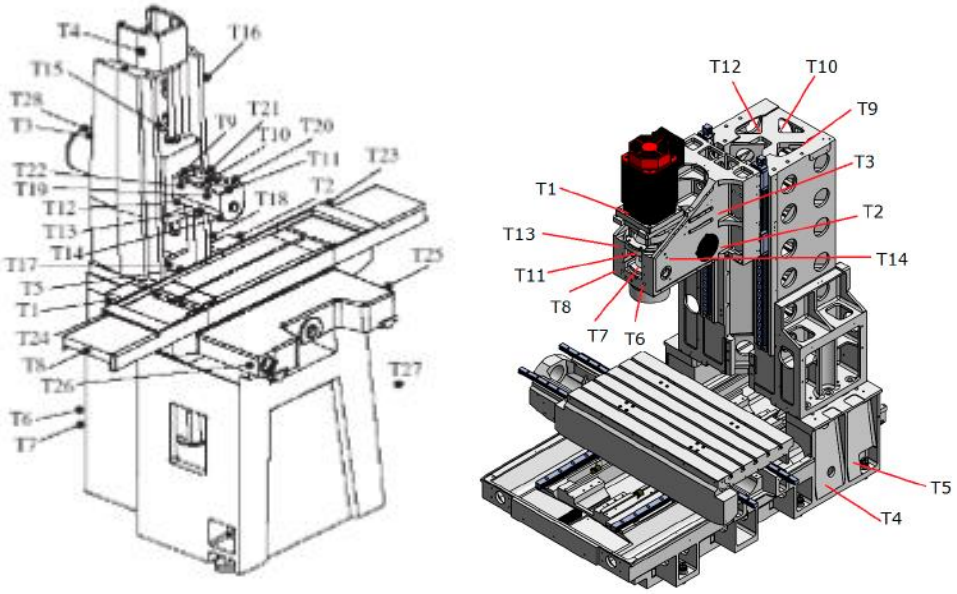

a. b.

Figure 2.8. Thermocouple setup for temperature distribution analysis in two different machine tools a. (Kang et al., 2007) b. (Chen et al., 2016)

2.4.5 Table-based error compensation

Controllers are equipped with several predefined compensation tables whereby the associated parameters can be modified to ameliorate the machining quality towards making more precise parts. Also, a general compensation facility is provided in some controllers for the users for generating complex lookup tables that are not predefined in the controller. In the table-based error compensation method, the controller uses the table entries to compensate the input commands directly without interruption in the feedback loop resulting in saving time and increasing the precision.

2.4.5.1 Standard – ISO/TR 16907

ISO/TR 16907 (ISO/TR16907, 2015) has classified typical geometric error compensation for conventional machine tools with up to six axes, two or three linear axes, and up to three rotary axes. The classification clarifies the type of geometric errors to be compensated. Some examples are positioning, straightness, squareness error, and angular error motions.

Based on ISO/TR 16907 (ISO/TR16907, 2015), some of the compensation facilities are for compensating the translational volumetric error effects such as L-POS (compensation for positioning errors of linear axes along specific lines), L-STR (compensation for straightness errors of linear axes along specific lines), L-SQR (compensation for squareness error between axes of linear motion at specific lines), L-ANG (compensation for the angular error motions of linear axes on 3-D position of functional point in the working volume) and L-VOL (volumetric compensation of linear axes) while some of the others are for compensating the angular volumetric error effects such as R-RAX (compensation for radial and axial error motion of the rotary axes), FOR (physical compensation for errors in functional orientation) and R-ANG (compensation for position and orientation errors of the rotary axes). Based on ISO/TR 16907 (ISO/TR16907, 2015), there are also some compensation types by which the volumetric error effect can be compensated, like L-VOL+ (volumetric compensation of linear axes including functional orientation), which includes L-VOL and FOR.

The grid compensation table structure is explained in ISO/TR 16907 (ISO/TR16907, 2015), where the spatial grid compensation tables for the linear axes and the rotary axes are separately presented. The spatial compensation grid for linear axes contains the sampling points for each linear axis and three-dimensional positioning or angular errors or their relative compensation values. Figure 2.9 illustrates a spatial grid structure for linear axes. Similarly, to generate the spatial grid compensation tables for the rotary axes, sampling points for each rotary axis and three-dimensional linear and angular errors or their relative compensation values are required.

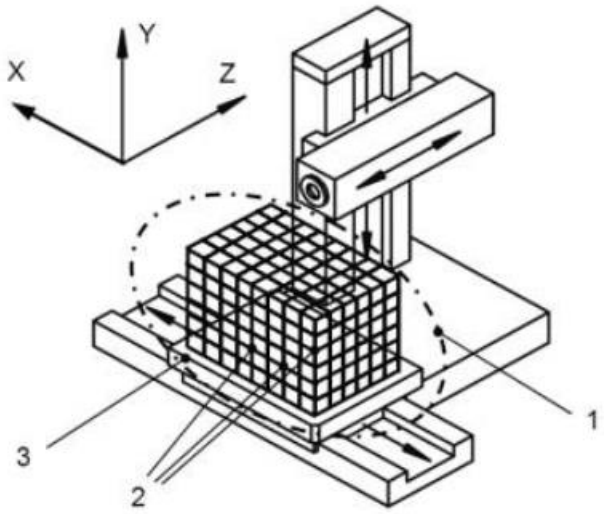

Figure 2.9. A spatial grid structure for linear axes (ISO/TR16907, 2015).

2.4.5.2 Control parameter modification

Each type of controller may contain a series of compensation facilities for compensating positioning, backlash, straightness, and thermal errors ("Fanuc Controller," Series 30i/Model A; "Siemens Controller," SINUMERIK 840D/840Di/810D Extended Functions). Those facilities are like simple lookup tables embedded for individual error parameter compensation. However, the general effect of compensation will indirectly impact the relative tool tip position to the workpiece position.

Another control parameter modification is three-dimensional error compensation embedded in Fanuc controller ("Fanuc Controller," Series 30i/Model A). Three-dimensional error compensation for the linear axes is a lookup table allowing the users to compensate translational volumetric errors. This type of compensation directly affects the tooltip linear position. It is a spatial error compensation wherein the table is constructed based on a mesh grid on the machine joint space. Three compensation values for the translational axes of X, Y, and Z are assigned to each 3D mesh grid node. By enabling the generated table, the controller uses the trilinear interpolation on the table entries when a G-code command is entered ("Fanuc Controller," Series 30i/Model A). Figure 2.10 shows the three-dimensional error compensation screen of Fanuc controller.

Fagor controller ("Fagor Controller, 8070 / 8065 CNC "), has a 3D error compensation table solution for Cartesian volumetric error compensation for CNC machine tools. Fagor controller

proposes an integrated calibration and compensation method called “Volumetric Compensation” to generate this table. Hence, a cloud of points on the Cartesian volume is defined, and the errors in each position are measured. The measured errors are then entered into the table.

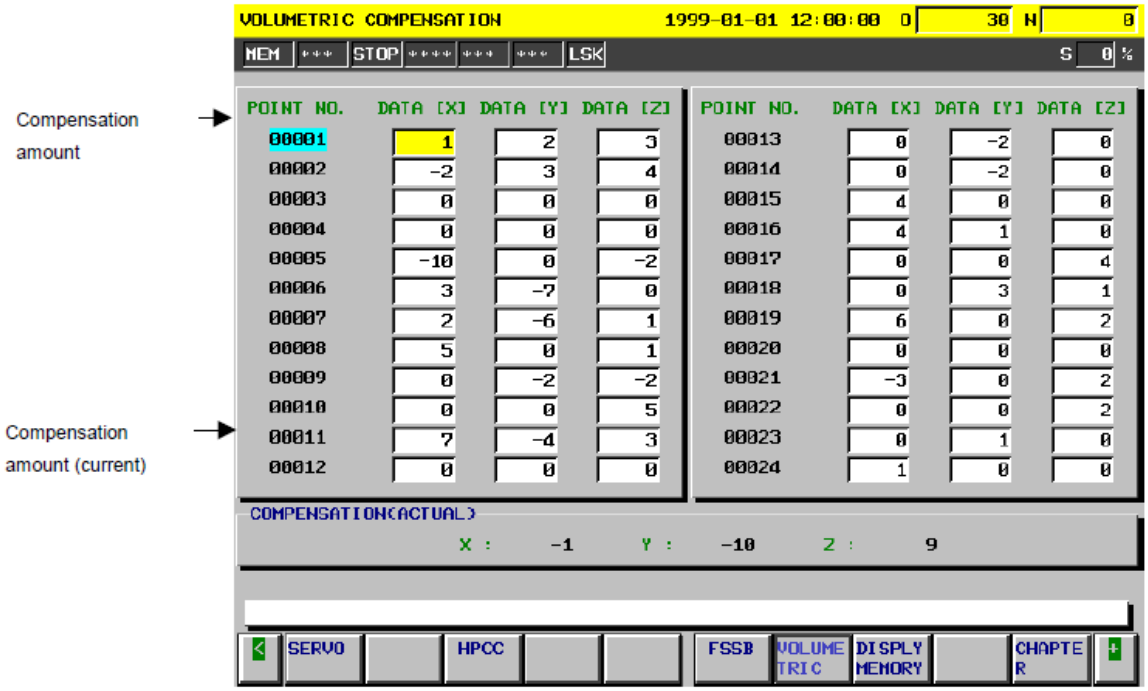

Figure 2.10. Three-dimensional error compensation screen of Fanuc controller ("Fanuc Controller," Series 30i/Model A).

2.4.5.3 General compensation facilities

The previous table-based compensation methods were limited to the tables already existed in the controllers, while the general compensation facility lets the users arrange the complex compensation tables based on their need. Those lookup tables can be also used for compensating volumetric errors (translational and angular errors) wherein the compensation is automatic. Hence, the user generates the tables based on the rules and the language of the specific controller under test. Summation and multiplication functionalities can be used in generating the tables. These tables can have different input and output axes. The input axis is an axis on which the table function is based, and the output axis is the one on which the table will be applied. By enabling the controllers' tables, the controller performs linear interpolation on the table entries while entering a G-code command. Figure 2.11 illustrates a table function graph, the linear interpolation concept, and the

required criteria in generating a table ("Siemens Controller," SINUMERIK 840D/840Di/810D Extended Functions).

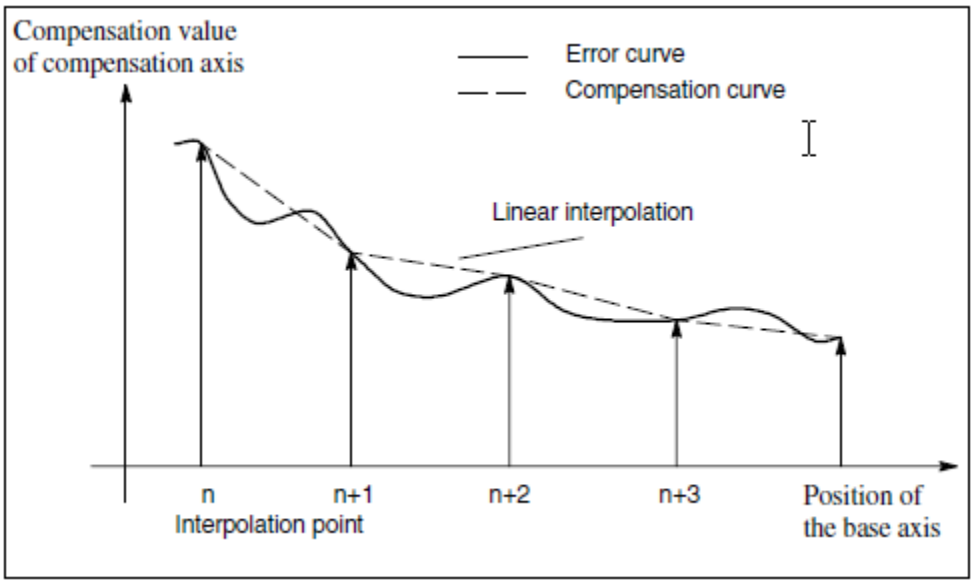

Figure 2.11. Linear interpolation between the interpolation points ("Siemens Controller," SINUMERIK 840D/840Di/810D Extended Functions).

ISO/TR 16907 does not specifically explain the combinatory tables or the required table functions (ISO/TR16907, 2015). However, an industrial table-based package like VCS was developed by Siemens (AG, 2010) for volumetric error compensation. The laserTRCAER is used for 21 machine tool error measurements, followed by calculating the tool tip's volumetric error. The NC program, including the tables, is then provided for the controller (AG, 2010). Similarly, KinematicsComp provides volumetric compensation in Heidenhain Controller ("Heidenhain Controller: iTNC 530 "), and “Extended Screw Compensation” is offered by Fidia controller ("Fidia Controller: C10 - C20 - C20 Vision,") to compensate for 21 machine error parameters. Fidia controller has offered another compensation feature calling “Volumetric Axes Compensation”. By combining VAC and rotary axes error compensation, maximum accuracy for all linear and rotary axes errors is achieved ("Fidia Controller: C10 - C20 - C20 Vision,").

Recent researches tend towards using these kinds of tables. Creamer et al. (Jennifer Creamer et al., 2016) proposed 25 tables, five tables per axis, in producing the complex tables. Summation functionalities have been utilized in generating those tables. They claimed their methodology in

developing the tables fulfills compensating the volumetric errors in the five-axis machine tool under the test. Later, they studied generating the optimal set of tables for the machine tool under the test. Their study is beneficial where the numbers of the tables are limited (J. Creamer, Bristow, & Landers, 2017). The multiplication functionalities were also used to develop the LUTs in a five-axis gantry machine. The volumetric error compensation was studied without considering inter- and intra-axis error parameters sources (J. Li, Mei, Shuai, Liu, & Liu, 2019).

A complex table includes one to several simple tables. The input to each simple table is an axis joint command, and the output is the associated correction to the output axis. Based on ISO/TR 16907 ("ISO/TR 16907. Technical report: Machine tools - Numerical compensation of geometric errors, 2015,"), identifying the nominal position, the direction to be compensated, the input, and the output axis must be defined while generating the lookup tables. Noted that the rules in developing the tables may vary from one controller to the other, which may affect the number of the tables required for compensating specific types of machine error parameters. For instance, the function that allows the users to generate these complex tables in Siemens controller is called Interpolatory compensation ("Siemens Controller," SINUMERIK 840D/840Di/810D Extended Functions). Some rules of the LUTs above are,

1. There are one input axis and one output axis as per each table. The input and output axes might be any mechanical axis of the machine tool. They are defined in the NC code by the syntaxes of $AN_CEC_INPUT_AXIS and $AN_CEC_OUTPUT_AXIS.
2. The table function can be anything but just one input axis-dependent.
3. The tables can be summed up or multiplied to each other by previously defining them in the NC program by the syntax $AN_CEC_MULT_BY_TABLE. If the syntax is equal to 0, no multiplication is applied, and the table is added to the others who have the same output axis. If the syntax is not 0, the table is multiplied by the table whose table number is equal to this syntax.
4. One table can be multiplied by several tables as long as the output axes are the same.
5. Each table can possess one weight which is constant for that table.

6. The user may define a table to be applied on a specific range of stroke length of the machine by considering the minimum and the maximum coverage with syntax $AN_CEC_MIN and $AN_CEC_MAX.
7. The tables entries' numbers are defined by the step value chosen for a range of stroke length with syntax $AN_CEC_STEP.
8. The LUT may be activated in a positive or negative direction or both. This option is essential where there is a backlash, and so the values in the positive direction might be different from the negative one with syntax $AN_CEC_DIRECTION.
9. There is an option called modulo function for compensating the rotary axes, which lets the user expect the table to be still applicable when the rotation is more than 360°. The associated syntax is $AN_CEC_IS_MODULO.

A simple NC code is illustrated in Figure 2.12 where table 1 is multiplied by table 2. The number of the table entries for the first and second tables are 10 and 15, respectively. The input axes for the first and second tables are Z- and Y-axis, respectively, and the output axis for both of them is X-axis. By entering any axis joint command of X and Y, the two tables' outputs are multiplied together.

```
%_N_NC_CEC_INI

METRIC

CHANDATA(1)
$AN_CEC[0,0]=0.0048
$AN_CEC[0,1]=0.0037
$AN_CEC[0,2]=0.0026
...
$AN_CEC[0,8]=-0.0039
$AN_CEC[0,9]=-0.0050
$AN_CEC_INPUT_AXIS[0]=AX3
$AN_CEC_OUTPUT_AXIS[0]=AX1
$AN_CEC_STEP[0]=50
$AN_CEC_MIN[0]=-450
$AN_CEC_MAX[0]=0
$AN_CEC_IS_MODULO[0]=0
$AN_CEC_DIRECTION[0]=0
$AN_CEC_MULT_BY_TABLE[0]=0
$AN_CEC[1,0]=0.0055
$AN_CEC[1,1]=0.0047
$AN_CEC[1,2]=0.0040
...
$AN_CEC[1,13]=-0.0041
$AN_CEC[1,14]=-0.0048
$AN_CEC_INPUT_AXIS[1]=AX2
$AN_CEC_OUTPUT_AXIS[1]=AX1
$AN_CEC_STEP[1]=50
$AN_CEC_MIN[1]=-700
$AN_CEC_MAX[1]=0
$AN_CEC_IS_MODULO[1]=0
$AN_CEC_DIRECTION[1]=0
$AN_CEC_MULT_BY_TABLE[1]=1
$AN_CEC[2,0]=0.032
$AN_CEC[2,1]=0.053
$AN_CEC[2,2]=0.031
M17
```

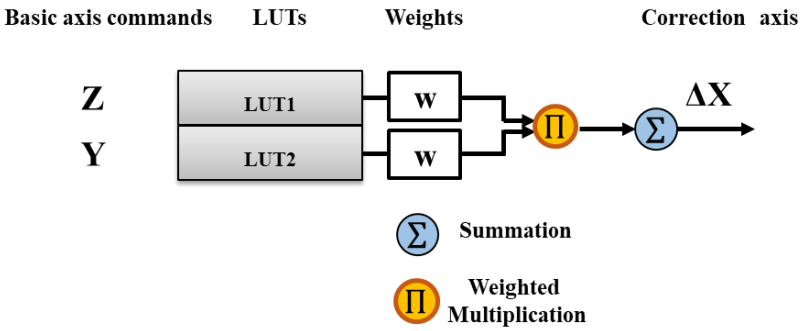

Figure 2.12. NC code for a sample of table multiplication.

CHAPTER 3 ORGANIZATION OF THE WORK

This chapter presents the general organization of the work. Four main research articles have been proposed to achieve the project's objectives and answer the research questions. The researches contain table-based translational and volumetric error compensation. All the experimental tests have been done on five-axis machine tools. Among various types of NC facilities that existed in the controllers for precision enhancement, the author has focused on two types of lookup tables that existed in Fanuc and Siemens controllers.

Chapter 4 includes the first article entitled “Generation of a 3D error compensation grid from ISO 230-1 error parameters obtained by a SAMBA indirect calibration and validated by a ball-bar spherical test”. It was published in the International Journal of Advanced Manufacturing Technology. This paper answers the question “Which criteria indicate machine tool error compensation?”. The paper proposes generating a three-dimensional error compensation table wherein the mesh grid nodes' numbers have been optimized. The table can compensate translational volumetric errors and not the angular volumetric errors. The experiments were run on a five-axis machine tool called HU40 and SAMBA indirect method is used to calibrate the machine. Two error models were developed, each containing a certain number of machine error parameters. A ball-bar spherical test including several meridians and an equator movement was designed to validate the compensation method. Two pseudo three-dimensional compensation tables were generated based on the two error models' error parameters. The ball-bar test was run three times, the first of which there was no use of the table and the second and the third of which the pseudo tables were used to compensate the joint positions located on the meridians and equator. The effectiveness of the table for the target machine tool was over 82%.

Chapter 5 includes the second article entitled “Five-axis machine tool volumetric and geometric error reduction by indirect geometric calibration and lookup tables”. It was published in the Journal of Manufacturing Science and Engineering. This paper proposes compensating volumetric error compensation using complex tables, interpolatory tables. This article focuses on using summation functionalities in generating such tables. The experiments were run on a five-axis machine tool called Kolibri. The indirect RUMBA method was used to calibrate the machine tool. 25 pseudo tables, five tables per axis, were developed to compensate two error models error parameters and

volumetric errors. Chase-the-ball was used for validation purposes. The data of chase-the-ball was processed two times, before and after applying for the compensation. For after compensation, the data were treated using generated 25 pseudo tables. The results showed a good improvement for the geometric and volumetric errors but not perfect.

Because using just summation functionalities in generating the tables did not provide a perfect compensation, the idea of using the multiplication and summation functionalities was developed in the third article presented in chapter 6. This paper was entitled “Trigonometrically enriched weighted lookup tables - a combinatorial scheme for accuracy improvement of a five axis machine tool” submitted to the International Journal of Machine Tools and Manufacture. The paper proposes 23Trigo-T consisting of the terms present in the Jacobian and the inverse Jacobian of command. Comparing the kinematic-based, 25 and 23 tables compensation results answers the question “How to optimize and predict joint correction?”. The table entries for 25 tables were calculated using iterative method, and for 23 tables, they were calculated using a classic optimization method. The results show that adding multiplication functionalities and the trigonometric terms in generating the tables improves the table-based compensation model while bringing the model closer to the kinematic-based error compensation. Also, the scheme is simulated on a non-orthogonal machine with excellent results supporting the potential generality of this work.

The idea of the fourth article came from the results of the third article. It answers the questions of “What is the relationship between the geometric errors and the command corrections required for volumetric error compensation?”, “How to build compensation tables to mimic the kinematic-based error compensation?” and “How many tables are required to fully compensate the errors?”. Chapter 7 includes the fourth article entitled “CNC table based compensation of inter-axis and linear axis scale gain errors for a five-axis machine tool from symbolic variational kinematics”. It was submitted to the CIRP Journal of Manufacturing Science and Technology. The forward inverse kinematics LUTs scheme (FIK-LUT) was developed in this paper, where the direct relationship between the geometric errors and the required joint corrections for the target machine tool was achieved. Summation and multiplication functionalities were used in generating such complex tables. The target machine was a non-perpendicular five-axis machine tool calling Huron. The results show that the exact model, consisting of 40 tables, can mimic the kinematic-based error

compensation and compensate the 13 error parameters in a 13-error model. FIK-LUT compensated over 79% of the mean estimated volumetric error. Figure 3.1 highlights the articles' structure.

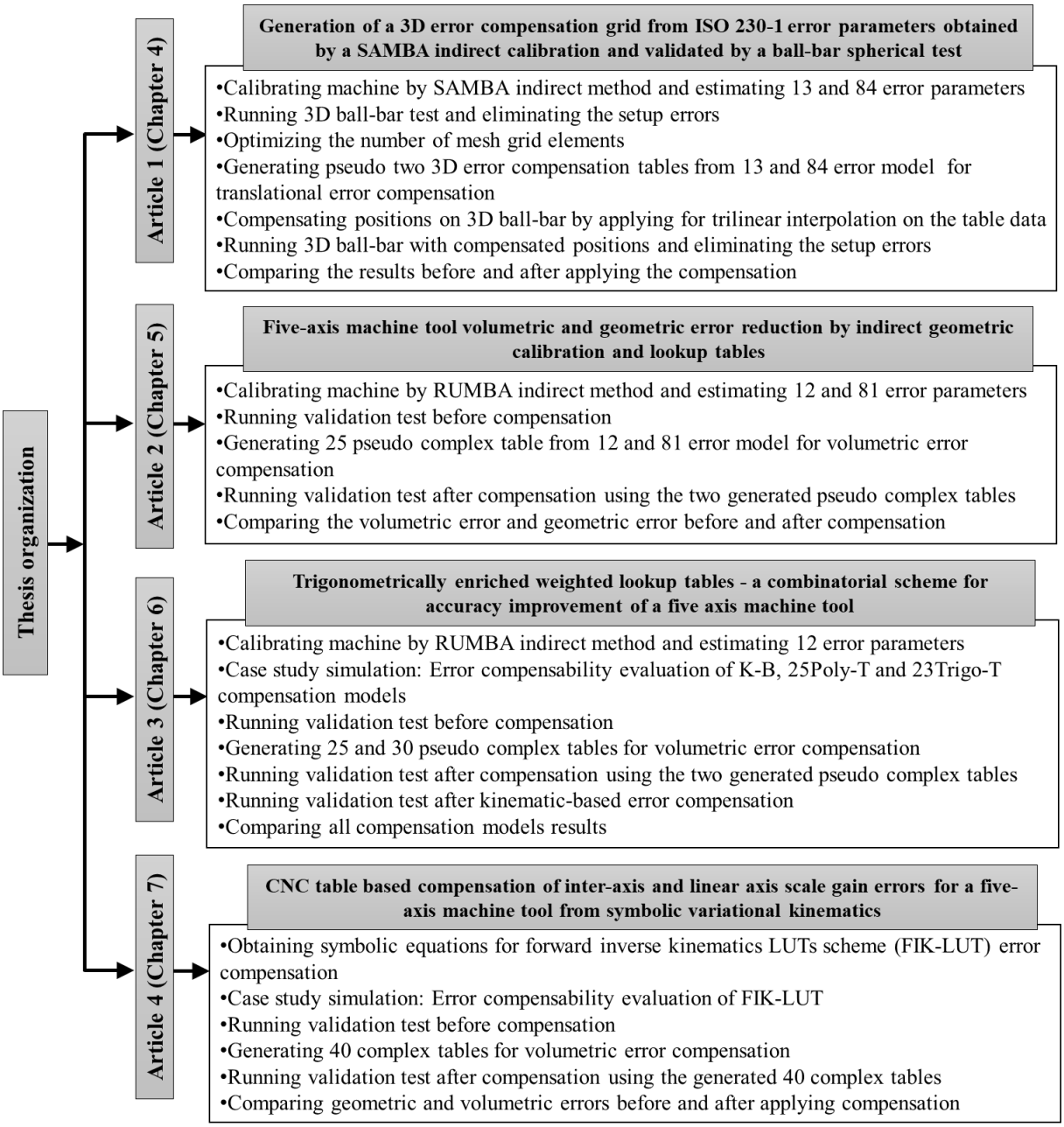

Figure 3.1. Thesis organization.

CHAPTER 4 ARTICLE 1: GENERATION OF A 3D ERROR COMPENSATION GRID FROM ISO 230-1 ERROR PARAMETERS OBTAINED BY A SAMBA INDIRECT CALIBRATION AND VALIDATED BY A BALL-BAR SPHERICAL TEST

Sareh M. Esmaeili*, J.R.R. Mayer

**Email: sareh.esmaeili-marzdashti@polymtl.ca *Tel.: +15143404711 Ext.: 2292, *Fax: (514) 340-5170*

**Address: Department of Mechanical Engineering, École Polytechnique (Montréal), P.O. Box 6079, Station Downtown, H3C 3A7 Montréal, QC, Canada*

NOTE: Based on the paper published in the International Journal of Advanced Manufacturing Technology: volume 106, pages 4649–4662(2020)

4.1 Abstract

Tool path deviation reduces machined parts quality. To enhance machine tool accuracy, compensation tables are provided in most controllers to automatically apply small corrections to axis commands. A model-based approach, considering the ISO 230-1 machine geometric error parameters, is proposed to generate the table entries. The error parameters are estimated using model-based indirect calibration results from a scale and master balls artefact probing (SAMBA) test. Two models are used, one with primarily the axis alignment errors and scale errors and the other including many error motions. The 3D grid error compensation is generated with a minimal optimum mesh grid dimension to achieve a preset precision considering the estimated model error parameters. The efficiency of the table is evaluated using a 3D ball-bar test consisting of various circular trajectories along several meridians and the equator before and after applying the table-based error compensation. It is shown that the volumetric errors due to out-of-squareness errors and linear axis linear positioning errors can be compensated using a 2x2x2, 8 nodes, grid. However, when including error motions the optimum grid dimension depends on the specific error values of the machine. For the tested machine, a 19x19x19 for 6859 nodes grid was required, with which the out-of-sphericity of the tool trajectory relative to the workpiece frame is improved by over 82%.

***Keywords**: CNC machine tool, table-based error compensation, geometric error parameters, Cartesian volumetric error*

4.2 Introduction

Machine tools impart a trajectory to a cutting tool relative to a workpiece. Any error in the path actually followed by the tool is likely to affect the quality of the machined part. Trajectory errors originate from the numerical control, the servo-drives, thermal deformation and geometric errors to name a few. Geometric errors are the focus of this paper. Different methods have been developed to reduce the effect of geometric errors through compensation such as cutter location file compensation, G-code compensation and direct axis command compensation either through inverse kinematics calculation or through table-based compensation. Koliskor (Koliskor, 1971) proposed an early error compensation technique wherein he corrected the tool path trajectory, by G-code compensation, for subsequently machined parts by applying a post-machining inspection of previously machined parts. Cartesian volumetric error compensation was applied by Lee et al. (Eung-Suk, Suk-Hwan, & Jin-Wook, 1998) wherein the tool tip position was corrected using the homogeneous transformation matrix (HTMs) followed by the G-code modification. Mahbubur et al. (R. M. Mahbubur, J. Heikkala, K. Lappalainen, & J. A. Karjalainen, 1997) proposed to alter the CL-data to modify the tool path trajectory so that the nominal G-code generation process yields a corrected tool path when ran on the erroneous machine. Nojdeh et al. (Vahebi Nojedeh, Habibi, & Arezoo, 2011) applied laser interferometry measurements to directly measure the 21 error parameters for a three-axis machine tool. They estimated the volumetric error at the tool tip using the forward kinematics. Then, using the reverse kinematics, they developed an NC program editor which uses the inverse kinematics to provide axis command corrections and generate a corrected G-code. G-code correction for a five-axis machine tool error compensation was proposed by Givi and Mayer (Givi & Mayer, 2014). They calculated the volumetric error of the tool in the desired cutter location (DCL) frame and then used the control Jacobian to calculate the axis command corrections needed to compensate this volumetric error. Zhu et al. (Zhu et al., 2012) estimated 27 machine error parameters including 21 geometric errors for the linear axes and 6 angular geometric error parameters for the rotary axes followed by error compensation using the inverse kinematics and then NC code modification. Xiang et al. (Xiang & Altintas, 2016) measured 30 intra-axis errors and 11 inter-axis errors of a five-axis machine using laser interferometry and ball-bar

measurements. The volumetric errors due to those components errors were then calculated at the tooltip for the erroneous machine tool and then compensated, all using screw theory. Cui et al. (Cui, Lu, Li, Gao, & Yao, 2012) introduced a geometric error compensation interface in which they used the inverse kinematics to reconstruct NC program for the purpose of error compensation. The G-code modification provided the compensated G-code for positioning, linear and circular movements.

Khan et al. (Khan & Chen, 2010) proposed the error compensation algorithm using the inverse kinematics by which they could find the corrected joint positions in a five-axis machine tool followed by correcting the G-code. They validated their technique by measuring the typical standard machined workpieces. Lei et al. (Lei & Hsu, 2003a) developed a methodology using 3D probe-ball and spherical test to estimate link errors. They also proposed a real-time model-based volumetric error compensation method for a five-axis machine tool using the inverse kinematics for any tool pose.

Machine tool controllers are equipped with compensation lookup tables. Some of the tables are predefined for specific purposes such as straightness errors, positioning errors, backlashes, squareness error compensation and so on ("Fanuc Controller," Series 30i/Model A; "Siemens Controller," SINUMERIK 840D/840Di/810D Extended Functions) and their values can be modified by the user. They are offered as simple and complex tables. The latter can be generated by combining the simple tables with multiplication or weighted summations. Some controllers provide spatial compensation grid tables which may be separately generated for linear axes and rotary axes (ISO/TR16907, 2015). The predefined lookup tables are mostly simple tables for correcting specific geometric error sources. As an example, the Sinumerik 840D controller proposes a volumetric compensation system (VCS) package. It provides the user the ability of error measurement, the error compensation data evaluation and finally the error compensation table generation. The tables are then transmitted to the NC program for volumetric error compensation (AG, 2010).

Most previous works (Cui et al., 2012; Eung-Suk et al., 1998; Givi & Mayer, 2014; Khan & Chen, 2010; Koliskor, 1971; R. M. Mahbubur et al., 1997; Vahebi Nojedeh et al., 2011; Xiang & Altintas, 2016; Zhu et al., 2012) focused on compensating the errors using kinematics-based error compensation. However, Creamer et al. (Jennifer Creamer et al., 2016) proposed two models, a

kinematics-based and a table-inspired one to generate a total of 25 compensation lookup tables. Each axis compensation is the sum of five tables output, one table per axis. The initial data are coordinate readings of a tool tip, an optical target, at random locations taken by a laser tracker. The kinematic model has six geometric errors, modeled as Chebyshev polynomials after each nominal axis moves similar to Mir et al. (Y. A. Mir, Mayer, & Fortin, 2005) but using small error approximated matrices. The two error models are used to generate optimized compensation table values via Chebyshev polynomial regression. Creamer et al. (J. Creamer et al., 2017) proposed an artificial intelligence approach to select an optimal set of combination of compensation tables. They performed their approach while limiting the number of tables to six instead of 25 for a five-axis machine tool.

One widely available compensation scheme in CNC to reduce Cartesian volumetric error is a 3-dimensional (3D) grid error compensation table (ISO/TR16907, 2015). The machine user is responsible for generating the table but the CNC performs the compensation automatically. 3D grid tables contain sets of compensation values corresponding to sets of linear axes positions. The compensation values are added to the commanded linear axes positions, to bring the tool to the desired position. For commanded positions not located at the mesh grid nodes, the corrections are interpolated. Since the resolution of the tables may be limited in some controllers, a method to obtain the minimal mesh grid dimension for 3D grid table is needed in order to compensate the machine errors. The mesh grid dimension becomes important when the machine errors have nonlinear behaviour. The primary contribution of this paper is proposing a novel methodology in using two error modeling framework for automatically generating the table entries from indirectly measured ISO 230-1 inter- and intra-axis error parameters. The second contribution of the paper is selecting the optimal mesh grid dimension in producing the 3D grid table. The compensation-table generating algorithm for each error model is presented and experimental evaluation of both methods are obtained and compared. The paper is organized as follows; in section 4.3, the kinematic model of the tested machine tool is introduced. Section 4.4 describes the mathematics of volumetric error calculations. Section 4.5 explains the process of determining values for the table and identifying its input and output. In section 4.6, the experimental case study is explained including calibration test and error compensation validation. The results are presented and discussed in section 4.7. Finally, the conclusion follows in Section 4.8.

4.3 Machine modeling

4.3.1 Machine configuration

Figure 4.1 shows a five-axis machine tool with topology wCBXFZYSt including three prismatic axes (X, Y and Z), two rotary axes (B and C) and a spindle (S) with stroke lengths of 610, 560 and 560 mm in the X, Y and Z directions, respectively. The workpiece branch consists of the X-, B- and C-axis and the tool branch consists of the Z- and Y-axis and the spindle. The foundation frame called F has its origin on the B-axis so that the x axis of the F frame hits the C-axis. The alignment of the F-frame is defined by the X- and Z-axis as primary and secondary axes respectively. The B-, C- and spindle axes are nominally parallel to Y-, Z- and again Z-axis, respectively. The w, S and t letters represent the workpiece, the spindle and the tool, respectively.

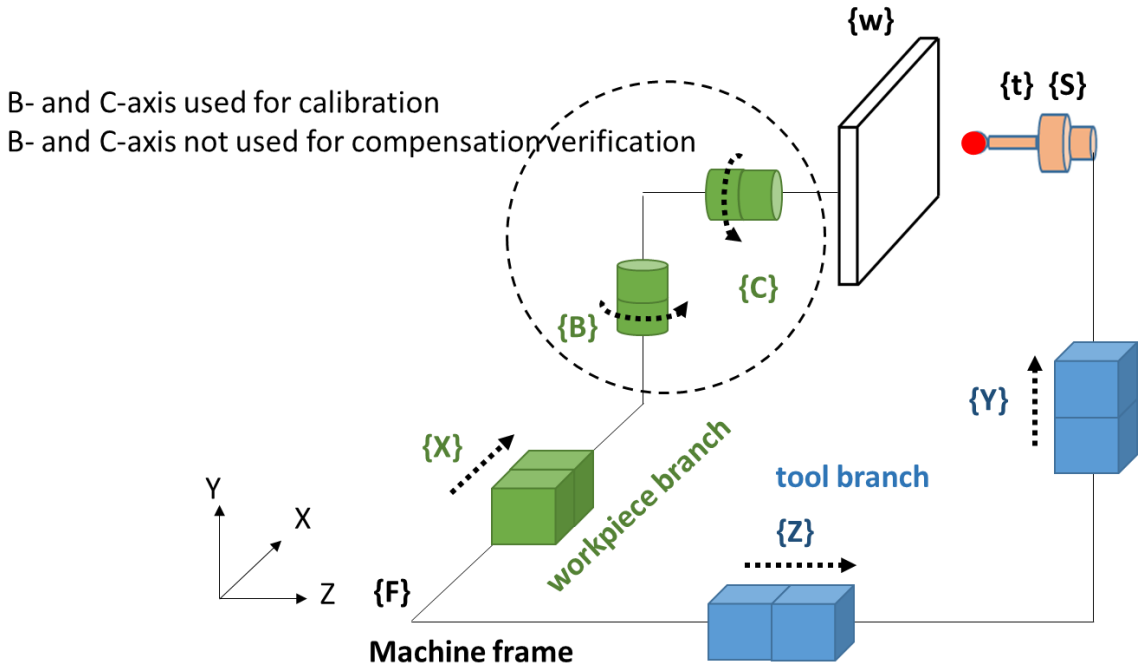

Figure 4.1. Machine tool kinematics with topology wCBXFZYSt.

4.3.2 Kinematic model

A machine tool can be seen as an open kinematic chain from workpiece to tool. Under the assumption of rigid body behaviour, the arbitrary transformation matrix between the pose of frame i relative to frame j is given by,

$$ {}^{j}\boldsymbol{T}_{i} = \begin{bmatrix} R_{3\times3} & P_{3\times1} \\ 0_{1\times3} & 1 \end{bmatrix} \tag{1} $$

where $R_{3\times3}$ and $P_{3\times1}$ are the rotation submatrix and the translation vector, respectively. In order to model the relative perfect movement of the tool relative to the workpiece, a series of homogeneous transformation matrices are multiplied in sequence as,

$$ {}^{w_n}\boldsymbol{T}_{t_n} = {}^{w_n}\boldsymbol{T}_{F}\,{}^{F}\boldsymbol{T}_{t_n} = ({}^{C}\boldsymbol{T}_{w_n}{}^{-1}\,{}^{B}\boldsymbol{T}_{C}{}^{-1}\,{}^{X}\boldsymbol{T}_{B}{}^{-1}\,{}^{F}\boldsymbol{T}_{X}{}^{-1})({}^{F}\boldsymbol{T}_{Z}\,{}^{Z}\boldsymbol{T}_{Y}\,{}^{Y}\boldsymbol{T}_{S}\,{}^{S}\boldsymbol{T}_{t_n}) \tag{2} $$

where the first parenthesis denotes the kinematic chain of the workpiece branch showing the HTM of the workpiece to the foundation frame (F) and the second one denotes the HTM of the tool relative to the foundation frame. In the presence of geometric errors, the kinematics of the target machine tool is completed with HTMs containing errors as follows:

$$ \begin{aligned} {}^{w_a}\boldsymbol{T}_{t_a} = {}&{}^{w_n}\boldsymbol{T}_{w_a}{}^{-1}\,{}^{C'}\boldsymbol{T}_{w_n}{}^{-1}\,{}^{C}\boldsymbol{T}_{C'}{}^{-1}\,{}^{C_0'}\boldsymbol{T}_{C}{}^{-1}\,{}^{C_0}\boldsymbol{T}_{C_0'}{}^{-1}\,{}^{B'}\boldsymbol{T}_{C_0}{}^{-1}\,{}^{B}\boldsymbol{T}_{B'}{}^{-1}\,{}^{B_0'}\boldsymbol{T}_{B}{}^{-1}\,{}^{B_0}\boldsymbol{T}_{B_0'}{}^{-1}\,{}^{X'}\boldsymbol{T}_{B_0}{}^{-1}\,{}^{X}\boldsymbol{T}_{X'}{}^{-1}\,{}^{X_0'}\boldsymbol{T}_{X}{}^{-1} \\ &{}^{X_0}\boldsymbol{T}_{X_0'}{}^{-1}\,{}^{F}\boldsymbol{T}_{X_0}{}^{-1}\,{}^{F}\boldsymbol{T}_{Z_0}\,{}^{Z_0}\boldsymbol{T}_{Z_0'}\,{}^{Z_0'}\boldsymbol{T}_{Z}\,{}^{Z}\boldsymbol{T}_{Z'}\,{}^{Z'}\boldsymbol{T}_{Y_0}\,{}^{Y_0}\boldsymbol{T}_{Y_0'}\,{}^{Y_0'}\boldsymbol{T}_{Y}\,{}^{Y}\boldsymbol{T}_{Y'}\,{}^{Y'}\boldsymbol{T}_{S}\,{}^{S}\boldsymbol{T}_{S'}\,{}^{S'}\boldsymbol{T}_{t_n}\,{}^{t_n}\boldsymbol{T}_{t_a} \end{aligned} \tag{3} $$

where X_0 , Y_0 , Z_0 , B_0 , C_0 , w_n , S and t_n describe the nominal joint locations and X, Y, Z, B and C describe the nominal movement of each axis. The actual joint locations before movement are X_0' , Y_0' , Z_0' , B_0' and , C_0' and actual locations of the axes, workpiece and tool are X', Y' , Z' , B', C' , w_a , S' and t_a .

The geometric errors in a five-axis machine tool are classified into two groups: intra- and inter-axis errors. In order to remove the redundancy between the two groups and provide a better estimation while calculating error parameters by indirect measurement methods, different error models are defined in which several intra- and inter-axis errors (M. M. Rahman & Mayer, 2015) participate. Those intra- and inter-axis errors are equivalent to the motion and link errors in ISO

230-1 (Zhu et al., 2012), respectively. Inter-axis (link) errors are defined as the errors of position and orientation between the average line of axes of movement and intra-axis (motion) errors are the motion imperfections of each individual mechanical axis (Schultschik, 1977). Two error models are studied, the first one is called the 13-error model. It requires the eight inter-axis error parameters of the five axes and two translation error parameters for the spindle axis apposition relative to the two main rotary axes of the machine. Finally, three intra-axis error modeling the scale gain errors of the positioning errors of the linear axes are included (Mayer, 2012). The other error model, called the 84-error model, includes many intra- and inter-axis errors and also the two angular positioning backlashes of the B- and C-axis. This model uses ordinary polynomials for modeling the error parameters (McHichi & Mayer, 2014). The 84-error model is made of the polynomials coefficients. The error coefficients and parameters relative to the two models are detailed in section 4.6, Table 4-2 and Table 4-3.

To calibrate the machine tool, an indirect technique called SAMBA (Mayer, 2012) is applied. The SAMBA hardware is an artefact consisting of a variable number of master balls, typically four, and a fixed length scale bar which are probed following a specific strategy to cover the maximum working volume and the maximum rotation of the rotary axes in order to enable better estimation of the machine error parameters (McHichi & Mayer, 2014). The measurement data are then processed using the Newton-Gauss to estimate the best values for the unknown inter- and intra-axis error parameters that match the measurements in a least square sense (Y. A. Mir et al., 2005).

4.4 Volumetric error compensation

A kinematics-based approach is used to calculate the axis command correction necessary to reduce the volumetric error. The volumetric errors are the relative linear and angular deviation of the tool to the workpiece calculated by,

$$ {}^{\{t\},w}E_{Vt} = twist(({}^{w_n}\boldsymbol{T}_{t_n}(q))^{-1}\,{}^{w_a}\boldsymbol{T}_{t_a}(q)) \tag{4} $$

for command position *q*, where ${}^{\{t\},w}E_{Vt}$ is the volumetric error twist expressed in the tool frame. The twist function extracts the three linear and three angular deviations from the tool relative to the workpiece HTM (4×4). *q* is,

$$q = [q_X \quad q_Y \quad q_Z \quad q_B \quad q_C] \tag{5}$$

where q_X, q_Y, q_Z, q_B and q_C are the components of the nominal command in X, Y, Z, B and C directions, respectively. As in (Givi & Mayer, 2014), assuming small angular volumetric errors, the necessary volumetric correction twist is given by,

$$E_{CV} = -{}^{\{t\},w}E_{Vt} \tag{6}$$

and

$$E_{CV} = \begin{bmatrix} E_{XCV} & E_{YCV} & E_{ZCV} & E_{ACV} & E_{BCV} & E_{CCV} \end{bmatrix}^T \tag{7}$$

is the volumetric correction twist where E_{CVX}, E_{CVY} and E_{CVZ} are its linear elements and, E_{CVA}, E_{CVB} and E_{CVC} are its the angular elements. In order to calculate the axis command correction, the sensitivity matrix, J_q, is calculated which describes the linear relationship between differential changes in axis command correction and the volumetric error. Therefore, the relationship between E_{CV} and the axes command correction, Δq_{Comp}, for each set of commands is given by,

$$\Delta q_{Comp} = J_q{}^{\dagger} E_{CV} \tag{8}$$

where,

$$\Delta q_{Comp} = \begin{bmatrix} \Delta q_X & \Delta q_Y & \Delta q_Z & \Delta q_A & \Delta q_B & \Delta q_C \end{bmatrix}^T \tag{9}$$

$J_q{}^{\dagger}$ is the pseudo-inverse of J_q. A Gauss-Newton iterative method is applied for a numerically exact solution.

4.5 3D error compensation table - generation and interpolation

4.5.1 Table generation

The 3D table is a mesh grid, Figure 4.2, with its node coordinates corresponding to the mechanical axes nominal commands and each node is attributed an axis command correction vector. For commands not corresponding exactly to a grid node, an interpolation using surrounding nodes is conducted. The input values to the table are the nominal axis commands and the output are the axis command correction values to be added to the nominal commands to reduce the effect of machine tool errors. For this 3D grid table only the linear axes are considered.

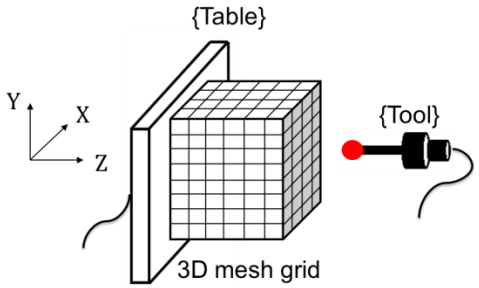

Figure 4.2. Schematic of a sample 3D mesh grid dimension.

The 3D table mesh grid dimension may affect the compensation quality since the interpolation is applied linearly for the commands located in between the mesh grid nodes. This may also depend on the nature of the dominant error parameters, and whether their effects are proportional to axis commands or nonlinear. The objective is to obtain the optimal mesh grid dimension based on the specific machine error parameters' values. Hence, an algorithm is used in Figure 4.4 in which the process of obtaining the minimal optimum mesh grid nodes is illustrated. This procedure uses, as inputs, the estimated machine error parameters and a set of random commands in the Cartesian working volume.

The smallest mesh grid dimension is 2x2x2. A 1x1x1 mesh grid would apply the same correction to every nominal command set which is akin to a workpiece reference frame offset and is handled by other G-code functions. To generate a 3D table for a specific mesh grid dimension, the volumetric error at the nominal command associated with each mesh grid node is calculated by Eq. (4). A number is assigned to each mesh grid node which is then used as an entry in the 3D table.

Then, the compensated volumetric error is obtained by Eq. (6). Afterwards, the corresponded command correction is computed by Eq. (8). This process corresponds to the Conversion algorithm in Figure 4.4. Ultimately, the table is generated with the nominal mesh grid node numbers and their associated commands and the corresponding nominal commands corrections (Figure 4.3).

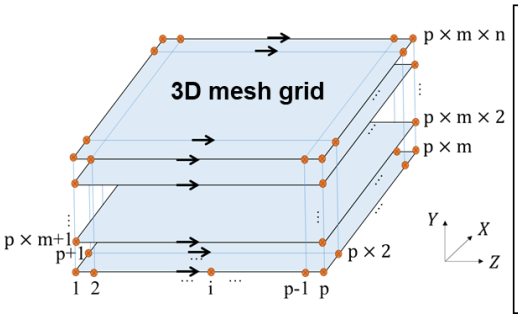

3D error compensation table

Mesh grid node Number	Joint command (X)	Joint command (Y)	Joint command (Z)	Joint correction (X)	Joint correction (Y)	Joint correction (Z)
1	q_{X1}	q_{Y1}	q_{Z1}	Δq_{X1}	Δq_{Y1}	Δq_{Z1}
2	q_{X2}	q_{Y2}	q_{Z2}	Δq_{X2}	Δq_{Y2}	Δq_{Z2}
⋮	⋮	⋮	⋮	⋮	⋮	⋮
i	$q_{X(i)}$	$q_{Y(i)}$	$q_{Z(i)}$	$\Delta q_{X(i)}$	$\Delta q_{Y(i)}$	$\Delta q_{Z(i)}$
⋮	⋮	⋮	⋮	⋮	⋮	⋮
p×m×n	$q_{X(p\times m\times n)}$	$q_{Y(p\times m\times n)}$	$q_{Z(p\times m\times n)}$	$\Delta q_{X(p\times m\times n)}$	$\Delta q_{Y(p\times m\times n)}$	$\Delta q_{Z(p\times m\times n)}$

Figure 4.3. The 3D mesh grid and the error compensation table.

To decide on the optimality of the selected mesh grid dimension, the table is used for 2000 random commands $(q_{Xn} \quad q_{Yn} \quad q_{Zn} \quad 0 \quad 0)$, where the compensated command $(q_{XC} \quad q_{YC} \quad q_{ZC} \quad 0 \quad 0)$ is calculated by adding the command correction $(\Delta q_X \quad \Delta q_Y \quad \Delta q_Z \quad 0 \quad 0)$ achieved by applying the interpolation explained in section 4.5.2 to the nominal command $(q_{Xn} \quad q_{Yn} \quad q_{Zn} \quad 0 \quad 0)$,

$$\begin{bmatrix} q_{XC} & q_{YC} & q_{ZC} & 0 & 0 \end{bmatrix} = \begin{bmatrix} q_{Xn} & q_{Yn} & q_{Zn} & 0 & 0 \end{bmatrix} + \begin{bmatrix} \Delta q_X & \Delta q_Y & \Delta q_Z & 0 & 0 \end{bmatrix}. \tag{10}$$

The remaining volumetric error, after using the 3D grid table, is recalculated by Eq. (4). Regarding the initial and also the optimal grid dimension, choosing this number as random commands seems to be reasonable. The number of mesh grid nodes are increased until the norm of the differences of the root mean square (RMS) of the Cartesian volumetric errors for the random commands in the considered working volume after numerically using the 3D grid table become less than a preset threshold of 10^{-4} mm. The preset threshold is introduced as the decision parameter for the simulated machine, which has no other errors than the modeled errors. So that,

$$if \quad \| (RMS(E_{VtK(i)}) - RMS(E_{VtK(i-1)})) \| < preset\ threshold\ . \tag{11}$$

where K can be substituted by X, Y and Z. $E_{VtK(i)}$ is the volumetric error for step i and $E_{VtK(i-1)}$ for step (i − 1). The RMS of the volumetric error in the K direction (E_{VtK}) is calculated by,

$$RMS(E_{VtK}) = \frac{1}{2000}\sqrt{\sum_{j=1}^{2000}(E_{VtKj})^2}\ . \tag{12}$$

where j = 1 to 2000 for the 2000 random commands.

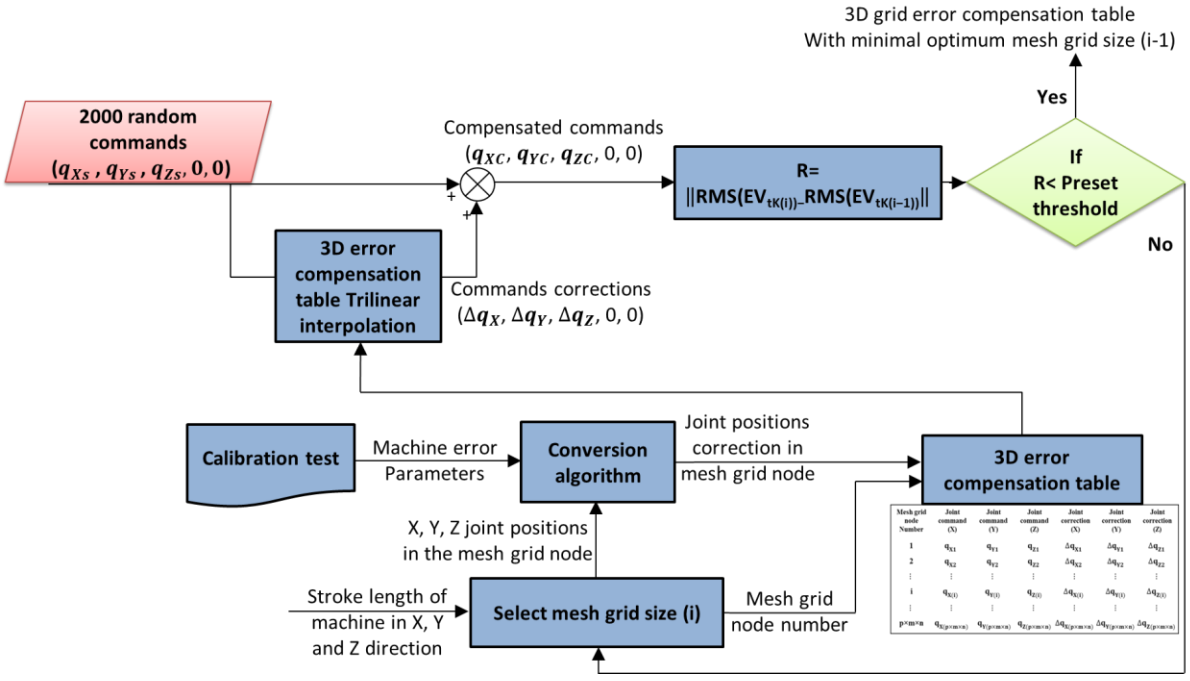

Figure 4.4. Process of generating the table with optimal mesh grid dimension.

Two simulated error models, the 84- and the 13-error models, are used for verifying the proposed method to generate the 3D grid table. This 84-error model uses cubic polynomials to model the error motion and so can model nonlinear errors while the 13-error model one contains errors having linear behaviour. As seen in Figure 4.5, the initial grid has a dimension 2x2x2 for 8 nodes. For a threshold of 10^{-4} mm and using a step of 1 for each grid dimension, e.g. 2x2x2, 3x3x3, 4x4x4, etc., the optimum 3D tables for the two simulated parameter and coefficient value sets of the 84-error model are shown in Figure 4.5. The dimension of the mesh grid that fulfils the *preset threshold* is different for the two simulated error sets. The optimum mesh grid dimension for the first simulated

84-error models error parameters' set is 14×14×14, 2744 nodes, while for the second simulated error parameters' set, the optimum mesh grid dimension is 19×19×19, 6859 nodes. Hence, depending on the specific error parameters values of the 84-error model, the optimum mesh grid dimension may vary. However, the grid dimension of 2x2x2 is appropriate for the simulated erroneous machine tool having 13 error parameters to reach to the predetermined threshold for 2000 random commands. This may be due to the quasi-linear relationship between the effect of those errors and the nominal commands. The relevant errors are the out-of-squarenesses between the linear axes and the linear axes linear positioning errors.

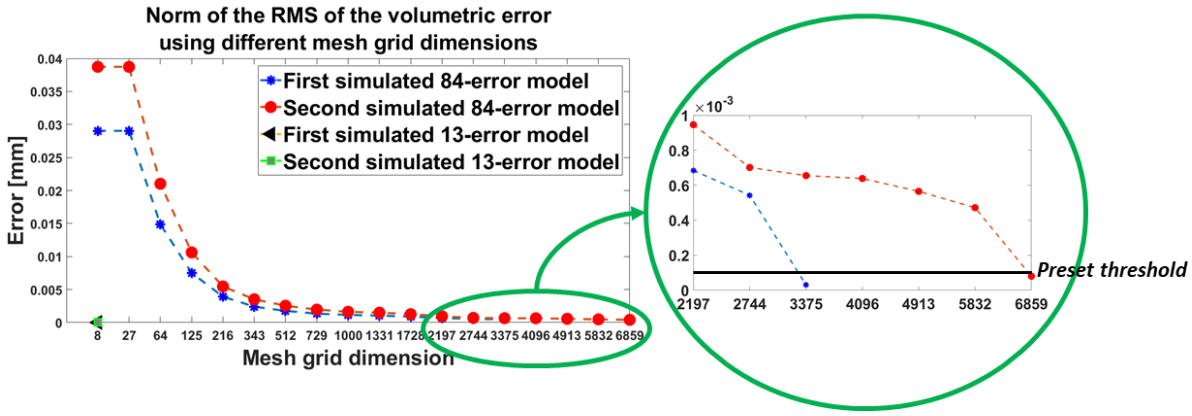

Figure 4.5. The norm of the Root Mean Square of the volumetric errors for the 2000 random commands in the stroke length of the machine while using the 3D grid table with different mesh grid dimension for the two simulated 13- and 84-error model parameters.

4.5.2 Interpolation

Because of the number of entries for the tables are limited, typically controllers interpolate for commands located between the mesh grid nodes. For instance, the mesh grid dimension in the Fanuc controller is 15625 or 25x25x25 for the X, Y and Z-axis ("Fanuc Controller," Series 30i/Model A). Intermediate values are calculated using a multivariate trilinear interpolation ("Fanuc Controller," Series 30i/Model A). Assuming P as the command needed to be compensated, the process can be simplified to perform the interpolation in an element forming a rectangular prism using the eight command corrections on the lattice points surrounding P (Figure 4.6).

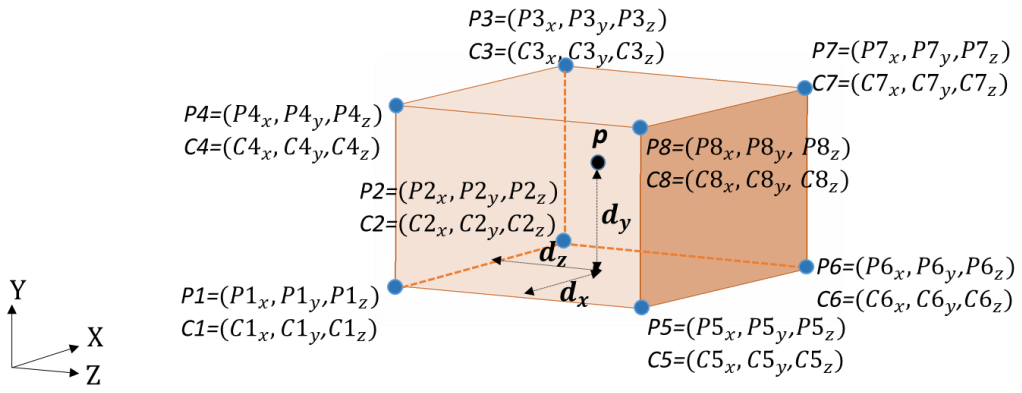

Figure 4.6. Schematic of a rectangular prism for applying trilinear interpolation.

Considering *p1*, *p2*, *p3*, *p4*, *p5*, *p6*, *p7* and *p8* as the rectangular prism corners, ratios *rx*, *ry* and *rz* are respectively calculated in the X, Y and Z directions by (Bourke, 1999),

$$rx = \frac{|p_x - p1_x|}{|p2_x - p1_x|} = \frac{d_x}{|p2_x - p1_x|}, ry = \frac{|p_y - p1_y|}{|p4_y - p1_y|} = \frac{d_y}{|p4_y - p1_y|}, rz = \frac{|p_z - p1_z|}{|p5_z - p1_z|} = \frac{d_z}{|p5_z - p1_z|} \tag{13}$$

where P_x, P_y and P_z are the x, y and z target joint positions in the joint space. In cases where the joint command is located at a mesh grid node, the program returns the value of zero to the associated ratio. The correction values in the X direction, C_x in the following equation, for position P is given by (Bourke, 1999),

$$\begin{aligned} C_x = {} & C1_x(1-rx)(1-ry)(1-rz) + C2_x rx(1-ry)(1-rz) + C3_x rxry(1-rz) + C4_x(1-rx)ry(1-rz) \\ & + C5_x(1-rx)(1-ry)rz + C6_x rx(1-ry)rz + C7_x rxryrz + C8_x(1-rx)ryrz \end{aligned} \tag{14}$$

where $C1_x$, $C2_x$, $C3_x$, $C4_x$, $C5_x$, $C6_x$, $C7_x$ and $C8_x$ are the scalar correction values at each rectangular prism corner, obtained from the 3D grid table. Similarly, the correction values in the Y and Z directions, C_y and C_z, are calculated by respectively substituting $C1_x$, $C2_x$, $C3_x$, $C4_x$, $C5_x$, $C6_x$, $C7_x$ and $C8_x$ with $C1_y$, $C2_y$, $C3_y$, $C4_y$, $C5_y$, $C6_y$, $C7_y$ and $C8_y$ and $C1_z$, $C2_z$, $C3_z$, $C4_z$, $C5_z$, $C6_z$, $C7_z$ and $C8_z$ in Eq. (14).

4.6 Experimental case study

To study the efficiency of the generated 3D grid error compensation table, a series of experimental tests were conducted including machine error parameters identification test (SAMBA) followed by 3D ball-bar validation tests. The experimental validation procedure is illustrated in Figure 4.9. In order to reduce thermal effect differences between the calibration and the validation tests, the tests were executed in the sequence 3D ball-bar, SAMBA and 3D ball-bar. Although a SAMBA test could be applied as validation a 3D ball-bar test was chosen instead as it provides a more independent validation means. Machine error parameters and error coefficients are estimated for both the 13- and 84-error error models from the SAMBA test data conducted "before compensation". Then, "after compensation", the SAMBA procedure is repeated just to ensure similar thermal states of the machine. The mean values of the radial errors (ball-bar measurements of the volumetric error along its sensitive direction) before compensation (e1, e2) and after compensation ($e1_c$, $e2_c$) were used for analyzing the effectiveness of the compensation. The calibration zone, mesh grid zone and 3D ball-bar test zone are shown in Figure 4.8. The test zone is entirely contained with the calibration zone in order to avoid error extrapolation. Because the tested machine does not have a 3D compensation table option a pseudo 3D table was produced by which the command compensation process was conducted offline and a compensated G-code produced. As shown in Figure 4.9, before comparing the two mean measured radial errors, the effect of ball-bar setup errors, i.e. eccentricity of the ball-bar tool ball circular trajectory relative to the workpiece ball, are removed using a linearized geometric error model. The resulting Jacobian of the first partial derivatives of the radial errors to the setup error was constructed. So that,

$$\rho = \underbrace{[\sin\theta\cos\phi \quad \sin\theta\sin\phi \quad \cos\theta]\begin{bmatrix}1 & 0 & 0\\ 0 & 1 & 0\\ 0 & 0 & 1\end{bmatrix}}_{J_{setup\ error}}\underbrace{\begin{bmatrix}u\\ v\\ w\end{bmatrix}}_{E_{setup\ error}} = J_{setup\ error}E_{setup\ error} \tag{15}$$

where $J_{setup\ error}$ is the projected Jacobian for the setup error, ρ is the ball-bar reading column matrix, $E_{setup\ error}$ is a column matrix containing the setup errors and *u*, *v* and *w* are the setup errors in the X, Y and Z directions, respectively. The θ and ϕ are respectively the polar and the azimuthal angles (Figure 4.7).

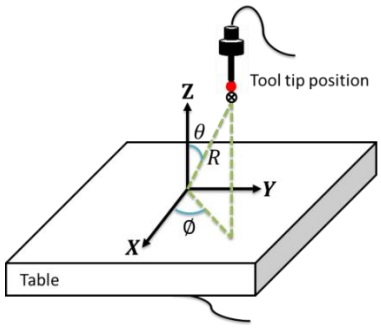

Figure 4.7. Projection of the tool tip position in the ball-bar direction.

Because the balls of the tool and the workpiece have the same effect on the Jacobian, one set of setup errors is kept and the other is redundant. Therefore, the setup error is denoted by,

$$E_{setup\ error} = J^{-1}{}_{setup\ error}\,\rho \tag{16}$$

and the setup error compensated measurement data is then calculated by,

$$\rho' = \rho - J_{setup\ error}\begin{bmatrix} u \\ v \\ w \end{bmatrix}. \tag{17}$$

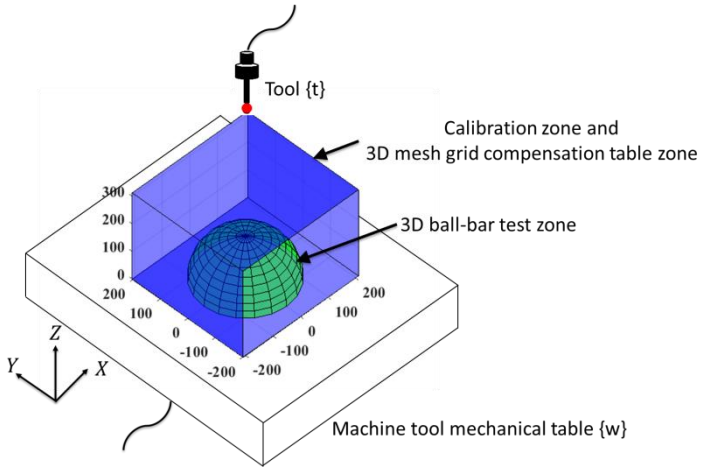

Figure 4.8. The calibration zone, mesh grid zone and 3D ball-bar test zone.

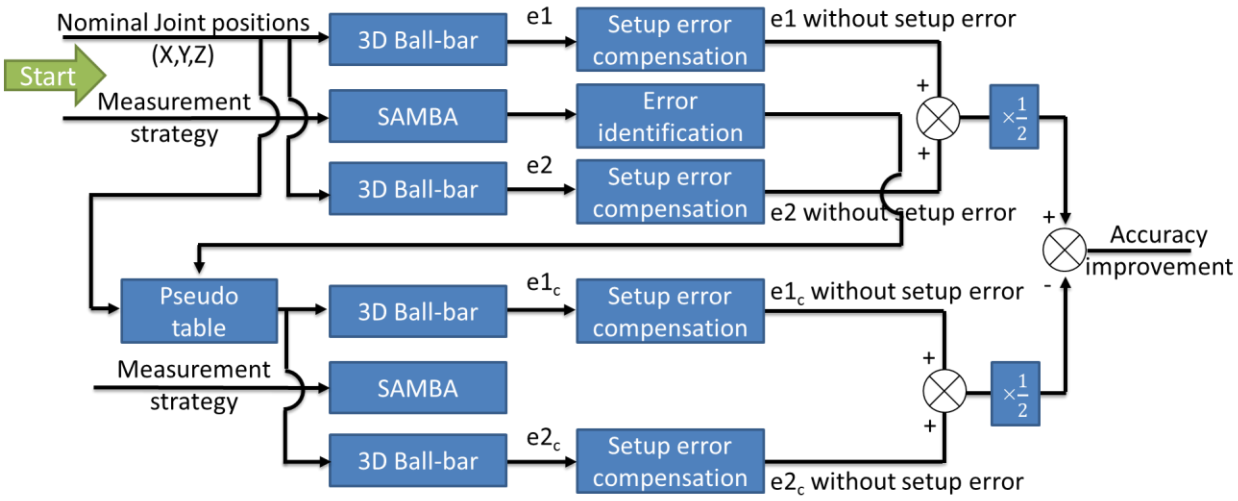

Figure 4.9. Experimental test procedure. (e1, e2): the measured radial error before compensation, (e1c, e2c): the measured radial error after compensation using pseudo table of the 13-error model or the 84-error model.

4.6.1 Machine error parameters identification

Figure 4.10 shows the calibration system (SAMBA) with the four 9.525 mm radius precision master balls and the scale bar artefact with a 304.6686 mm (U = 1.2 µm) length installed on the pallet of the tested machine tool. The rotary B- and C-axis are indexed within the ranges of -90º to 90º and -360º to 360º, respectively. A Renishaw machine tool touch trigger probe (MP700) with a total tool length of 275.86 mm measures the x, y and z coordinate of the balls' positions for 32 sets of B and C angular position pairs. The measurement strategy is designed to cover the full rotation of the rotary axes to have a better estimation of machine error parameters. However, depending on the accessibility of the probe to the target balls, the number of balls measured in different indexations may vary. The measurement strategy is shown in Table 4-1. As seen, the spindle (S-axis) is also indexed at 60º, 120º, 180º, 240º and 300º which allow distinguishing the stylus tip offsets from the spindle position error parameters. In the conducted tests, the scale bar is also probed to allow the three scale gain errors to be estimated with respect to the international meter. The SAMBA data is processed to estimate the machine error model. The tests were repeated five times over five consecutive days. Each test for measuring 123 positions lasted for 3H10M (3 h and 10 min). The room temperature was between 21°C and 22°C during the test.

Table 4-1. Strategy of measurement in SAMBA technique.

Index number	Indexation (°) (S,B,C)	Ball ID	Index number	Indexation (°) (S,B,C)	Ball ID
1	(0,10,30)	3,4,5	**17**	(0,0,90)	1,2,3,4,5,6
2	(0,30,90)	3,4,5	**18**	(0,0,240)	3,4,5
3	(0,50,150)	3,4,5	**19**	(0,0,300)	3,4,5
4	(0,70,210)	3,4,5	**20**	(0,0,180)	1,2,3,4,5,6
5	(0,90,270)	3,4,5,6	**21**	(0,0,45)	1,2,3,4,5,6
6	(0,60,180)	3,4,5	**22**	(0,0,-45)	1,2,3,4,5,6
7	(0,40,120)	3,4,6	**23**	(0,0,-180)	1,2,3,4,5,6
8	(0,20,60)	3,4,6	**24**	(0,0,-300)	3,4,5
9	(0,-10,-30)	3,4,5	**25**	(0,0,-240)	3,4,5
10	(0,-30,-90)	3,4,5	**26**	(0,0,-90)	1,2,3,4,5,6
11	(0,-50,-150)	3,4,5	**27**	(0,0,0)	1,2,3,4,5,6
12	(0,-70,-210)	3,4,5	**28**	(60,0,0)	3
13	(0,-90,-270)	3,4,5,6	**29**	(120,0,0)	3
14	(0,-60,-180)	3,4,5	**30**	(180,0,0)	3
15	(0,-40,-120)	3,4,6	**31**	(240,0,0)	3
16	(0,-20,-60)	3,4,6	**32**	(300,0,0)	3

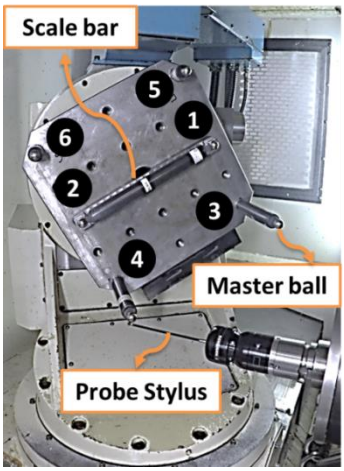

Figure 4.10. SAMBA artefact (1-2: Scale bar), (3,4,5,6: Master ball) used to estimate the machine tool error parameters and coefficients to be used to prepare the compensation table.

4.6.2 3D ball-bar test with single setup for compensation validation

The telescopic magnetic ball-bar measures the distance between its two ball centers using its internal linear transducer and an external calibrated distance in the form of two kinematic ball seats

separated by a calibrated distance, on which the ball-bar can be temporarily mounted. The nominal ball-bar length is 150 mm with an uncertainty of ±1.4 μm on the readings and a measuring range of approximately ±1 mm. Figure 4.11 shows the 3D ball-bar test. Five half meridian travels form a hemisphere while transiting between the meridians via arcs on the equator. The first engagement is at the first position (position “A”), the feed in and feed out are located on the third forward meridional travel (position “B”) and the disengagement is at the end in front of the engagement point (position “C”). The G-code before compensation uses the nominal trajectories. To minimize error contribution from the NC linear interpolation between the programmed points an angular increment of 0.1 degree along the meridians was used thus ensuring a maximum distance of 0.00014 μm between the meridians and the trajectory linear segments. As a result, 19809 positions are programmed with G01 commands. The number of ball-bar measurements is controlled by the Renishaw software. At the slower feed rate of 200 mm/min is selected for the test, the slower sampling rate is automatically selected by the ball-bar software yielding a total of 5990 distance readings. The 3D ball-bar test was run before and after compensation.

Any compensation table present on the machine controller, such as linear axis positioning and angular axis positioning, were deactivated for all tests. The room temperature was between 21°C and 22°C during the test but fluctuations outside this range were possible overnight between tests. The test was repeated ten times over five consecutive days while the machine was assumed to be in the same environmental situation. Each test lasted 37 minutes without considering the setup time.

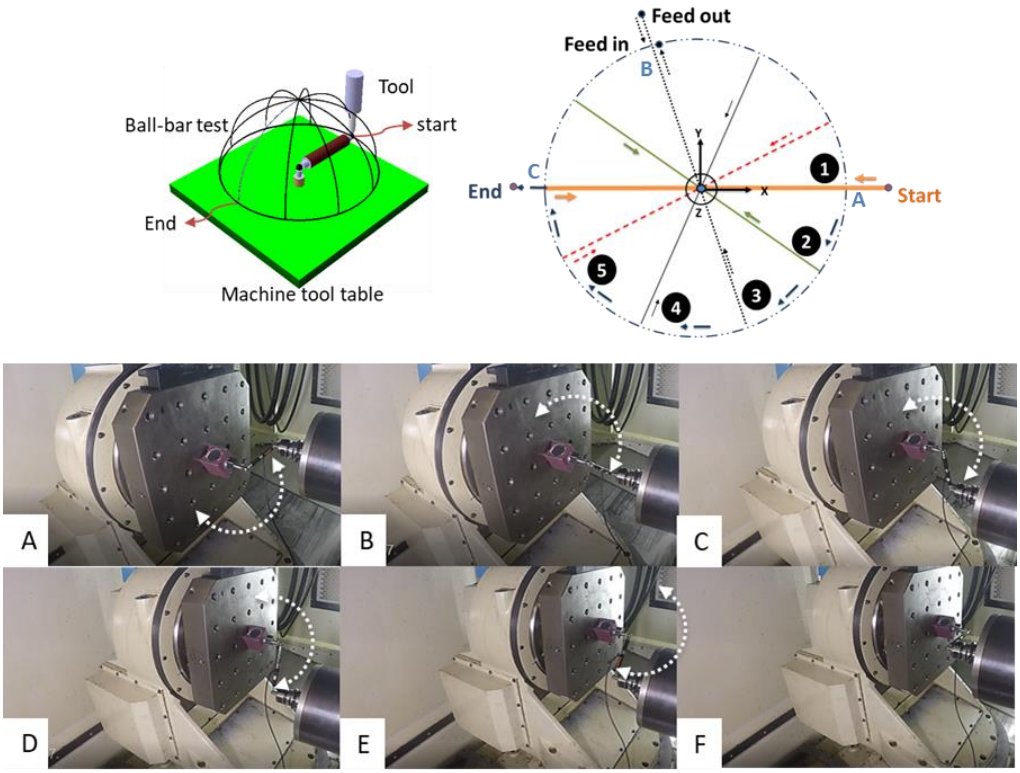

Figure 4.11. 3D ball-bar validation test used to evaluate the effectiveness of the compensation. (A: start-travel 1, B: travel 2, C: travel 3, D: travel 4, E: travel 5, F: end).

4.7 Results and discussions

Table 4-2 lists the error coefficients for the 84-error model obtained by SAMBA calibration. Each intra-axis error is fitted with third degree ordinary polynomials. However, some of them are partially confounded as is expected for ordinary polynomials. The errors are presented for each axis separately in Table 4-2. The 84-error model is capable of providing positioning backlashes for the two rotary axes as well. Table 4-3 lists the error parameters and coefficients for the 13-error model obtained by SAMBA calibration. The maximum standard deviations of the five repeated measurements (SAMBA test) along X, Y and Z were 0.8, 1.2 and 1.1 µm, respectively.

The 3D ball-bar tests data before and after compensation are compared for compensation validation. The setup error calculated by Eq. (16), accounted for less than 5% of the 3D ball-bar data before compensation. For 3D ball-bar "after compensation" test, first, the pseudo 3D grid error compensation table was provided for the two error models. A simulator was developed for the target machine tool topology which used the erroneous machine tool forward kinematics. By

entering the tool specification and the machine tool error parameters estimated from the SAMBA test for one of the two error models, the volumetric errors for each mesh grid node position are predicted. The optimal mesh grid was obtained for the two error models with the error parameters and coefficients values listed in Table 4-2 and Table 4-3 using the process explained in Figure 4.4. Starting the initial guess for the mesh grid dimension as 2x2x2 (resulting in eight nodes) and considering a step of 1 for the mesh grid dimension in the optimization process, the 2x2x2 mesh grid dimension was appropriate for the 13-error model but for the 84-error model, the minimal optimum grid dimension for the real data was 19x19x19 for 6859 nodes. Two pseudo 3D grid error compensation tables were then generated and the trilinear interpolation used to compensate the nominal G-code for the 3D ball-bar tests. No corrections exceeded 100 µm. The setup error was recalculated for the 3D ball-bar data after compensation by Eq. (16) showing less than 5% of the 3D ball-bar data after compensation. The radial errors before and after G-code 3D grid error compensation are shown in Figure 4.12 and Figure 4.13 for 13- and 84-error parameter models, respectively. The machine tool exhibits scale errors before applying the compensation. The discrepancy between the maximum and the minimum ball-bar measurements was 33.6 µm before compensation. This discrepancy was reduced to 6.3 µm and 5.8 µm after compensation for the 13- and 84-error model, respectively. Thus, the machine tool accuracy was improved by 81.25% and 82.74% for 13- and 84-error, respectively. The root mean square (RMS) of the Cartesian volumetric error was reduced from 24.5 µm before compensation down to 4.3 µm and 3.5 µm after compensation for the 13- and 84-error model, respectively. The two error models do not estimate linear axes backlashes. However, independent circular ball-bar tests showed a backlash of around 5 µm for the linear axes. The 84-error model contains more error parameters but only performed marginally better than the 13 error parameter model probably because the parameters which were common in the two models were the dominant ones.

Table 4-2. Calibration results for 84-error model. It estimates 84 error coefficients.

X-axis		Y-axis		Z-axis		B-axis		C-axis	
Name	Value	Name	Value	Name	Value	Name	Value	Name	Value
E_{XX1}	-3.13E-04	E_{XY0}	-2.41E-02	E_{XZ1}	2.29E-04	E_{XB0}	-1.08E-01	E_{XC1}	-5.06E-04
E_{XX2}	7.53E-08	E_{XY2}	3.43E-08	E_{XZ2}	-6.27E-07	E_{XB1}	-1.21E-02	E_{XC2}	2.81E-05
E_{XX3}	1.35E-10	E_{XY3}	-5.12E-10	E_{XZ3}	5.55E-10	E_{XB2}	4.19E-02	E_{XC3}	3.39E-05
E_{YX2}	-2.74E-09	E_{YY0}	6.10E-02	E_{YZ2}	5.12E-07	E_{XB3}	1.53E-02	E_{YC1}	2.08E-04
E_{YX3}	1.22E-10	E_{YY1}	-1.09E-04	E_{YZ3}	-3.06E-10	E_{YB1}	-1.58E-03	E_{YC2}	-7.80E-05
E_{ZX2}	-1.57E-08	E_{YY2}	-2.46E-08	E_{ZZ1}	1.04E-04	E_{YB2}	-4.16E-04	E_{YC3}	-2.51E-05
E_{ZX3}	-1.32E-11	E_{YY3}	3.64E-11	E_{ZZ2}	-3.76E-07	E_{YB3}	-4.16E-04	E_{ZC1}	-2.74E-04
E_{AX0}	-5.99E-04	E_{ZY2}	3.30E-08	E_{ZZ3}	3.26E-10	E_{ZB1}	-1.08E-02	E_{ZC2}	-4.94E-05
E_{AX1}	2.86E-08	E_{ZY3}	-1.19E-10	E_{AZ0}	-2.60E-04	E_{ZB2}	-4.89E-02	E_{ZC3}	1.40E-05
E_{AX2}	2.97E-10			E_{AZ1}	-1.15E-07	E_{ZB3}	1.05E-02	E_{AC1}	5.41E-07
E_{AX3}	-1.82E-13			E_{AZ2}	4.06E-10	E_{AB0}	3.00E-04	E_{AC2}	-1.35E-08
E_{BX1}	-7.27E-08			E_{AZ3}	-5.07E-13	E_{AB1}	-3.62E-04	E_{AC3}	-5.51E-08
E_{BX2}	-1.10E-10			E_{CZ0}	-4.28E-04	E_{AB2}	-1.30E-04	E_{BC1}	1.89E-06
E_{BX3}	3.61E-13			E_{CZ1}	3.47E-06	E_{AB3}	5.03E-05	E_{BC2}	-5.42E-08
E_{CX0}	-3.62E-03			E_{CZ2}	-8.99E-09	E_{BB0}	1.95E-05	E_{BC3}	-1.58E-07
E_{CX1}	6.46E-08			E_{CZ3}	7.56E-12	E_{BB1}	-2.39E-05	E_{CC1}	1.64E-06
E_{CX2}	-2.59E-11					E_{BB2}	3.92E-06	E_{CC2}	9.84E-08
E_{CX3}	-1.82E-12					E_{BB3}	1.51E-05	E_{CC3}	-9.73E-08
						E_{BBb}	7.12E-06	E_{CCb}	5.76E-06
						E_{CB1}	3.13E-04		
						E_{CB2}	-1.55E-04		
						E_{CB3}	-4.66E-05		

Units examples:

R and H are the linear axes: E_{RH0}[mm], E_{RH1}[mm/mm], E_{RH2}[mm/mm^2], E_{RH3}[mm/mm^3], E_{RHb}[mm]
R is the rotary axis and H is the linear axis: E_{RH0}[rad], E_{RH1}[rad/mm], E_{RH2}[rad/mm^2], E_{RH3}[rad/mm^3], E_{RHb}[rad]
R and H are the rotary axes: E_{RH0}[rad], E_{RH1}[rad/rad], E_{RH2}[rad/rad^2], E_{RH3}[rad/rad^3], E_{RHb}[rad]
R is the linear axis and H is the rotary axis: E_{RH0}[mm], E_{RH1}[mm/rad], E_{RH2}[mm/rad^2], E_{RH3}[mm/rad^3], E_{RHb}[mm]

Table 4-3. Calibration results for 13-error model. It estimates 13 error parameters.

Error definition	Symbol [unit]	Value
Out-of-squareness angle of the B-axis relative to the Z-axis	E_{A0B} [rad]	-0.000040
Out-of-squareness angle of the B-axis relative to the X-axis	E_{C0B} [rad]	-0.000001
Offsets between the B and C axes	E_{X0C} [mm]	-0.095600
Out-of-squareness of the C-axis relative to the B-axis	E_{A0C} [rad]	-0.000012
Out-of-squareness of the C-axis relative to the X-axis	E_{B0C} [rad]	0.000011
Out-of-squareness of the Z-axis relative to the X-axis	E_{B0Z} [rad]	-0.000010
Out-of-squareness of the Y-axis relative to the Z-axis	E_{A0Y} [rad]	-0.000038
Out-of-squareness of the Y-axis relative to the X-axis	E_{C0Y} [rad]	0.000015
Offset of the spindle relative to the C-axis in Y	E_{Y0S} [mm]	0.029300
Offset of the spindle relative to the B-axis in X	E_{X0S} [mm]	-0.100000
Positioning linear error of the X-axis	E_{XX1} [mm/mm]	-0.000017
Positioning linear error of the Y-axis	E_{YY1} [mm/mm]	-0.000023
Positioning linear error of the Z-axis	E_{ZZ1} [mm/mm]	-0.000032

The results before and after compensation are also compared by inspecting the radial residuals of a least squares sphere fitted to the ball-bar data. The size error (isotropic effect) is the deviation between the radii of fitted sphere and that of the nominal trajectory while the form error is defined as the residuals. Figure 4.14 shows the errors of size and form before and after applying the compensation for forward and backward movements. The reference sphere is also shown. The results are listed in Table 4-4. The compensated machine tool has size errors larger than the form errors. The radius of the fitted sphere before compensation was 19.3 µm bigger than the reference sphere. However, after applying the error compensation technique and using the 13- and 84–error models, the radii of the fitted spheres respectively became 3.8 µm and 2.6 µm bigger than the reference sphere. The standard deviation of the residuals was changed from 4.1 before compensation to 1.1 and 0.7 after compensation using the 13- and 84-error model, respectively.

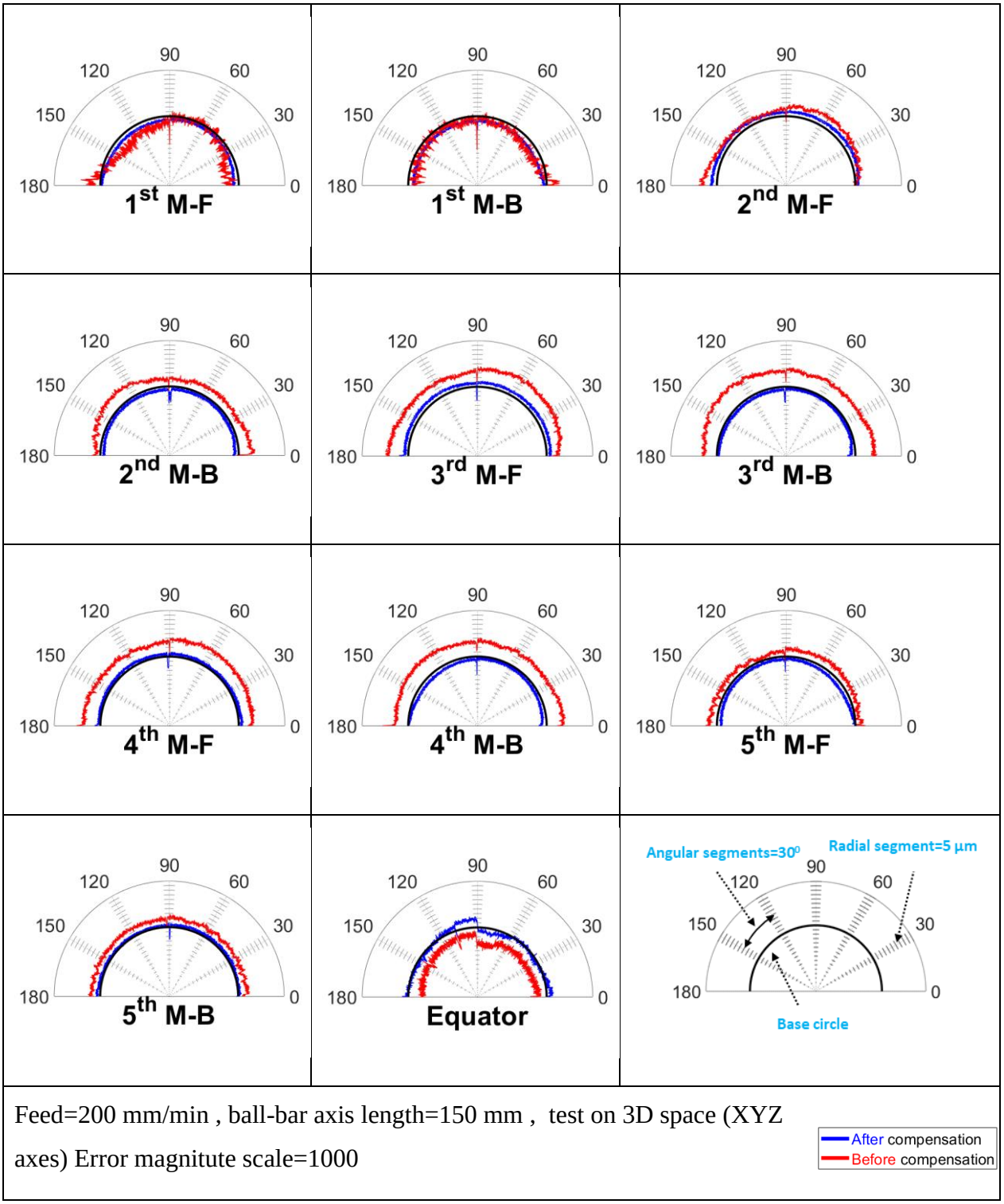

Figure 4.12. Projection of volumetric Cartesian error on the ball-bar axis direction before compensation (red) and after compensation through using 3D grid error compensation from the 13-error model (blue).

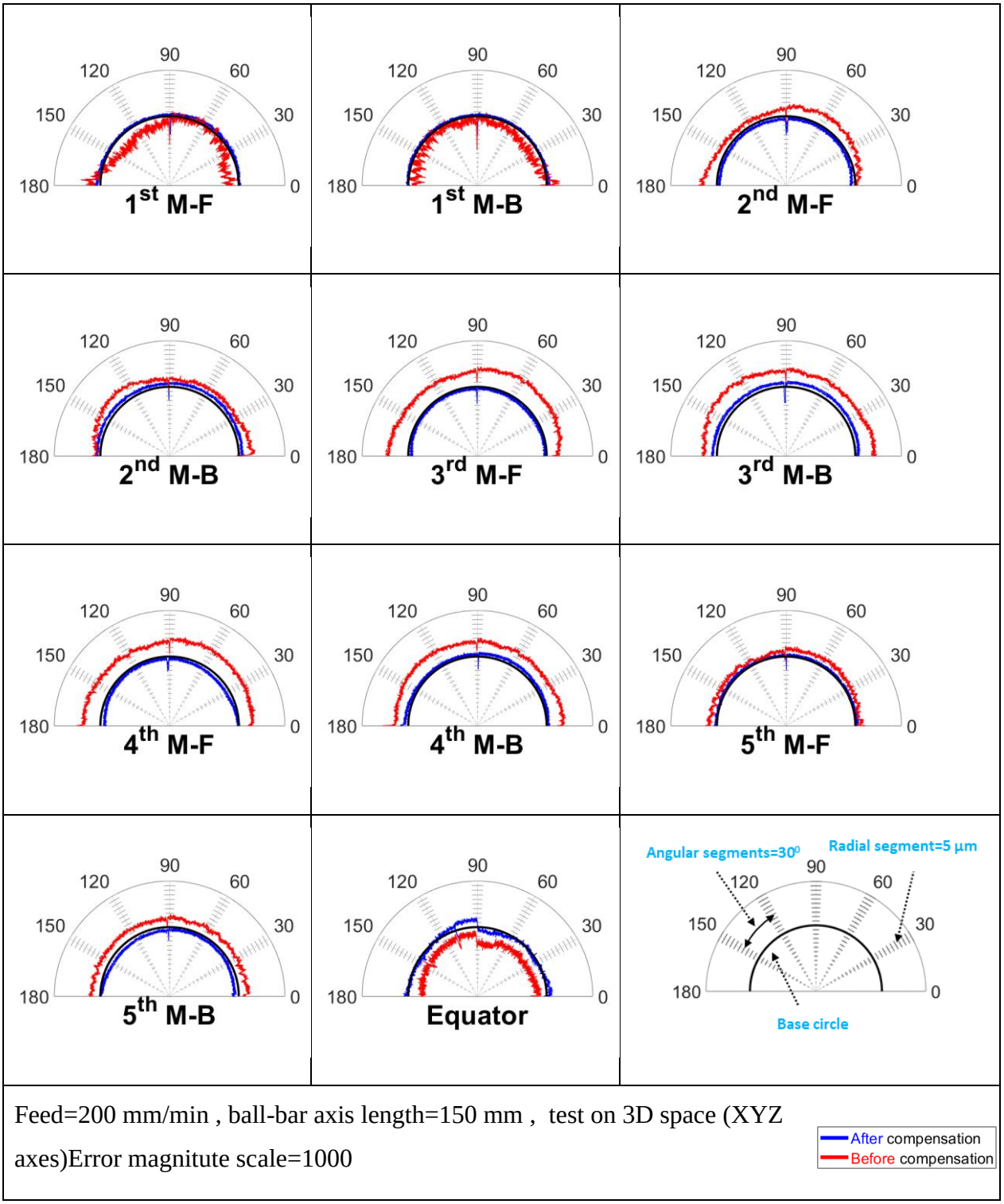

Figure 4.13. Projection of volumetric Cartesian error on the ball-bar axis direction before compensation (red) and after compensation through using 3D grid error compensation from the 84-error model (blue).

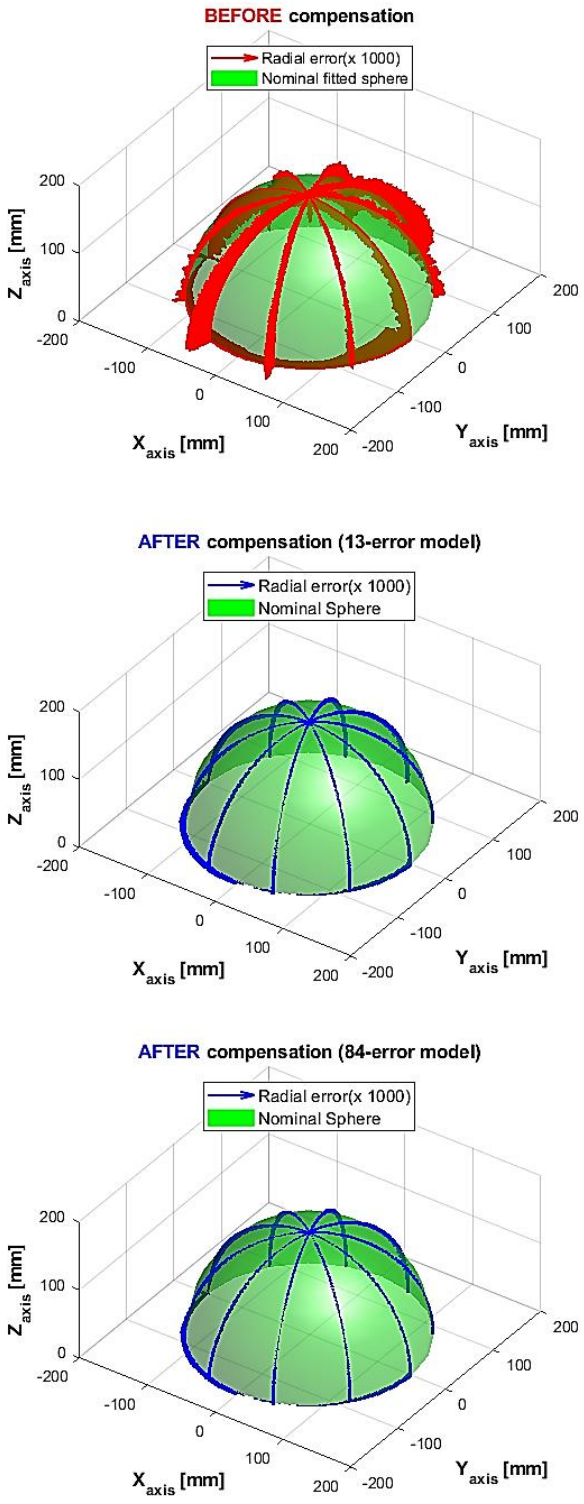

Figure 4.14. Projected volumetric error (radial error) before and after the error compensation for bi-directional travels.

Table 4-4. The calculations regarding the size and form errors before and after applying the error compensation.

Category	Calculations	Before compensation	After compensation using 13-error model	After compensation using 84-error model
Form error	$\max(\text{residuals}) - \min(\text{residuals})$	14.1	1.7	1.3
Form error	$\text{std}(\text{residuals})$	4.1	1.1	0.7
Size error	$\text{radius}_{\text{fitted}} - \text{radius}_{\text{nominal}}$	19.3	3.8	2.6

4.8 Conclusion

3D compensation table were generated from an indirectly estimated ISO-230-1:2012 machine tool error parameters, and the forward kinematic model, to compensate the Cartesian volumetric error of a five axis machine tool in 3-axis operation mode. The effect of the number of nodes, the dimension of the table was studied in order to find the minimal mesh grid dimension necessary to achieve a given compensation precision. Two machine error models were calibrated using the SAMBA method, one model includes inter-axis errors and numerous intra-axis errors as 84 error polynomial coefficients and the other models includes only the inter-axis errors and linear axes scale factors with 13 error parameters. The errors of the 13-error model, as far as the linear axes are concerned, could be compensated with an eight node grid which is coherent with the linear nature of these error parameters such as out-of-squarenesses and linear axes linear positioning errors. As for the 84-error model, the optimum dimension of the table depends on the actual error parameters values. For the tested machine a 19x19x19 for 6859 nodes tables was needed to achieve the preset threshold of 0.1 micrometer if the machine had no other errors than the estimated ones. To verify the efficiency of the generated tables, a validation test consisting in a 3D ball-bar test was used. The path best fit sphere radius deviation from the nominal sphere (size error) was reduced from 19.3 µm, before compensation, down to 3.8 and 2.6 µm after compensation for the 13- and 84-error model, respectively. The standard deviations of the residuals (form error) were reduced from 4.1 µm, before error compensation, down to 1.1 and 0.7 µm after error compensation for the 13- and 84-error models, respectively. The discrepancy between the maximum and minimum radial residuals (form error) were reduced from 14.1 µm before compensation, down to 1.7 and 1.3 µm after error compensation for the 13- and 84-error models, respectively. The machine tool showed

significant scale errors which were modeled by the two error models and compensated. The experimental average effectiveness of the 3D grid error compensation table was over 82%.

4.9 Acknowledgement

The authors would like to thank the valuable support of CNC machine technician, Vincent Mayer during the experimental tests. This research was supported by Natural Sciences and Engineering Research Council of Canada (NSERC) under the CANRIMT Strategic Research Network Grant NETGP 479639-15.

4.10 References

AG, S. (2010). Function description VCS (Volumetric Compensation System).

Bourke, P. (1999). Nearest neighbour weighted interpolation.

Controller, F. Series 30i/Model A.

Controller, S. SINUMERIK 840D.

Creamer, J., Bristow, D. A., & Landers, R. G. (2017). Selection of limited and constrained compensation tables for five-axis machine tools. *The International Journal of Advanced Manufacturing Technology, 92*(1-4), 1315-1327. doi:10.1007/s00170-017-0230-4

Creamer, J., Sammons, P. M., Bristow, D. A., Landers, R. G., Freeman, P. L., & Easley, S. J. (2016). Table-Based Volumetric Error Compensation of Large Five-Axis Machine Tools. *Journal of Manufacturing Science and Engineering, 139*(2). doi:10.1115/1.4034399

Cui, G., Lu, Y., Li, J., Gao, D., & Yao, Y. (2012). Geometric error compensation software system for CNC machine tools based on NC program reconstructing. *The International Journal of Advanced Manufacturing Technology, 63*(1-4), 169-180. doi:10.1007/s00170-011-3895-0

Eung-Suk, L., Suk-Hwan, S., & Jin-Wook, S. (1998). A Comprehensive Method for Calibration of Volumetric Positioning Accuracy of CNC-Machines. *Advanced Manufacturing Technology, 14*, 43-49.

Givi, M., & Mayer, J. R. R. (2014). Volumetric error formulation and mismatch test for five-axis CNC machine compensation using differential kinematics and ephemeral G-code. *The International Journal of Advanced Manufacturing Technology, 77*(9-12), 1645-1653. doi:10.1007/s00170-014-6558-0

ISO-16907. (2015). Machine Tools-Numerical Compensation of Geometric Errors, ISO/TR 16907,".

ISO 230-1. (2012). *Test code for machine tools-Part1: Geometric accuracy of machines operating under no-load or quassi-static conditions*.

Khan, A. W., & Chen, W. (2010). A methodology for systematic geometric error compensation in five-axis machine tools. *The International Journal of Advanced Manufacturing Technology, 53*(5-8), 615-628. doi:10.1007/s00170-010-2848-3

Koliskor, A. (1971). Compensating for automatic-cycle machining errors. *Machines and Tooling, 41*, 1-14.

Lei, W. T., & Hsu, Y. Y. (2003). Accuracy enhancement of five-axis CNC machines through real-time error compensation. *International Journal of Machine Tools and Manufacture, 43*(9), 871-877. doi:10.1016/s0890-6955(03)00089-0

Mahbubur, R. M., Heikkala, J., Lappalainen, K., & Karjalainen, J. A. (1997). Positioning Accuracy improvement in five-axis milling by post processing. *International Journal of Machine Tools and Manufacture, 37*, 223-236.

Mayer, J. R. R. (2012). Five-axis machine tool calibration by probing a scale enriched reconfigurable uncalibrated master balls artefact. *CIRP Annals, 61*(1), 515-518. doi:10.1016/j.cirp.2012.03.022

McHichi, N. A., & Mayer, J. R. R. (2014). Axis Location Errors and Error Motions Calibration for a Five-axis Machine Tool Using the SAMBA Method. *Procedia CIRP, 14*, 305-310. doi:10.1016/j.procir.2014.03.088

Mir, Y. A., Mayer, J. R. R., & Fortin, C. (2005). Tool path error prediction of a five-axis machine tool with geometric errors. *Proceedings of the Institution of Mechanical Engineers, Part B: Journal of Engineering Manufacture, 216*(5), 697-712. doi:10.1243/0954405021520391

Rahman, M. M., & Mayer, J. R. R. (2015). Five axis machine tool volumetric error prediction through an indirect estimation of intra- and inter-axis error parameters by probing facets on a scale enriched uncalibrated indigenous artefact. *Precision Engineering, 40*, 94-105. doi:10.1016/j.precisioneng.2014.10.010

Schultschik, R. (1977). The Components of the Volumetric Accuracy. *CIRP Annals, 25*, 223-228.

Vahebi Nojedeh, M., Habibi, M., & Arezoo, B. (2011). Tool path accuracy enhancement through geometrical error compensation. *International Journal of Machine Tools and Manufacture, 51*(6), 471-482. doi:DOI: 10.1016/j.ijmachtools.2011.02.005

Xiang, S., & Altintas, Y. (2016). Modeling and compensation of volumetric errors for five-axis machine tools. *International Journal of Machine Tools and Manufacture, 101*, 65-78. doi:https://doi.org/10.1016/j.ijmachtools.2015.11.006

Zhu, S., Ding, G., Qin, S., Lei, J., Zhuang, L., & Yan, K. (2012). Integrated geometric error modeling, identification and compensation of CNC machine tools. *International Journal of Machine Tools and Manufacture, 52*(1), 24-29. doi:10.1016/j.ijmachtools.2011.08.011

CHAPTER 5 ARTICLE 2: FIVE-AXIS MACHINE TOOL VOLUMETRIC AND GEOMETRIC ERROR REDUCTION BY INDIRECT GEOMETRIC CALIBRATION AND LOOKUP TABLES

Sareh M. Esmaeili [a,*], J.R.R. Mayer [a], Mark P. Sanders [b], J. Philipp Dahlem [b], Kanglin Xing [a]

[a] *Department of Mechanical Q1 Engineering, École Polytechnique (Montréal), P.O. Box 6079, Station Downtown, Montréal, QC H3C3A7, Canada*

[b] *Laboratory for Machine Tools and Production Engineering (WZL), RWTH Aachen University, Aachen, Germany*

[*] Corresponding author. *Email: sareh.esmaeili-marzdashti@polymtl.ca [*]Tel.: +15143404711 Ext.: 2292, [*]Fax: (514) 340-5170*

NOTE: Based on the paper published in the Journal of Manufacturing Science and Engineering: volume 143, pages 1-14(2021), doi:10.1115/1.4049846

5.1 Abstract

Modern CNC machine tools provide lookup tables to enhance the machine tool's precision but the generation of table entries can be a demanding task. In this paper, the coefficients of the 25 cubic polynomial functions used to generate the LUTs entries for a five-axis machine tool are obtained by solving a linear system incorporating a Vandermonde expansion of the nominal control jacobian. The necessary volumetric errors within the working volume are predicted from machine's geometric errors estimated by the indirect error identification method based on the on-machine touch probing measurement of a reconfigurable uncalibrated master ball artefact (RUMBA). The proposed scheme is applied to a small Mitsubishi M730 CNC machine. Two different error models are used for modeling the erroneous machine tool, one estimating mainly inter-axis errors and the other including numerous intra-axis errors. The table-based compensation is validated through additional on-machine measurements. Experimental tests demonstrate a significant reduction in volumetric errors and in the effective machine error parameters. The LUTs reduce most of the dominant machine error parameters. It is concluded that although being effective in correcting some geometric errors, the generated LUTs cannot compensate some axis misalignments such as EB(OX)A and EB(OX)Z. The Root Mean Square of the translational volumetric errors are

improved from 87.3, 75.4 and 71.5 µm down to 24.8, 18.8 and 22.1 µm in the X, Y and Z directions, respectively.

Keywords: Lookup Table, Five-axis machine tool, Table-based error compensation, Geometric error, Volumetric error

5.2 Introduction

The need for producing geometrically complex parts meeting tight tolerances on one hand and increasing the productivity on the other hand brings the necessity to maintain the accuracy of the machine tool while limiting machine downtime for mechanical realignment of its various components. The tool positioning errors mostly result from inter- and intra-axis errors, thermal errors and force-induced errors (Srivastava et al., 1995). Considering the errors that are at least partly repeatable, their calibration and compensation using a table-based error compensation scheme is potentially cost-effective when compared to the downtime resulting from mechanical maintenance and overhaul operations or producing scrap parts due to out-of-tolerance part features.

Numerical compensation, used to improve machine accuracy requires machine calibration and introducing the error correction in the machine controller. Machine calibration approaches have been categorized into direct and indirect methods (Sartori & Zhang, 1995). The direct methods use instruments and setups that either measure the resulting volumetric errors, i.e. the inaccurate position and orientation of the tool relative to the workpiece, or measure the causal geometric error parameters individually. The indirect methods measure the combined effects, as volumetric errors, of more than one causal error parameter and estimate their respective values through mathematical models (Schwenke et al., 2008). Indirect methods facilitate machine tool calibration (Abbaszadeh-Mir et al., 2002; Esmaeili & Mayer, 2020; Lei & Hsu, 2003a; Montavon, Dahlem, & Schmitt, March 2019; Suh, Lee, & Sohn, 1999) by relaxing many instrument related constraints. Such models often rely on homogenous transformation matrices (HTM) which are a convenient mathematical tool to build the error model and have been widely used in indirect machine tool calibration and also for geometric error compensation (Lei & Hsu, 2003a; Suh et al., 1999). In such model, the geometric errors can be limited to the relative axes location (Abbaszadeh-Mir et al., 2002) or can also incorporate general shape functions, such as polynomials as in (Y A. Mir, Mayer, & Fortin, 2002), to model the intra-axis errors of each axis.

Error compensation has been widely studied (J. G. Li, Zhao, Yao, & Liu, 2007; Ramesh, Mannan, & Poo, 2000b; Shih-Ming Wang, Yu, & Liao, 2005; Xi, Poo, Hong, & Huo, 2010; H. Zhang, Yang, Zhang, Shen, & Wang, 2010). Compensation schemes were implemented either through off-line modifications of NC codes (M. Rahman, Heikkala, & Lappalainen, 2000) or real-time error compensation (Yuan & Ni, 1998). Ji-Hun et al. (Jung, Choi, & Lee, 2006) modified G-code program in a three-axis machine tool to compensate linear and circular interpolation movements. Srivastava et al. (Srivastava et al., 1995) enriched the HTM model with time-varying terms in order to also model thermal errors to compensate the tool path. Wang et al. (Shih-Ming Wang, Liu, & Kang, 2002) proposed an automatic volumetric error compensation wherein the error sources resulted from static or quasi-static errors. The mathematical error model for the three-axis machine tool uses shape functions and considers the machine's non-rigid body behavior. The compensation is implemented using a modified G-code. Khan et al. (Khan & Chen, 2010) proposed a case study of volumetric error compensation in a five-axis machine tool using the nominal tool position from CAD/CAM software and the actual tool position through the kinematic chain of the erroneous machine tool. The deviations between the nominal and actual tool positions were then applied to the tool path by modifying the NC program.

Most research for compensating machine tool error has focused on G-code modifications (Givi & Mayer, 2014; Koliskor, 1971; R. M. Mahbubur et al., 1997). However, volumetric errors lookup tables (LUT) have been available on CNCs, for over a decade, by which there is no need to modify each G-code separately for compensation purposes. Published research in this area is recent (J. Creamer et al., 2017; Jennifer Creamer et al., 2016, November 15-21, 2013, San Diego, California, USA; M. Esmaeili & Mayer, 2020). Various LUTs are embedded in CNCs for pitch, straightness, rotational, squareness and backlash error compensation ("Fanuc Controller," Series 30i/Model A; "Siemens Controller," SINUMERIK 840D/840Di/810D Extended Functions). Some controllers offer more complex user configurable tables ("Siemens Controller," SINUMERIK 840D/840Di/810D Extended Functions). Creamer et al. (Jennifer Creamer et al., 2016) used a laser tracker to measure the volumetric errors of a five-axis machine tool at randomized location in the machine workspace. Two models are then produced. One, called 6DoF, uses a homogenous transformation matrix based approach where each geometric error matrix is modeled by Chebyshev polynomials of each axis command. The other model, called Axis Perturbation (AP), has a form much closer to the proposed LUT scheme. It generates, for each axis, a command correction that

should bring the actual machine to the same position as the nominal machine. Each axis correction is the sum of five corrections each a univariate Chebyshev polynomial of one of the five-axis nominal command. The 6DoF model can also be used to generate the 25 Chebyshev polynomials that are then discretized to populate the compensation LUTs, available in the Siemens controller (Sinumerik 840D), which operate much like the AP model. The AP model is directly discretized to populate the tables. The models' coefficients are optimized to correct the laser tracker indications as pseudo-measurements obtained using the estimated models. They validated their compensation approach by re-measuring the machine's volumetric errors in positioning mode with the laser tracker after compensation. Creamer et al. (J. Creamer et al., 2017) did another study to select a limited number of compensation tables because most of the controllers are not equipped with 25 compensation tables as their previous work required. They applied an artificial intelligence based (genetic algorithm GA) methodology to select an optimal set of tables and compared them with a full set of compensation tables. The compensation tables achieved by GA methodology include eleven tables, five fixed base tables of pitch error compensation plus six others selected by GA. The GA compensation tables have a respective mean and maximum volumetric error 8 μm and 11 μm larger than a full set of compensation tables.

While the previous works (J. Creamer et al., 2017; Jennifer Creamer et al., 2016, November 15-21, 2013, San Diego, California, USA) in generating the LUTs are validated when the machine is in machining mode, this paper presents a compensation LUTs generation process validated when the machine tool is in measurement mode. Also, two alternate error models, differing only in the number of modeled intra-axis errors, are considered. The first model uses the minimum complete ISO axis alignment (inter-axis) error parameters and the second uses the ISO error motion (intra-axis) parameters. The process of generating the table and optimizing the table coefficients uses the predicted volumetric error, as opposed to directly measured ones, calculated from the estimated machine geometric error parameters, for the sets of commands located at a 5D mesh grid of the five axis commands. Univariate ordinary polynomials are used as table functions. Constructing the Jacobian of the sensitivity of the required volumetric corrections to the LUT function coefficients in order to directly calculate the coefficients is another novelty of this paper. Finally, the criteria for the effectiveness of the compensation are not only the remaining volumetric errors but also the actual geometric errors before compensation and their effective values after compensation when the machine is used in measurement mode.

The paper is organized as follows; in section 5.3, the two error model used for calibration are introduced. In section 5.6, the table-based volumetric error compensation is explained. In section 5.7, the error compensation verification in measurement and machining modes are presented. In section 5.8 details the experimental validation procedure including the calibration and compensation tests on a five-axis machine tool. The results and discussions are presented in section 5.9 followed by conclusion in section 5.10.

5.3 Machine tool modeling and error models

The target machine tool used in this work has an open serial kinematic chain made of two branches. It is a five-axis compact-sized CNC milling machine tool with a Mitsubishi M730 CNC controller and Mitsubishi servomotors. It has no linear encoders. The topology of the kinematic chain of the machine tool is described as wCAYFXZSt, as illustrated in Figure 5.1, in which C and A are the rotary axes, X, Y and Z are the linear axes and the w, S and t symbols stand for the workpiece, spindle and tool, respectively. The machine (or foundation) frame, F, is nominally located at the intersection of the A- and C-axis.

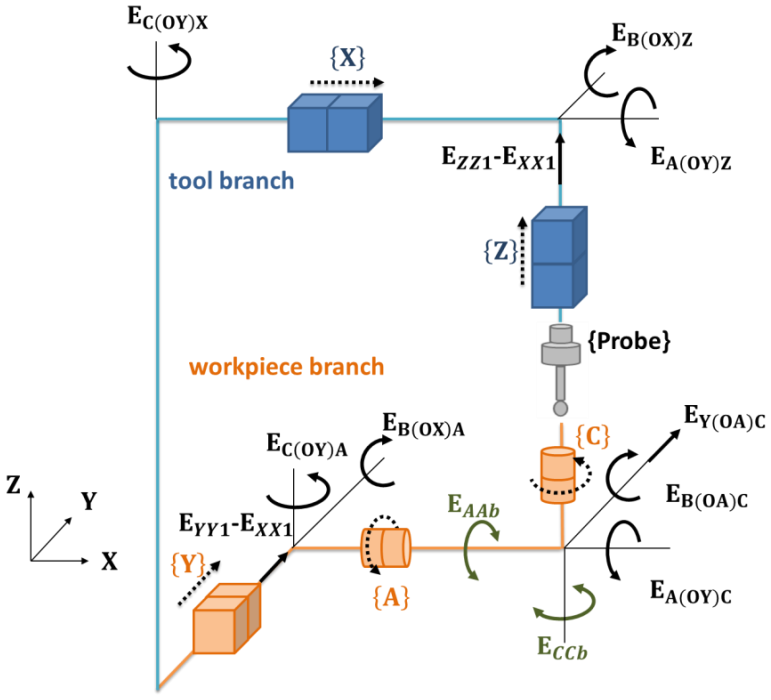

Figure 5.1 Schematic of the machine tool kinematics with the 12-error model parameters.

The kinematic chain of the nominal machine which generates the relative movement of the tool relative to the workpiece is mathematically modeled as follows:

$$ {}^{w_n}\boldsymbol{T}_{t_n} = \left({}^{F}\boldsymbol{T}_{Y}\,{}^{Y}\boldsymbol{T}_{A}\,{}^{A}\boldsymbol{T}_{C}\,{}^{C}\boldsymbol{T}_{w_n} \right)^{-1} \left({}^{F}\boldsymbol{T}_{X}\,{}^{X}\boldsymbol{T}_{Z}\,{}^{Z}\boldsymbol{T}_{S}\,{}^{S}\boldsymbol{T}_{t_n} \right) \tag{18} $$

where *T* stands for a 4×4 homogenous transformation matrix (HTM), embedding the translation and the angular movement of one component relative to the previous component.

A machine tool has intra-axis and inter-axis errors. Intra-axis error, also called error motion, motion errors or position dependent geometric error parameters, are the imperfect motion of each mechanical axis whereas inter-axis, also called axis location error or position independent geometric error parameters, are the imperfect relative location of the mechanical axes (Soichi Ibaraki & Knapp, 2012). A five-axis machine tool, without considering the spindle, has five sets of six intra-axis errors for a total of 30 intra-axis errors, and eight inter-axis errors to represent the errors in relative location of its five axes. This yields a total of 38 errors. The intra-axis errors vary with their respective axis position and so a number of error function coefficients are needed to model each intra-axis error. Now considering the spindle, one could add six intra-axis errors, up to four inter-axis errors and a Z offset for the tool attachment plane. However, in this work only the two lateral offsets (x and y) inter-axis errors of the spindle are included due to the measurement method limitations.

5.4 12-error model

One of the two error model studied in this paper is the 12-error model consisting of the eight necessary and sufficient axis location errors (Abbaszadeh-Mir et al., 2002; Zhu et al., 2012), two backlashes of the rotary axes and, since no length reference is measured, two relative gain errors of the linear axes. These 12 errors are listed in Table 5-1 and shown in Figure 5.1.

Table 5-1. The error parameters of the 12-error model.

Error definition	Symbol[1]
Out-of-squareness angle of the A-axis relative to the X-axis	$E_{B(OX)A}$
Out-of-squareness angle of the A-axis relative to the Y-axis	$E_{C(OY)A}$
Offset between the C and A axes	$E_{Y(OA)C}$
Out-of-squareness of the C-axis relative to the Y-axis	$E_{A(OY)C}$
Out-of-squareness of the C-axis relative to the A-axis	$E_{B(OA)C}$
Out-of-squareness of the X-axis relative to the Y-axis	$E_{C(OY)X}$
Out-of-squareness of the Z-axis relative to the Y-axis	$E_{A(OY)Z}$
Out-of-squareness of the Z-axis relative to the X-axis	$E_{B(OX)Z}$
Backlash of the A-axis	E_{AAb}
Backlash of the C-axis	E_{CCb}
Relative positioning linear errors of the X and Y axes	E_{YY1}- E_{XX1}
Relative positioning linear errors of the X and Z axes	E_{ZZ1}- E_{XX1}

1-$E_{U(0V)W}$ where U is the nature of the error, V is the datum axis and W is the axis which has the error.

5.5 81-error model

The 81-error model uses ordinary cubic polynomials to model intra-axis error which were found by Slamani et al. (M. Slamani, Mayer, & Cloutier, 2011) to provide good representativity for the machines they tested. The inter-axis errors are not added explicitly to this model because they can be modeled by the coefficients of the polynomials of some of the intra-axis errors (Y A. Mir et al., 2002). As an example, suppose the straightness error of the Y-axis in the X direction is modeled as,

$$E_{XY} = E_{XY0} + E_{XY1}y + E_{XY2}y^2 + E_{XY3}y^3 + \dot{b}_Y E_{XYb} \tag{19}$$

where E_{XY0}, E_{XY1}, E_{XY2} and E_{XY3} are the coefficients for the zero to third degree terms of the polynomials, respectively and E_{XYb} is the hysteretic effect coefficient. The first degree term (and the third degree term due to some coupling occurring in ordinary polynomials) can model the out-of-squareness between the X- and Y-axis, which is an inter-axis error. Modeling all 30 error parameters with a third-degree polynomial defines 120 error coefficients which are listed in Table 5-2. Adding the positioning backlashes to the model, the number of variables is increased to 125. However, there are unnecessary and also unobservable coefficients. In order to have reliable estimates, based on the condition number and rank of the Jacobian matrix, the number of independent error coefficients must be reduced to 81. A procedure is applied to eliminate

redundancies and confounded coefficients by removing some zero degree and first degree polynomial coefficients while maintaining the rank of the estimation Jacobian (M. M. Rahman & Mayer, 2015). Table 5-2 shows the retained error coefficients in black and the discarded ones in red. After considering the redundancies, only two backlashes, EAAb and ECCb, can be detected by this measurement strategy.

Table 5-2. All possible error coefficients for a five-axis machine tool. The 81-error model variable are shown in black color.

			X-axis												
E_{XX}	E_{YX}	E_{ZX}	E_{AX}	E_{BX}	E_{CX}	E_{XY}	E_{YY}	E_{ZY}	E_{AY}	E_{BY}	E_{CY}	E_{XZ}	E_{YZ}	E_{ZZ}
E_{XX0}	E_{YX0}	E_{ZX0}	E_{AX0}	E_{BX0}	E_{CX0}	E_{XY0}	E_{YY0}	E_{ZY0}	E_{AY0}	E_{BY0}	E_{CY0}	E_{XZ0}	E_{YZ0}	E_{ZZ0}
E_{XX1}	E_{YX1}	E_{ZX1}	E_{AX1}	E_{BX1}	E_{CX1}	E_{XY1}	E_{YY1}	E_{ZY1}	E_{AY1}	E_{BY1}	E_{CY1}	E_{XZ1}	E_{YZ1}	E_{ZZ1}
E_{XX2}	E_{YX2}	E_{ZX2}	E_{AX2}	E_{BX2}	E_{CX2}	E_{XY2}	E_{YY2}	E_{ZY2}	E_{AY2}	E_{BY2}	E_{CY2}	E_{XZ2}	E_{YZ2}	E_{ZZ2}
E_{XX3}	E_{YX3}	E_{ZX3}	E_{AX3}	E_{BX3}	E_{CX3}	E_{XY3}	E_{YY3}	E_{ZY3}	E_{AY3}	E_{BY3}	E_{CY3}	E_{XZ3}	E_{YZ3}	E_{ZZ3}
E_{XXb}	E_{YXb}	E_{ZXb}	E_{AXb}	E_{BXb}	E_{CXb}	E_{XYb}	E_{YYb}	E_{ZYb}	E_{AYb}	E_{BYb}	E_{CYb}	E_{XZb}	E_{YZb}	E_{ZZb}

Z-axis			A-axis						C-axis					
E_{AZ}	E_{BZ}	E_{CZ}	E_{XA}	E_{YA}	E_{ZA}	E_{AA}	E_{BA}	E_{CA}	E_{XC}	E_{YC}	E_{ZC}	E_{AC}	E_{BC}	E_{CC}
E_{AZ0}	E_{BZ0}	E_{CZ0}	E_{XA0}	E_{YA0}	E_{ZA0}	E_{AA0}	E_{BA0}	E_{CA0}	E_{XC0}	E_{YC0}	E_{ZC0}	E_{AC0}	E_{BC0}	E_{CC0}
E_{AZ1}	E_{BZ1}	E_{CZ1}	E_{XA1}	E_{YA1}	E_{ZA1}	E_{AA1}	E_{BA1}	E_{CA1}	E_{XC1}	E_{YC1}	E_{ZC1}	E_{AC1}	E_{BC1}	E_{CC1}
E_{AZ2}	E_{BZ2}	E_{CZ2}	E_{XA2}	E_{YA2}	E_{ZA2}	E_{AA2}	E_{BA2}	E_{CA2}	E_{XC2}	E_{YC2}	E_{ZC2}	E_{AC2}	E_{BC2}	E_{CC2}
E_{AZ3}	E_{BZ3}	E_{CZ3}	E_{XA3}	E_{YA3}	E_{ZA3}	E_{AA3}	E_{BA3}	E_{CA3}	E_{XC3}	E_{YC3}	E_{ZC3}	E_{AC3}	E_{BC3}	E_{CC3}
E_{AZb}	E_{BZb}	E_{CZb}	E_{XAb}	E_{YAb}	E_{ZAb}	E_{AAb}	E_{Bab}	E_{CAb}	E_{XCb}	E_{YCb}	E_{ZCb}	E_{ACb}	E_{BCb}	E_{CCb}

The forward kinematic model of the erroneous machine tool is given by,

$$
\begin{aligned}
{}^{w_a}\boldsymbol{T}_{t_a} = & \left({}^{F}\boldsymbol{T}_{Y_0}\,{}^{Y_0}\boldsymbol{T}_{Y_0'}\,{}^{Y_0'}\boldsymbol{T}_{Y}\,{}^{Y}\boldsymbol{T}_{Y'}\,{}^{Y'}\boldsymbol{T}_{A_0}\,{}^{A_0}\boldsymbol{T}_{A_0'}\,{}^{A_0'}\boldsymbol{T}_{A}\,{}^{A}\boldsymbol{T}_{A'}\,{}^{A'}\boldsymbol{T}_{C_0}\,{}^{C_0}\boldsymbol{T}_{C_0'}\,{}^{C_0'}\boldsymbol{T}_{C}\,{}^{C}\boldsymbol{T}_{C'}\,{}^{C'}\boldsymbol{T}_{w_n}\,{}^{w_n}\boldsymbol{T}_{w_a}\right)^{-1} \\
& \left({}^{F}\boldsymbol{T}_{X_0}\,{}^{X_0}\boldsymbol{T}_{X_0'}\,{}^{X_0'}\boldsymbol{T}_{X}\,{}^{X}\boldsymbol{T}_{X'}\,{}^{X'}\boldsymbol{T}_{Z_0}\,{}^{Z_0}\boldsymbol{T}_{Z_0'}\,{}^{Z_0'}\boldsymbol{T}_{Z}\,{}^{Z}\boldsymbol{T}_{Z'}\,{}^{Z'}\boldsymbol{T}_{S}\,{}^{S}\boldsymbol{T}_{t_n}\,{}^{t_n}\boldsymbol{T}_{t_a}\right)
\end{aligned}
\tag{20}
$$

where X_0, Y_0, Z_0, A_0, C_0, stand for the nominal axis locations before movement; X_0', Y_0', Z_0', A_0' and C_0' stand for the actual axis locations, accounting for inter-axis errors, before movement; X, Y, Z, A and C show axis location after nominal movement; and X′, Y′, Z′, A′, C ′, represent the actual axis locations, accounting for intra-axis errors, after movement. S, w_n and t_n are the spindle

and the nominal locations of the workpiece and tool, respectively. The actual locations of the workpiece, and tool are w_a and t_a, respectively.

All error parameters and coefficients are estimated using the indirect measurement approach based on a reconfigurable uncalibrated master ball artefact (RUMBA) (Mayer, 2012). The estimation process, requires solving the following linearized error model:

$$E_V = (J)(E_P) \tag{21}$$

where E_V is the column matrix of raw volumetric error vectors, E_P is the column matrix of unknown error coefficients or error parameters, and some setup errors and J is the Jacobian matrix. E_P is calculated by applying the iterative Gauss-Newton method with a combination of the forward model of Eq. (2) and the following inverse model

$$E_P = (J^+)(E_V), \tag{22}$$

using a suitably updated Jacobian matrix at each iteration until convergence to a pre-defined threshold.

5.6 Table-based volumetric error compensation

Table-based compensation uses an open programming environment within the CNC with its own commands and rules sets that the machine user can exploit to generate corrections to the machine axes. The CNC uses these user instructions automatically. Data can be provided as lookup tables interpolated by the CNC in real-time and as weights. The environment does not provide any guidance as to the necessary tables, their combination, weights, entries or maximum correction values. These functionalities are separate from the specific pre-programmed black box compensation options that CNC manufacturers offer as paid licenses. The functions that combine the tables' output represent the complexity of the tables. Figure 5.2 illustrates the relationship between the basic axis and the compensation axis when generating complex tables for the compensation scheme used. The basic axis is the machine tool axis whose position is used as input to the table to interpolate its entries and produce an output. The interpolated output of the compensation table is applied to the compensation axis. The basic axis and the compensation axis may be the same or different axes. As shown, the weights for each table outputs are W_{11}, W_{21},

W_{31}… W_{55}. The weighted summation functions (∑) add together the weighted corrections for a particular axis. The bounds define maximum compensation values to avoid excessive corrections.

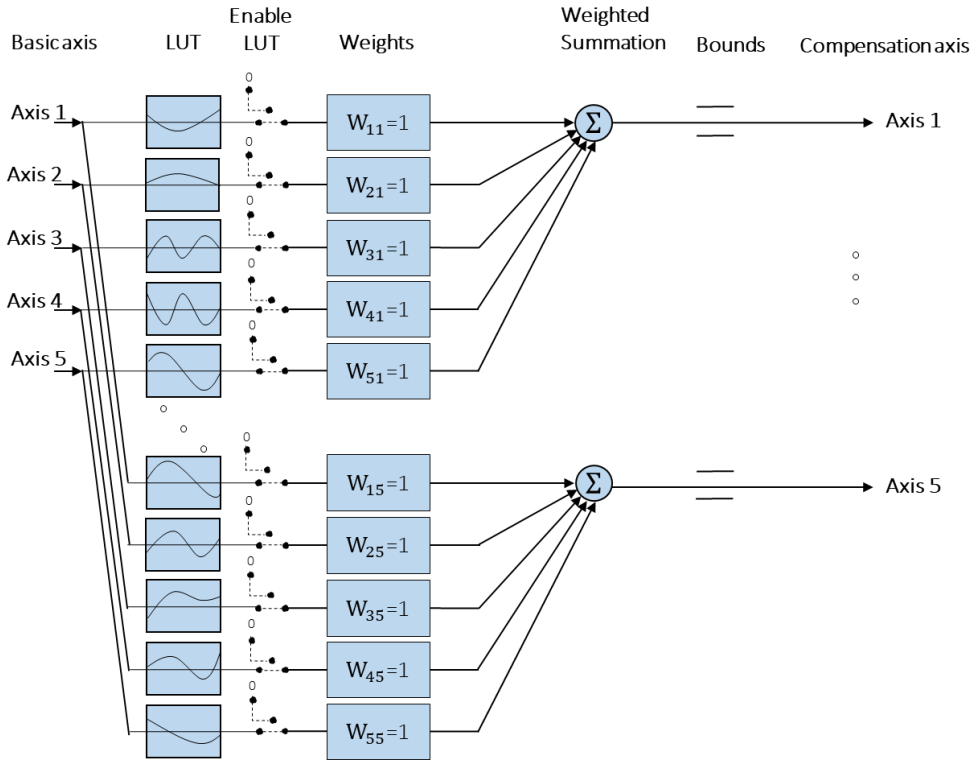

Figure 5.2. Schematic of the 25 tables compensation scheme showing the basic axes, LUTs, weights, summing operators, compensation axes corrections and their bounds.

The controller automatically corrects the axis' commands using the enabled tables' outputs as illustrated in Figure 5.3. The process of generating the table uses the machine calibration results and the associated machine error model to predict the volumetric error at the nodes of a 5D mesh grid of axis commands generated within the stroke lengths and angles of the machine tool axes. For each set of five axis commands corresponds a mesh grid node at which the associated volumetric error is calculated using Eq. (2). Then, the functions that will be used to populate the LUTs are optimised so that the compensation scheme corrections closely match the volumetric errors at the node. All weights are equal to 1 in this study.

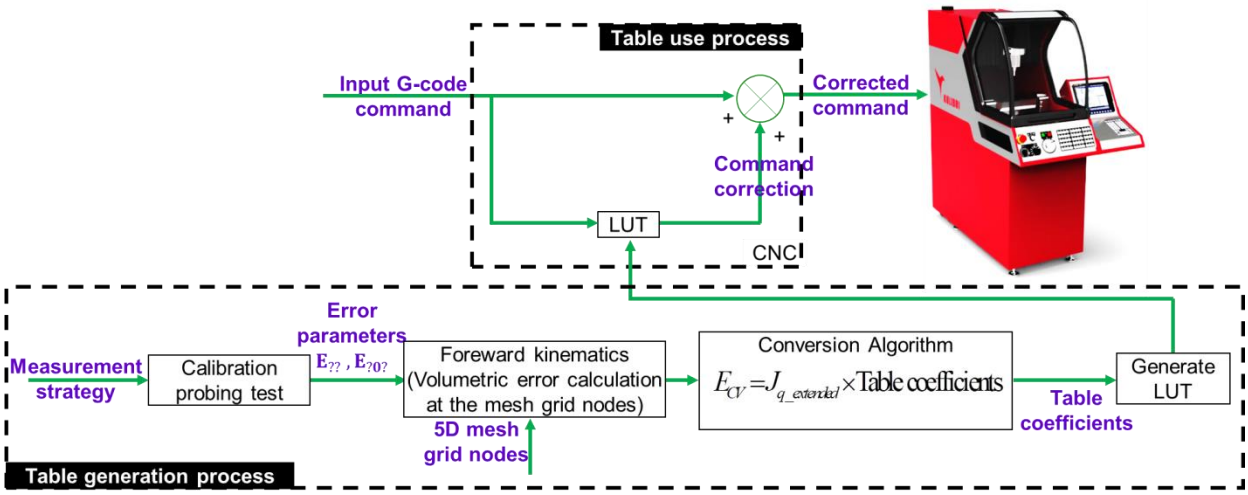

Figure 5.3. The procedure of generating and using the lookup table (LUT).

Figure 5.4 shows a series of possible compensation tables for the i^{th} compensation axis. Considering the summation characteristic of the tables, the correction value for compensation axis *i* is (Jennifer Creamer et al., 2016),

$$\Delta q_i = f_{i,x}(q_X) + f_{i,y}(q_Y) + f_{i,z}(q_Z) + f_{i,a}(q_A) + f_{i,c}(q_C) = \sum_{j=X,Y,Z,A,C} f_{i,j}(q_j) \tag{23}$$

where *i* stands for the compensation axis, Δq_i is the compensation value for the compensation axis, q_j is the nominal position command for basic axis *j* and $f_{i,j}$ are the table functions. Cubic polynomials are used here so that $f_{i,j}$ is denoted by,

$$f_{i,j}(q_j) = a_{i,j,0} + a_{i,j,1} q_j + a_{i,j,2} q_j^{\,2} + a_{i,j,3} q_j^{\,3} \tag{24}$$

where $a_{i,j,0}, a_{i,j,1}, a_{i,j,2}, a_{i,j,3}$ are the fitted function coefficients. Hence, Δq_i is fitted by the sum of five univariate polynomial functions. Note that these polynomials are likely different and serve an entire different purpose from those used to model the geometric errors of the machine tool in the 81-error model as presented in section 5.5.

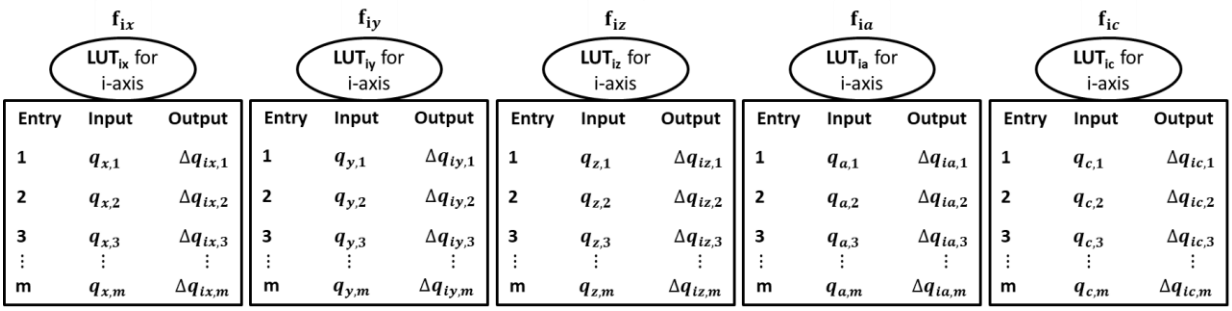

Figure 5.4. A series of the possible compensation tables for the ith axis.

According to Givi and Mayer (Givi & Mayer, 2014), in order to bring the tool tip to the desired location, the required tool tip volumetric error compensation in a five-axis machine tool is the reverse of the tool tip volumetric error, assuming small volumetric errors. Again assuming small errors, there is a linear relationship between the volumetric error compensation value at the tool tip, corresponding to a set of nominal axis position or command set (q_X, q_Y, q_Z, q_A, q_C), and the required axis command corrections (Δq_X, Δq_Y, Δq_Z, Δq_A, Δq_C) as,

$$E_{CV} = J_q \left[\Delta q_X \ \Delta q_Y \ \Delta q_Z \ \Delta q_A \ \Delta q_C\right]^T \tag{25}$$

where E_{CV} is the volumetric error compensation defined as a twist of three translational and three rotational errors at the tool tip relative to the workpiece,

$$E_{CV} = \left[E_{XCV} \ E_{YCV} \ E_{ZCV} \ E_{ACV} \ E_{BCV} \ E_{CCV}\right]^T \tag{26}$$

and J_q, a 6×5 matrix, is the control Jacobian of the machine as the set of partial derivatives of the volumetric errors (or their required compensation value) to the axis commands (or their correction values) as,

$$J_q = \begin{bmatrix} \frac{\partial E_{XCV}}{\partial q_X} & \frac{\partial E_{XCV}}{\partial q_Y} & \frac{\partial E_{XCV}}{\partial q_Z} & \frac{\partial E_{XCV}}{\partial q_A} & \frac{\partial E_{XCV}}{\partial q_C} \\ \frac{\partial E_{YCV}}{\partial q_X} & \frac{\partial E_{YCV}}{\partial q_Y} & \frac{\partial E_{YCV}}{\partial q_Z} & \frac{\partial E_{YCV}}{\partial q_A} & \frac{\partial E_{YCV}}{\partial q_C} \\ \frac{\partial E_{ZCV}}{\partial q_X} & \frac{\partial E_{ZCV}}{\partial q_Y} & \frac{\partial E_{ZCV}}{\partial q_Z} & \frac{\partial E_{ZCV}}{\partial q_A} & \frac{\partial E_{ZCV}}{\partial q_C} \\ \frac{\partial E_{ACV}}{\partial q_X} & \frac{\partial E_{ACV}}{\partial q_Y} & \frac{\partial E_{ACV}}{\partial q_Z} & \frac{\partial E_{ACV}}{\partial q_A} & \frac{\partial E_{ACV}}{\partial q_C} \\ \frac{\partial E_{BCV}}{\partial q_X} & \frac{\partial E_{BCV}}{\partial q_Y} & \frac{\partial E_{BCV}}{\partial q_Z} & \frac{\partial E_{BCV}}{\partial q_A} & \frac{\partial E_{BCV}}{\partial q_C} \\ \frac{\partial E_{CCV}}{\partial q_X} & \frac{\partial E_{CCV}}{\partial q_Y} & \frac{\partial E_{CCV}}{\partial q_Z} & \frac{\partial E_{CCV}}{\partial q_A} & \frac{\partial E_{CCV}}{\partial q_C} \end{bmatrix} \tag{27}$$

By substituting the command corrections with their polynomial representation given by Eq. (13), an extended Jacobian version of Eq. (15) can be generated using a Vandermonde expansion. Using third degree polynomials fitness functions, the extended Jacobian with a size of (6×100) is denoted by,

$$J_{q\_extended} = \begin{pmatrix} \frac{\partial E_{XCV}}{\partial a_{XX0}} & \cdots & \frac{\partial E_{XCV}}{\partial a_{CC3}} \\ \vdots & \ddots & \vdots \\ \frac{\partial E_{CVC}}{\partial a_{CX0}} & \cdots & \frac{\partial E_{CCV}}{\partial a_{CC3}} \end{pmatrix}_{[6\times100]} \tag{28}$$

which is then used as follows,

$$E_{CV} = J_{q\_extended} \left[a_{XX0}\ a_{XX1}\ a_{XX2}\ a_{XX3}\ a_{XY0} \cdots a_{CB3}\ a_{CC0}\ a_{CC1}\ a_{CC2}\ a_{CC3} \right]^T_{[100\times1]} \tag{29}$$

.

The table function coefficient column matrix has 100 elements: four coefficients per function, five functions per compensation axis (one for each basic axis) and five compensation axes. A solution for the unknown fitted function coefficients is obtained by pseudo inversing the Jacobian matrix within an iterative process to obtain convergence to a numerically precise solution

$$\left[a_{XX0}\ a_{XX1}\ a_{XX2}\ \cdots\ a_{CC1}\ a_{CC2}\ a_{CC3}\right]^T = J^+_{q\_extended} E_{CV}\ . \tag{30}$$

The tables are then generated by discretizing the table functions over the stroke lengths of the machine axes with a pre-determined number of entries for the tables, in this case 50 entries per table is used.

When a given axis command does not match a node of a compensation table, the table is linearly interpolated. Suppose a basic command q_j for axis *j* is located between $q_{j,l}$ and $q_{j,l+1}$ of the table entries in $LUT_{i,j}$, the output of this table is,

$$\Delta q_{i,j} = (\Delta q_{i,j,l+1} - \Delta q_{i,j,l}) \frac{q_j - q_{j,l}}{q_{j,l+1} - q_{j,l}} \tag{31}$$

where $\Delta q_{i,j,l}$ and $\Delta q_{i,j,l+1}$ are the command corrections associated with the i^{th} compensation axis and the j^{th} basic axis commands $q_{i,j,l}$ and $q_{i,j,l+1}$, respectively and $\Delta q_{i,j}$ is the interpolated compensated axis command correction.

5.7 Error compensation verification in measurement mode and machining mode

The machine used does not have LUTs facilities. So, offline pseudo-tables were used instead. The correction concept is different when a machine tool is used in measurement mode, using a touch trigger probe for example, as opposed to machining mode when using the pseudo tables. In machining mode, the purpose of compensation is to bring the tool from its actual to its nominal position. In measurement mode, the purpose is to calculate the actual position for a given set of uncompensated read axis positions. Let us assume q^n as the nominal G-code command, q^{read} as the read command following a triggering of the probe and *dq* as the required command correction to

compensate the effect of geometric errors. In machining mode, the error compensation is calculated by adjusting the axis command in such a way as to bring the tooltip to the desired location as,

$$q^{c}_{\text{machining mode}} = q^{n} + dq \tag{32}$$

where $q^{c}_{\text{machining mode}}$ is the corrected command in the machining mode. However, in the measurement mode the compensated command is achieved by subtracting the command correction from the read command. So,

$$q^{c}_{\text{measurement mode}} = q^{read} - dq \tag{33}$$

where $q^{c}_{\text{measurement mode}}$ is the corrected command in the measurement mode. Figure 5.5 illustrates a simplified example wherein the geometric error of a machine tool is defined as 1 mm (E_{YY}=1) positioning error in the Y direction. The nominal height of the tip of the master ball to the table or the nominal command is 5 mm. However, the machine tool reads 4 mm (q^{read}=4) because of its positioning error. The correction command required for compensation is –1 mm (dq=–1) in the Y direction. Hence, when the machine is used in machining mode the objective is to bring the tool at the tip of the master ball. So, the required compensated command is 4 mm, ($q^{c}_{machining\ mode} = 4$), obtained by Eq. (32). However, for the measurement mode, the objective is to obtain the nominal height of the master ball which is 5 mm, $(q^{c}_{\text{measurement mode}} = 5)$, obtained by Eq. (33). The measurement mode is studied in this paper.

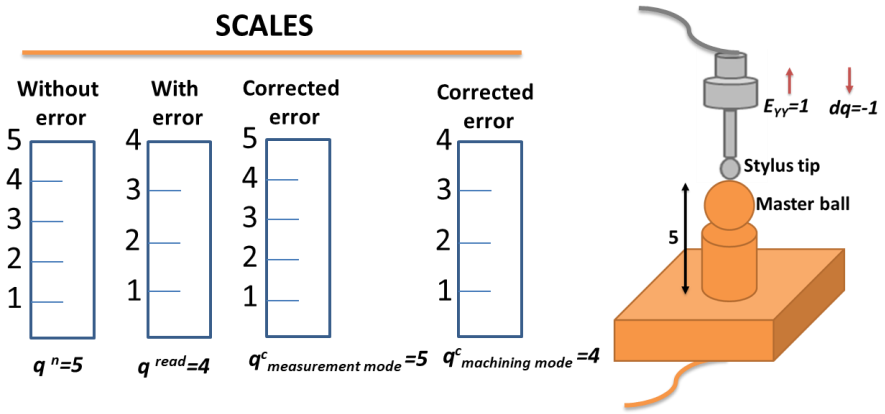

Figure 5.5. A simplified example for the definition of the error compensation concept in the machining mode and in the measurement mode.

The procedure for the calibration, error compensation and its validation is illustrated in Figure 5.6. It proceeds as follows:

1. The RUMBA measurement strategy for the calibration uses four setups, named 1 to 4. The raw probing data is then processed to estimate the machine error parameters and coefficients for the 12- and also for the 81-error models. The estimation results are used to generate grid node corrections from which the LUTs' functions are optimized and then discretized to populate the LUTs.
2. The procedure for the error compensation validation is divided into two phases, a and b.
    a. The validation measurement strategy is executed without any compensation (''before compensation'') and the collected raw probing data is processed to estimate the error parameters for the 12-error model and the error coefficients for the 81-error model.
    b. The raw probing data gathered in phase a is compensated using the LUTs generated by the 12-error model. The compensated probing data is then processed to estimate the error parameters of the 12-error model. This process is repeated but this time using the 81-error model to generate the LUTs.
3. Finally, the machine error parameters before and after compensation are compared.

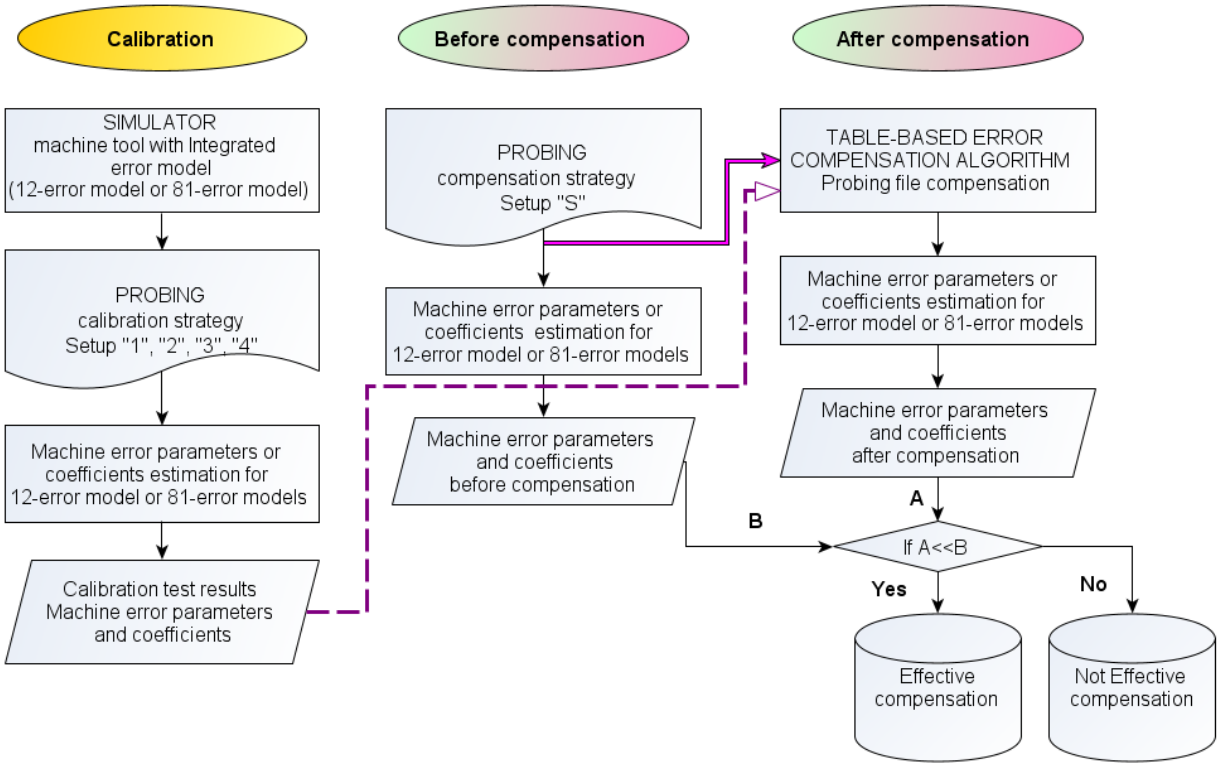

Figure 5.6. The procedure for the calibration (12- or 81-errror model), error compensation and its validation in measurement mode (12-error model).

5.8 Experimental design

The target machine tool has stroke lengths of 260, 420 and 240 mm in the X, Y and Z direction, respectively. The A-axis and C-axis have ranges of 240° and 360°, respectively. Given the relatively small size of the Kolibri machine tool, the RUMBA indirect calibration method is used. The ceramic master spheres' diameter is 20 mm. In the RUMBA method, typically four master balls are installed together while they are measured with different rotary axes indexations. However, to avoid potential interference and collisions, a single ball at a time was mounted and probed for the complete set of rotary axes indexations. So, four setups each with a different ball position were used. The master ball was screwed to the table. The heights from the center of the ceramic ball to the table were 37.5 mm for setups 1 and 2. However, an extension of 10 mm was used to change the height of the master ball to 47.5 mm for setups 3 and 4. The setups are shown in Figure 5.7.

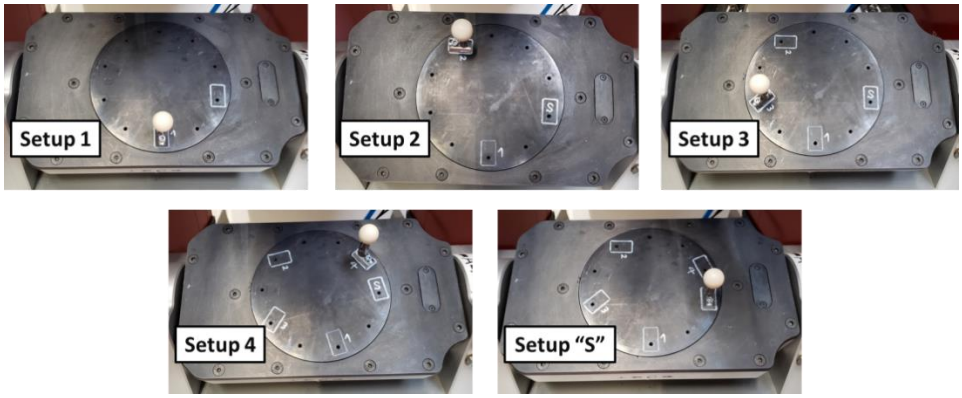

Figure 5.7. The four setups (1 to 4) for the calibration process and the one setup (S) for validating the volumetric error compensation in measurement mode.

Each ball probing includes touches from 5 different directions including four touches around the equator and one touch at the top of the sphere in order to calculate the center of the ball. The probing pattern at the equator is rotated by 45 degrees relative to the machine axes to avoid collision of the probe with the ball stem. The probing process is shown in Figure 5.8. The precise position of the ball is neither known a priori nor necessary. The coordinates of the balls in the last workpiece branch axis frame are estimated together with the machine geometric errors.

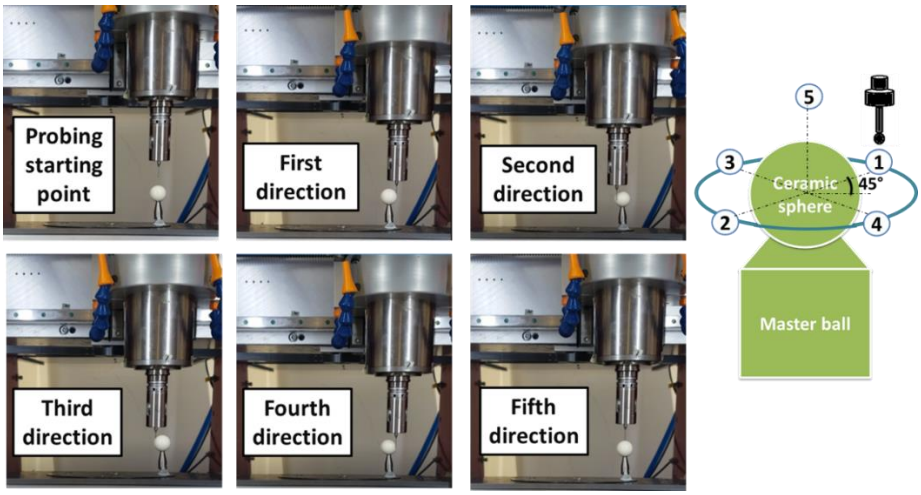

Figure 5.8. The probing process (probing starting point, first direction, second direction, third direction, fourth direction, fifth direction).

Table 5-3 lists the measurement strategy for the four setups which is defined by the A- and C-axis indexation pairs. The rotary A-axis is indexed between -55° and +55° while the C-axis is indexed for its maximum possible rotation during the measurement procedure. The reason of the partial

rotation of the A-axis during the measurement is that the master balls were not accessible for angles of the A-axis over +55° and under -55° in different setups. The touch probe Hexagon IRP40.50 was used for the measurement. The probe tip radius was 0.5 mm and the total height of the probe was 74 mm. The measurements for the four different setups were repeated three times for three consecutive days while the room temperature was around 21 and 22℃ in a climate-controlled workshop. Each probing lasted 1 min 50 sec for one master ball. The 81-error model has a total of 96 unknowns including the balls and tool setup errors. The 12-error model has 27 unknowns and so normally would require less data for a test time about three times shorter. However, in this study, the same calibration tests were run for both error models.

The validation setup (labeled "S") is shown in Figure 5.7. Using a single ball is a technique similar to the "Chase the ball" approach (Bringmann & Knapp, 2006). The ceramic ball was attached to the table with a holder of height 37.5 mm. It was probed using another measurement strategy consisting of 60 A- and C-axis indexation pairs. The strategy is listed in Table 5-4. Each complete measurement of the compensation validation strategy lasted 110 min and the tests were repeated three times while the room temperature was between 21℃ and 22℃. The data is then used for estimating the 12-error model parameters.

Table 5-3. The measurement strategy with different A and C indexation for the four machine calibration setups (1 to 4).

Calibration test (measurement strategy first to fourth setup) Rotary axes indexations (a° , c°)							
(15 , 60)	(30 , 180)	(45 , 280)	(55 , 340)	(40 , 240)	(20 , 120)	(0 , 0)	(-20 , -100)
(-40 , 250)	(-55 , 350)	(-50 , -310)	(-25 , -40)	(0 , 180)	(0 , 280)	(0 , 360)	(0 , 320)
(0 , 210)	(0 , -160)	(0 , -300)	(0 , -220)	(0 , -50)	(15 , 0)	(40 , 0)	(55 , 0)
(45 , 0)	(30 , 0)	(-20 , 0)	(-45 , 0)	(-55 , 0)	(-35 , 0)	(44 , -30)	(53 , -208)
(36 , -318)	(30 , 45)	(21 , 326)	(9 , 290)	(-16 , -12)	(-54 , -304)	(-40 , -10)	(-17 , 100)
(-38 , 197)	(-5 , 345)						

Table 5-4. The measurement strategy with different A and C indexation for fifth setup, used for validation of the compensation (setup S).

Table-based volumetric error compensation (Measurement strategy fifth setup)
Rotary axes indexations (a° , c°)

(8 , 55)	(16,120)	(40 , 180)	(38 , 240)	(55 , 300)	(50 , 330)	(45 , 270)	(36 , 210)
(23 , 150)	(12 , 90)	(4 , 30)	(-5 , -30)	(-12 , -90)	(-28 , -150)	(-31 , -210)	(-48 , -270)
(-52 , -330)	(-5 , -300)	(-43 , -240)	(-34 , -180)	(-23 , -120)	(-11 , -55)	(8 , 140)	(18 , 190)
(12 , 250)	(30 , 290)	(22 , 310)	(47 , 10)	(24 , 50)	(38 , 100)	(41 , 160)	(53 , 200)
(-34 , -45)	(-43 , -140)	(-50 , -170)	(-20 , -220)	(-15 , -280)	(-10 , -310)	(-5 , -70)	(-16 , 135)
(-50 , 280)	(-36 , 94)	(-10 , 20)	(-26 , 200)	(28 , -40)	(50 , -300)	(20 , -280)	(37 , -100)
(10 , -280)	(0 , 0)	(0 , 90)	(0 , 240)	(0 , 300)	(0 , 180)	(0 , 45)	(0 , -45)
(0 , -180)	(0 , -300)	(0 , -240)	(0 , -90)				

5.9 Results and discussions

5.9.1 Machine tool calibration

The raw probing data captured by the four setups (1, 2, 3 and 4) was processed using Eq. (7) in order to estimate the error parameters and coefficients of the two error models. The column normalized Jacobian condition number of the 12-error model and 81-error model were 200 and 3900, respectively. The Jacobian condition number of the 81-error model is larger as the numbers of unknowns participating in the former error model are larger and it includes coefficients of quadratic and cubic terms, unlike the 12-error model. It is also expected that some ordinary polynomial coefficients exhibit some amount of correlation. In Appendix, the two error model estimation results are listed in details. The pooled standard deviation for three repetitions of the probing measurements in the X, Y and Z directions are 1.8, 2.2 and 1.5 µm, respectively.

5.9.2 Experimental validation of the compensation scheme

The validation was conducted by comparing the estimated error parameters for the 12-error model obtained using the “S” validation setup raw probing data before and after compensation. Table 5-5 lists the 12-error model parameters computed from the uncompensated validation strategy data. These parameters should be close to those obtained with the raw probing data from setups 1 to 4. The error parameters listed in Table 5-5 are shown in Figure 5.9 with their respective units. As seen, the behavior of the two graphs are similar even though different measurement strategies are used.

Table 5-5. The estimated error parameters of the 12-error model for the uncompensated validation strategy (S) and for the calibration setups (1 to 4).

Symbol [unit]	Value Setup (S)	Mean volumetric error norm caused by each estimated model parameters in µm	Value Setup (1,2,3,4)	Mean volumetric error norm caused by each estimated model parameters in µm
EB(OX)A	1.290 mrad	50.60	1.090 mrad	42.40
EC(OY)A	-0.984 mrad	88.80	-0.869 mrad	76.50
EY(OA)C	41.400 µm	41.40	42.100 µm	42.10
EA(OY)C	0.073 mrad	6.38	0.069 mrad	5.89
EB(OA)C	0.032 mrad	2.83	0.029 mrad	2.46
EC(OY)X	0.150 mrad	4.96	0.143 mrad	4.54
EA(OY)Z	-0.480 mrad	33.80	-0.439 mrad	32.10
EB(OX)Z	0.153 mrad	10.80	0.114 mrad	8.30
EAAb	-0.015 mrad	1.07	-0.013 mrad	2.66
ECCb	-0.028 mrad	4.18	-0.024 mrad	3.20
EYY1-EXX1	-0.642 µm/mm	25.20	-0.607 µm/mm	22.00
EZZ1-EXX1	-0.253 µm/mm	36.50	-0.216 µm/mm	28.20

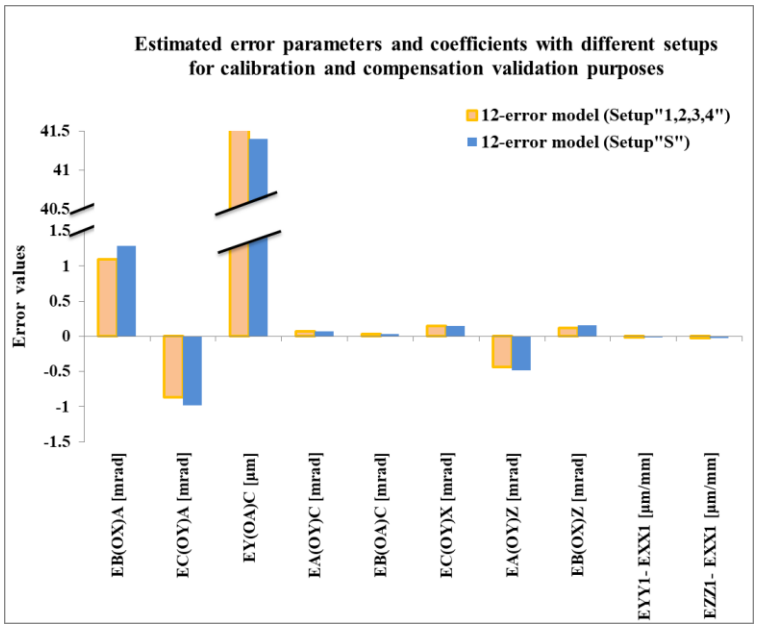

Figure 5.9. The estimated error parameters of the 12-error model for the uncompensated validation strategy (S) and for the calibration setups (1 to 4) (same data as in Table 5-5).

To generate the LUTs, first, the axis space where the compensation tables are needed to be applied is defined. The axis space is kept within the range of available calibration data in order to avoid extrapolating the model. For instance, although the A-axis stroke length is between $-120°$ and

$+120°$, the command correction values are considered from $-55°$ to $+55°$ thus within the calibration test range.

The 5D mesh grid was generated using 10 positions per axis for a total of 100000 sets of commands and corresponding grid nodes. Using the variables estimated from the calibration process from the 12- and then for the 81-error models and Eq. (3), the volumetric errors for 100000 set of commands were calculated for each model separately and the table coefficients were optimized and the tables populated. Because the controller of the target machine tool was not able to embed these compensation tables, the error compensation was conducted offline using pseudo tables. The 25 compensation table functions are shown in Figure 5.10 for the 12- and 81-error models. During the optimization process it was realized that offsets, or zero degree terms of the polynomials, of all basic axis functions for a given compensation axis correction have the same effect, and so are confounded. So, it was decided to only retain those terms for one basic axis per compensation axis i.e. for the table functions of f_{XX}, f_{YZ}, f_{ZX}, f_{AX} and f_{CX}. As expected, the table functions from the 81-error model reveal more complexity than the table functions from the 12-error model as it is better able to represent machine error patterns. Each set of five table functions in each column in Figure 5.10 are functions of a specific basic axis command: X, Y, Z, A or C-axis, respectively.

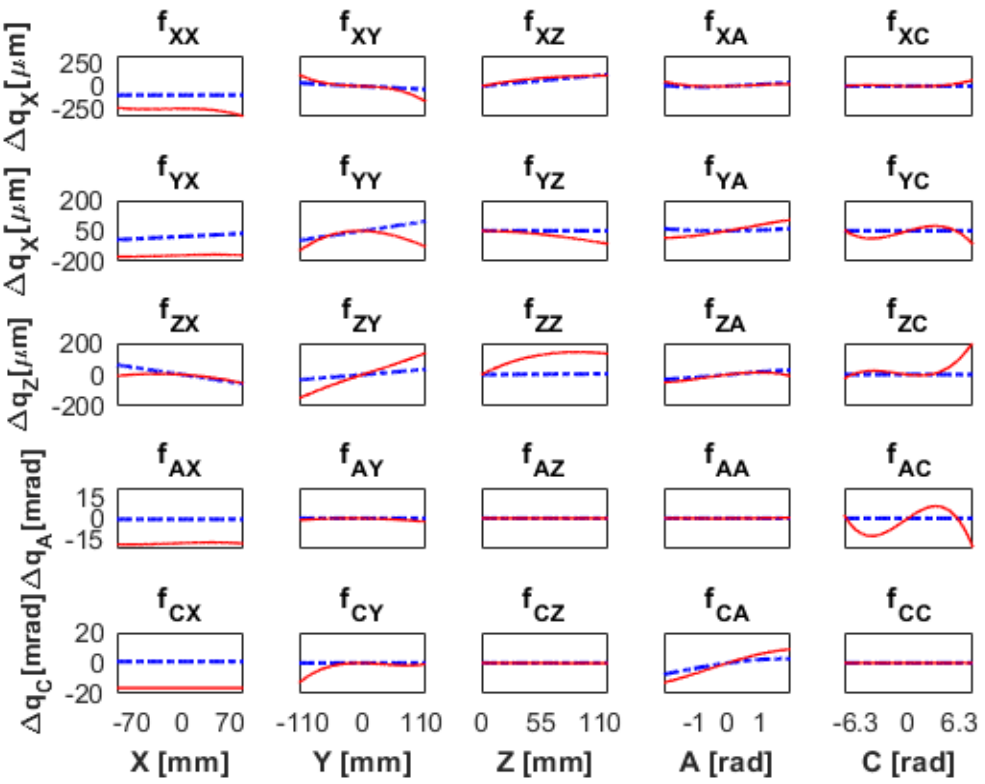

Figure 5.10. The 25 compensation table functions generated from the 81- and 12-error models. (81-error model: red continous line, 12-error model: blue long- and short-dashed line).

The validation strategy's probing results were processed to estimate the error models. The comparison of the 12-error parameters before and after using the compensation tables are shown in Figure 5.11. The compensated results for both the 12- and the 81-error model improve the effective geometry of the machine but the performance of the two models in improving the 12 geometric errors parameters of the 12-error model are quite similar. Table 5-6 lists results for the translational volumetric error norm. The ability of the two models to improve the measuring accuracy of the machine is quantified by the mean estimated translational volumetric error norm. This value is 125 µm for the 12-error model before compensation whereas the mean translational volumetric error norm unexplained by the model is 21 µm, showing a potential of compensation of 104 µm if only the 12 error parameters could be compensated. However, after using the pseudo tables of the 12- and 81-error models, the mean estimated volumetric error norms are reduced to 47 µm and 32 µm, respectively. As expected, by also modeling the intra-axis errors (81-error

model) the accuracy improves further although only by 12%, which suggests that axes misalignments and relative linear positioning errors are dominant**.** The mean unexplained volumetric error before compensation is 21 µm for the 12-error model. This indicates that the intra-axis error modelling and compensation using the 81-error model did not significantly improve the machine.

As seen in Table 5-5, the dominant errors for this machine tool are EC(OY)A, EB(OX)A and EY(OA)C as they exhibit the largest mean volumetric error norm caused by each estimated model parameters. Table 5-7 shows the error parameters magnitude before and after table-based error compensation and their standard deviation for setup "S" for three repetitions. Among the dominant errors, EC(OX)A and EY(OA)C are significantly reduced, after compensation, but not EB(OX)A. The mean volumetric error norm caused by each estimated model parameters for EB(OA)C and EC(OY)X are less than 5 µm before compensation. Since the magnitudes of the aforementioned errors before compensation are small, the effectiveness of the compensation model in compensating those errors is not clear.

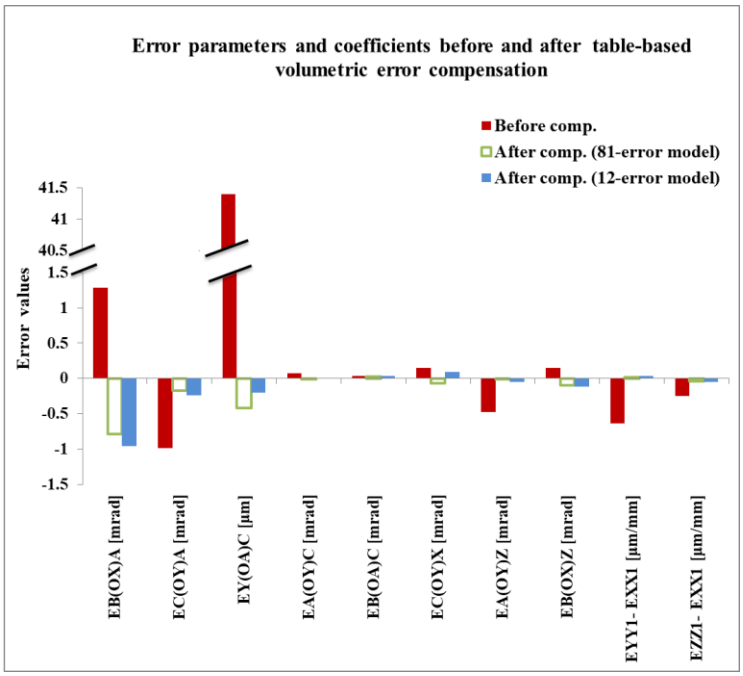

Figure 5.11. Comparison of the 12 error parameters before and after using the pseudo tables for the 81- and 12-error model compensation tables.

Table 5-6. The mean estimated translational volumetric error norm and mean unexplained translational volumetric error norm before and after compensation.

	Mean estimated translational volumetric error norm [µm]	**Mean unexplained translational volumetric error norm [µm]**
Before Comp.	125	21
After Comp. (12-error model)	47	21
After Comp. (81-error model)	32	19

Table 5-7. The effectiveness of two pseudo complex tables (81- and 12-error model) in terms of reducing the magnitudes of the 10 error parameters and coefficients (Setup "S").

Symbol	**Error parameters magnitude before and after table-based error compensation**			**Standard deviation**		
	Before Comp.	**After Comp. (12-error model)**	**After Comp. (81-error model)**	**Before Comp.**	**After Comp. (12-error model)**	**After Comp. (81-error model)**
EB(OX)A [mrad]	1.290	-0.962	-0.893	0.230	0.182	0.151
EC(OY)A [mrad]	-0.984	-0.242	-0.173	0.031	0.044	0.028
EY(OA)C [µm]	41.400	-0.941	-0.551	0.400	0.822	0.722
EA(OY)C [mrad]	0.073	0.002	-0.013	0.003	0.005	0.006
EB(OA)C [mrad]	0.032	0.031	0.030	0.004	0.003	0.004
EC(OY)X [mrad]	0.150	0.094	-0.071	0.003	0.003	0.004
EA(OY)Z [mrad]	-0.480	-0.047	-0.010	0.004	0.005	0.003
EB(OX)Z [mrad]	0.153	0.112	-0.096	0.003	0.002	0.004
EYY1- EXX1 [µm/mm]	-0.642	0.037	0.013	0.009	0.009	0.007
EZZ1- EXX1 [µm/mm]	-0.253	-0.047	-0.044	0.008	0.006	0.009

The histogram of the volumetric error vector components in the X, Y and Z directions and their norms for the 60 probings of the validation strategy (setup S) before and after using the two compensation models are shown in Figure 5.12. The distribution shows a clear reduction in the volumetric errors. The norm of the volumetric errors before compensation is between 20 to 70 µm while this value is reduced to less than 30 µm after using the two compensation models. The root

mean square (RMS) of the volumetric errors in the X, Y and Z direction before compensation are 87.3, 75.4 and 71.5 µm, respectively. Using the complex compensation tables generated from the 12-error model reduces the RMS of the volumetric errors to 24.8, 18.8 and 22.1 µm in the X, Y and Z directions, respectively. When using the 81-error model for compensation purposes, the RMS of the volumetric errors in the X, Y and Z directions become 18.6, 11.9 and 21.5 µm, respectively. Hence, the LUTs constructed by the 12- and 81-error models are respectively efficient by 72% and 74% in decreasing the volumetric errors.

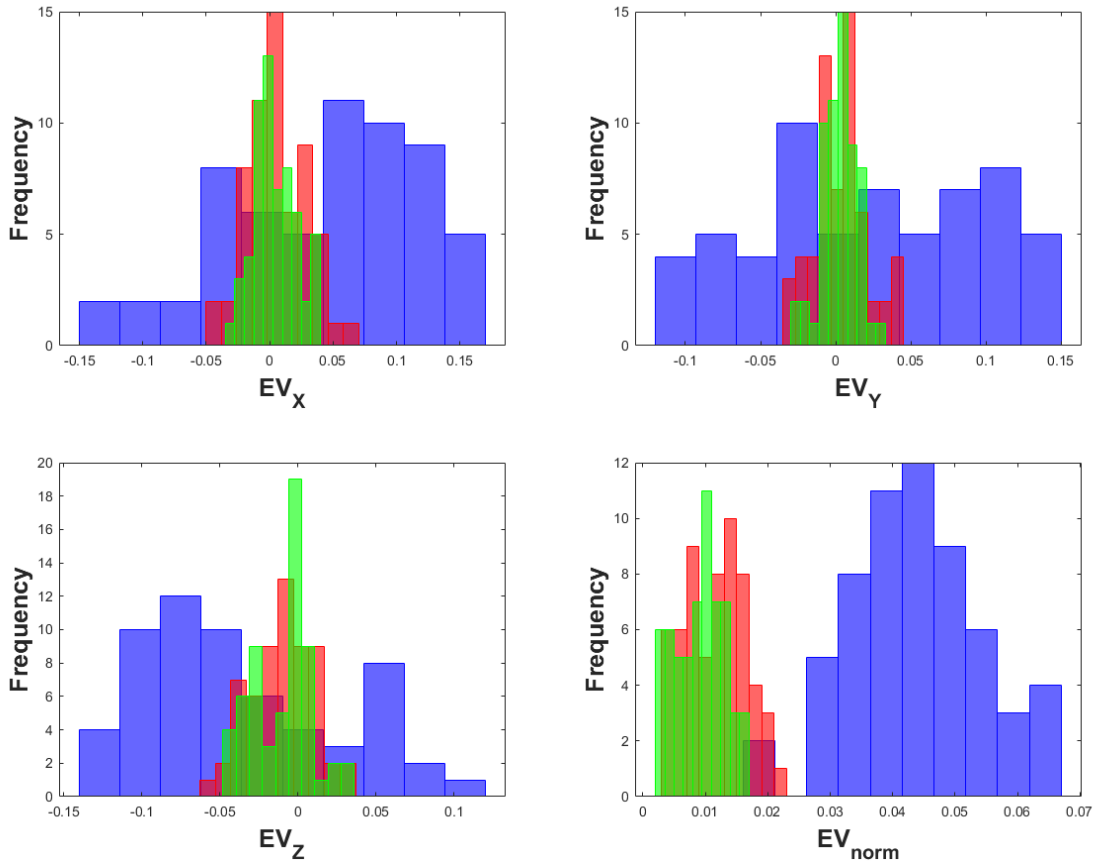

Figure 5.12. Histogram of the volumetric errors (EV) [mm] for 60 probings, before and after applying the compensation algorithm. (Before compensation: blue; after compensation 81-error model: green; after compensation 12-error model: red)

5.10 Conclusion

The generation, use and performance of a 25 lookup table compensation scheme, exploiting the summation functions, is studied. The automated probing based RUMBA indirect calibration

provides the error parameters and coefficients for two distinct error models, a 12- and an 81-error model. These models are used to predict volumetric error twists at the nodes of a 5D grid. The table functions are univariate ordinary cubic polynomials. An extended Jacobian matrix relating the volumetric error twists at the node to the table function coefficients yields optimum coefficients. These functions are discretized to populate the LUTs.

The criteria for the effectiveness of the procedure are the volumetric errors and the apparent machine error parameters of the 12-error model before and after compensation when the machine is in measurement mode. The compensation reduces the volumetric errors and all geometric errors. The 25 LUT scheme is appropriate to compensate most misalignments such as EC(OX)A, EY(OA)C, EA(OY)C, EA(OY)Z and the relative scale errors but had limited success in correcting EB(OX)A and EB(OX)Z. The RMS of the volumetric error vector components are reduced from 87.3, 75.4 and 71.5 µm down to 24.8, 18.8 and 22.1 µm for the 12-error model and to 18.6, 11.9 and 21.5 µm for the 81-error model in X, Y and Z directions, respectively. The effectiveness of the tables in reducing the volumetric errors is 72% and 74% respectively using the 12- and 81-error model.

5.11 Acknowledgments

This research was supported by Natural Sciences and Engineering Research Council of Canada (NSERC) under the CANRIMT Strategic Research Network Grant NETGP 479639-15 and by the Deutsche Forschungsgemeinschaft (DFG, German Research Foundation) under Germany's Excellence Strategy – EXC 2023 Internet of Production – 390621612.

5.12 References

Abbaszadeh-Mir, Y., Mayer, J. R. R., Cloutier, G., & Fortin, C. (2002). Theory and simulation for the identification of the link geometric errors for a five-axis machine tool using a telescoping magnetic ball-bar. *Int. J. Pod. Res, 40*, 4781-4797. doi:10.1080/00207540210164459

Bringmann, B., & Knapp, W. (2006). Model-based ‘Chase-the-Ball’ Calibration of a 5-Axes Machining Center. *CIRP Annals, 55*(1), 531-534. doi:10.1016/s0007-8506(07)60475-2

Controller, F. Series 30i/Model A.

Controller, S. SINUMERIK 840D.

Creamer, J., Bristow, D. A., & Landers, R. G. (2017). Selection of limited and constrained compensation tables for five-axis machine tools. *The International Journal of Advanced Manufacturing Technology, 92*(1-4), 1315-1327. doi:10.1007/s00170-017-0230-4

Creamer, J., Sammons, P. M., Bristow, D. A., Landers, R. G., Freeman, P. L., & Easley, S. J. (2016). Table-Based Volumetric Error Compensation of Large Five-Axis Machine Tools. *Journal of Manufacturing Science and Engineering, 139*(2). doi:10.1115/1.4034399

Creamer, J., Sammons, P. M., Bristow, D. A., Landers, R. G., Freeman, P. L., & Easley, S. J. (November 15-21, 2013, San Diego, California, USA). Table-Based Compensation for 5-Axis Machine Tools. *Proceedings of the ASME 2013 International Mechanical Engineering Congress and Exposition IMECE2013*.

Esmaeili, S., & Mayer, J. R. R. (2020). An Integrated Geometric and Hysteretic Error Model of a Three Axis Machine Tool and Its Identification With a 3D Telescoping Ball-Bar. *Journal of Manufacturing and Materials Processing, 4*(1). doi:10.3390/jmmp4010024

Givi, M., & Mayer, J. R. R. (2014). Volumetric error formulation and mismatch test for five-axis CNC machine compensation using differential kinematics and ephemeral G-code. *The International Journal of Advanced Manufacturing Technology, 77*(9-12), 1645-1653. doi:10.1007/s00170-014-6558-0

Ibaraki, S., & Knapp, W. (2012). Indirect Measurement of Volumetric Accuracy for Three-Axis and Five-Axis Machine Tools: A Review. *International Journal of Automation Technology, 6*, 110-124. doi:10.3929/ethz-a-007593181

ISO 230-1. (2012). *Test code for machine tools-Part1: Geometric accuracy of machines operating under no-load or quassi-static conditions*.

Jung, J.-H., Choi, J.-P., & Lee, S.-J. (2006). Machining accuracy enhancement by compensating for volumetric errors of a machine tool and on-machine measurement. *Journal of Materials Processing Technology, 174*(1-3), 56-66. doi:10.1016/j.jmatprotec.2004.12.014

Khan, A. W., & Chen, W. (2010). A methodology for systematic geometric error compensation in five-axis machine tools. *The International Journal of Advanced Manufacturing Technology, 53*(5-8), 615-628. doi:10.1007/s00170-010-2848-3

Koliskor, A. (1971). Compensating for automatic-cycle machining errors. *Machines and Tooling, 41*, 1-14.

Lei, W. T., & Hsu, Y. Y. (2003). Accuracy enhancement of five-axis CNC machines through real-time error compensation. *International Journal of Machine Tools and Manufacture, 43*(9), 871-877.

Li, J. G., Zhao, H., Yao, Y. X., & Liu, C. Q. (2007). Off-line optimization on NC machining based on virtual machining. *The International Journal of Advanced Manufacturing Technology, 36*(9-10), 908-917. doi:10.1007/s00170-006-0915-6

M. Esmaeili, S., & Mayer, J. R. R. (2020). Generation of a 3D error compensation grid from ISO 230-1 error parameters obtained by a SAMBA indirect calibration and validated by a ball-bar spherical test. *The International Journal of Advanced Manufacturing Technology, 106*(11-12), 4649-4662. doi:10.1007/s00170-020-04928-4

Mahbubur, R. M., Heikkala, J., Lappalainen, K., & Karjalainen, J. A. (1997). Positioning Accuracy improvement in five-axis milling by post processing. *International Journal of Machine Tools and Manufacture, 37*, 223-236.

Mayer, J. R. R. (2012). Five-axis machine tool calibration by probing a scale enriched reconfigurable uncalibrated master balls artefact. *CIRP Annals, 61*(1), 515-518. doi:10.1016/j.cirp.2012.03.022

Mir, Y. A., Mayer, J. R. R., & Fortin, C. (2002). Tool path error prediction of a five-axis machine tool with geometric errors. *Proceedings of the Institution of Mechanical Engineers, 216*, 697-712.

Montavon, B., Dahlem, P., & Schmitt, R. H. (March 2019). Fast machine tool calibration using a single Laser Tracker. *Laser Metrology and Machine Performance XIII*.

Rahman, M., Heikkala, J., & Lappalainen, K. (2000). Modeling, measurement and error compensation of multi-axis machine tools. Part I: theory. *International Journal of Machine Tools and Manufacture, 40*, 1535–1546.

Rahman, M. M., & Mayer, J. R. R. (2015). Five axis machine tool volumetric error prediction through an indirect estimation of intra- and inter-axis error parameters by probing facets on a scale enriched uncalibrated indigenous artefact. *Precision Engineering, 40*, 94-105. doi:10.1016/j.precisioneng.2014.10.010

Ramesh, R., Mannan, M. A., & Poo, A. N. (2000). Error compensation in machine tools — a review Part II: thermal errors. *International Journal of Machine Tools and Manufacture, 40*, 1257–1284.

Sartori, S., & Zhang, G. X. (1995). Geometric Error Measurement and Compensation of Machines. *CIRP Annals, 44*(2), 599-609. doi:10.1016/s0007-8506(07)60507-1

Schwenke, H., Knapp, W., Haitjema, H., Weckenmann, A., Schmitt, R., & Delbressine, F. (2008). Geometric error measurement and compensation of machines—An update. *CIRP Annals, 57*(2), 660-675. doi:10.1016/j.cirp.2008.09.008

Slamani, M., Mayer, J. R. R., & Cloutier, G. M. (2011). Modeling and Experimental Validation of Machine Tool Motion Errors Using Degree Optimized Polynomial Including Motion Hysteresis. *Experimental Techniques, 35*(1), 37-44. doi:10.1111/j.1747-1567.2009.00576.x

Srivastava, A. K., Veldhuis, S. C., & Elbestawlt, M. A. (1995). Modeling geometric and thermal errors in five-axis CNC machine tool *International Journal of Machine Tools and Manufacture, 35*, 1321-1337.

Suh, S.-H., Lee, E.-S., & Sohn, J.-W. (1999). Enhancement of Geometric Accuracy via an Intermediate Geometrical Feedback Scheme. *Journal of Manufacturing Systems, 18*, 12-21.

Wang, S.-M., Liu, Y.-L., & Kang, Y. (2002). An efficient error compensation system for CNC multi-axis machines. *International Journal of Machine Tools and Manufacture, 42*, 1235–1245.

Wang, S.-M., Yu, H.-J., & Liao, H.-W. (2005). A new high-efficiency error compensation system for CNC multi-axis machine tools. *The International Journal of Advanced Manufacturing Technology*, *28*(5-6), 518-526. doi:10.1007/s00170-004-2389-8

Xi, X.-C., Poo, A.-N., Hong, G.-S., & Huo, F. (2010). Experimental implementation of Taylor series expansion error compensation on a bi-axial CNC machine. *The International Journal of Advanced Manufacturing Technology*, *53*(1-4), 285-299. doi:10.1007/s00170-010-2843-8

Yuan, J., & Ni, J. (1998). The real-time error compensation technique for CNC machining systems. *Mechatronics*, *8*, 359-380.

Zhang, H., Yang, J., Zhang, Y., Shen, J., & Wang, C. (2010). Measurement and compensation for volumetric positioning errors of CNC machine tools considering thermal effect. *The International Journal of Advanced Manufacturing Technology*, *55*(1-4), 275-283. doi:10.1007/s00170-010-3024-5

5.13 Appendix

The estimation results of the error parameters and coefficients (81-error model).

X-axis		Y-axis		Z-axis		A-axis		C-axis	
Name	Value	Name	Value	Name	Value	Name	Value	Name	Value
E_{XX2}	6.09E-06	E_{XY2}	-2.85E-08	E_{XZ2}	1.60E-05	E_{XA1}	1.59E-02	E_{XC1}	-8.48E-04
E_{XX3}	1.29E-07	E_{XY3}	-9.54E-08	E_{XZ3}	-4.16E-08	E_{XA2}	1.40E-03	E_{XC2}	5.45E-04
E_{YX1}	1.18E-03	E_{YY1}	1.16E-04	E_{YZ2}	-1.05E-04	E_{XA3}	2.75E-02	E_{XC3}	1.14E-04
E_{YX2}	-1.25E-05	E_{YY2}	1.01E-05	E_{YZ3}	2.78E-07	E_{YA0}	1.59E-01	E_{YC1}	-9.21E-04
E_{YX3}	-3.08E-07	E_{YY3}	-2.00E-08	E_{ZZ1}	-4.00E-03	E_{YA1}	-7.04E-02	E_{YC2}	1.74E-04
E_{ZX2}	8.84E-06	E_{ZY2}	-5.46E-06	E_{ZZ2}	3.09E-05	E_{YA2}	-7.30E-01	E_{YC3}	6.40E-05
E_{ZX3}	3.65E-08	E_{ZY3}	1.05E-07	E_{ZZ3}	-5.77E-08	E_{YA3}	1.53E-02	E_{ZC1}	-9.57E-04
E_{AX0}	-1.20E-02	E_{AY1}	4.33E-06			E_{ZA1}	-1.55E-01	E_{ZC2}	2.83E-04
E_{AX1}	1.71E-05	E_{AY2}	1.05E-07			E_{ZA2}	3.24E-02	E_{ZC3}	8.51E-05
E_{AX2}	-1.05E-07	E_{AY3}	-2.21E-11			E_{ZA3}	2.35E-01	E_{AC1}	2.12E-06
E_{AX3}	-3.43E-09	E_{BY0}	2.63E-04			E_{AA0}	1.82E-04	E_{AC2}	2.07E-06
E_{BX0}	-1.60E-03	E_{BY1}	-2.69E-06			E_{AA1}	2.34E-04	E_{AC3}	4.48E-07
E_{BX1}	3.39E-06	E_{BY2}	-1.36E-08			E_{AA2}	-2.45E-04	E_{BC1}	1.45E-05
E_{BX2}	-1.01E-07	E_{BY3}	1.63E-10			E_{AA3}	-7.92E-05	E_{BC2}	-6.32E-06
E_{BX3}	-1.73E-09	E_{AY0}	1.65E-02			E_{AAb}	3.11E-07	E_{BC3}	-1.51E-06
		E_{AY1}	1.30E-06			E_{BA0}	9.85E-04	E_{CC1}	-3.25E-06
		E_{AY2}	6.68E-08			E_{BA1}	-1.73E-02	E_{CC2}	-2.66E-06
		E_{AY3}	-6.86E-10			E_{BA2}	-2.53E-04	E_{CC3}	-1.09E-08
						E_{BA3}	2.91E-03	E_{CCb}	-2.17E-04
						E_{CA1}	-7.50E-04		
						E_{CA2}	8.21E-03		
						E_{CA3}	2.04E-04		

Units examples:

R and H are the linear axes: E_{RH0}[mm], E_{RH1}[mm/mm], E_{RH2}[mm/mm^2], E_{RH3}[mm/mm^3], E_{RHb}[mm]

R is the rotary axis and H is the linear axis: E_{RH0}[rad], E_{RH1}[rad/mm], E_{RH2}[rad/mm^2], E_{RH3}[rad/mm^3], E_{RHb}[rad]

R and H are the rotary axes: E_{RH0}[rad], E_{RH1}[rad/rad], E_{RH2}[rad/rad^2], E_{RH3}[rad/rad^3], E_{RHb}[rad]

R is the linear axis and H is the rotary axis: E_{RH0}[mm], E_{RH1}[mm/rad], E_{RH2}[mm/rad^2], E_{RH3}[mm/rad^3], E_{RHb}[mm]

The estimation results for the error parameters and coefficients of the 12-error model obtained using the combined data from setups 1, 2, 3 and 4 used for calibration purpose.

Symbol [unit]	Value
EB(OX)A [mrad]	1.090
EC(OY)A [mrad]	-0.869
EY(OA)C [µm]	42.100
EA(OY)C [mrad]	0.069
EB(OA)C [mrad]	0.029
EC(OY)X [mrad]	0.143
EA(OY)Z [mrad]	-0.439
EB(OX)Z [mrad]	0.114
E_{AAb} [mrad]	-0.013
E_{CCb} [mrad]	-0.024
EYY1-EXX1[µm/mm]	-0.607
EZZ1-EXX1[µm/mm]	-0.216

CHAPTER 6 ARTICLE 3: TRIGONOMETRIC FUNCTIONS AND COMBINATORIAL LOOKUP TABLE SCHEME FOR INDIGENOUS CNC COMPENSATION OF A FIVE-AXIS MACHINE TOOL

Sareh M. Esmaeili [a,*], J.R.R. Mayer [a], J. Philipp Dahlem [b], Mark P. Sanders [b]

[a] *Department of Mechanical Q1 Engineering, École Polytechnique (Montréal), P.O. Box 6079, Station Downtown, Montréal, QC H3C3A7, Canada*

[b] *Laboratory for Machine Tools and Production Engineering (WZL), RWTH Aachen University, Aachen, Germany*

[*] Corresponding author. *Email: sareh.esmaeili-marzdashti@polymtl.ca [*]Tel.: +15143404711 Ext.: 2292, [*]Fax: (514) 340-5170*

NOTE: Based on the paper resubmitted to the International Journal of Machine Tools and Manufacture (2021)

6.1 Abstract

A CNC table-based volumetric error compensation model is proposed to enhance a five-axis machine tool's accuracy that uses discretized trigonometric functions to populate the lookup tables (LUTs). The proposed model is inspired by the terms present in the Jacobian of commands of the target machine tool. It results in 23 look up tables using the multiplication and summation functionalities of the CNC table generator. Simulations and experimental validations are used to evaluate the proposed model's effectiveness for compensating each geometric error parameter and reduce volumetric errors. An indirect measurement method estimating machine tool error parameters, as well as volumetric errors, is used to characterize the machine tool before and after compensation. The new procedure is compared with a 25 lookup table approach where cubic polynomials and only the summation functionality are used. The trigonometric function-based scheme further reduces the maximum volumetric error norm by 32%. All effective geometric errors are reduced by at least 87%, bringing the end result closer to the theoretically exact inverse kinematics approach.

6.2 Introduction

Industrial demand for producing parts with tight tolerances and high productivity requires keeping machine tools operating at accuracies close to their repeatability with minimum downtime for mechanical corrections. Machine tool inaccuracies may stem from geometric imperfections (Majda, 2012) resulting in volumetric errors. The geometric sources of volumetric errors are generally modeled using rigid body kinematics, mathematically described as homogeneous transformation matrices (Castro & Burdekin, 2005; Lei & Sung, 2008; Schwenke et al., 2009; Zhu et al., 2012).

To calibrate the machine tool and estimate the error parameters and the volumetric errors, indirect methods have been proposed (Soichi Ibaraki & Knapp, 2012). Some indirect methods are laser interferometry approaches such as the LaserTRACER and laser trackers. The LaserTRACER uses the quadrilateration principle for machine calibration consisting of multiple stations or setups of a tracking laser interferometer and a cat's eye type retro-reflector target installed at the tool holder. Each station measures the distances between the target and the LaserTRACER internal reference sphere (Schwenke et al., 2009). All 21 errors of the linear axes are estimated. A linearized set of equations is solved by a Gaussian fit (Härtig et al., 2009). Groos et al. (Groos et al., 2020) used the LaserTRACER to map the geometric errors with the effect of the ambient temperature and numerically compensated them. They claimed that some errors such as positioning and squareness errors of the linear axes are significantly influenced by the ambient temperature whereas straightness and rotational errors were much less affected. Zha et al. (Zha et al., 2020) used the LaserTRACER to calculate the geometric error in a 3-axis machine tool. The geometric error values were also verified with a conventional laser interferometer. They used cubic spline interpolation method to obtain volumetric error at the tool tip followed by modifying the G-code for machining a concave semi-spheroid test piece. The machining accuracy after compensation was reduced by 43%. Schwenke et al. (Schwenke et al., 2009) used the LaserTRACER to measuring the error motions of rotary axes on a five-axis machine tool. Laser trackers use two angles and a distance measure to produce spherical coordinates in one setup to estimate the machine tool geometric errors. Relying on angular readings reduces accuracy but using multiple setups overcomes this issue (Schwenke et al., 2005). Creamer et al. (J. Creamer et al., 2017; Jennifer Creamer et al., 2016) used the laser tracker to estimate the machine tool volumetric errors and to

generate compensation lookup tables. Another indirect calibration approach may use measurements of an artefact with proximity sensors or the on-machine touch trigger probe (Florussen & Spaan, 2007; Mayer, 2012; McHichi & Mayer, 2014; Md Mizanur & Mayer, 2015; Weikert, 2004). The R-test is used to calibrate the five-axis machine tool error parameters by measuring the 3D Cartesian deviations between the tool mounted sphere and the table mounted sensor array while maintaining their nominal coincidence during five-axis motion (Weikert, 2004). Probing data on precision spheres or on facets was also used for indirect estimation of geometric error parameters of five-axis machines (S. Ibaraki, Iritani, & Matsushita, 2010; Mayer, 2012; McHichi & Mayer, 2014; Md Mizanur & Mayer, 2015).

Error compensation, without mechanical corrections of the machine structure, requires modifying the axis commands from their nominal values. As Sartori et al. (Sartori & Zhang, 1995) explain, there are two phases: Error measurement and then compensation. Kinematic-based error compensation may be done by user (Hocken, 1993; Xiang & Altintas, 2016) or may be achieved by G-code modifications may be achieved by G-code modifications (Givi & Mayer, 2014, 2016). Donmez et al. (Donmez, Bloquist, Hocken, & Liu, 1986) presented a general kinematic-based error compensation method using rigid body kinematics. The online volumetric error compensation is performed by correction of the control command within the control loop (Ramesh, Mannan, & Poo, 2000a; H. Zhang et al., 2010).

Some modern CNCs have compensation tables such as pitch error, backlash, straightness error, thermal error, sag and angularity error compensation. The tables enable the machine to be compensated automatically without the need for continuously adapting G-codes as a machine geometry changes. Positioning, straightness, and out-of-squareness error compensation are commonly used on CNC controllers. Recent CNC controllers are equipped with tables to compensate many machine tool errors ("Siemens Controller," SINUMERIK 840D/840Di/810D Extended Functions). In ISO/TR 16907 (ISO/TR16907, 2015), 13 compensation schemes are proposed each addressing a particular combination of geometric errors with a number of limitations and overlaps. From the document it appears that no scheme specifically addresses the eight inter-axis errors but scheme L-SQR addresses linear axes inter-axis errors whereas scheme R-POR addresses rotary axes inter-axis errors. In ISO/TR 16907 (ISO/TR16907, 2015), grid tables are discussed while the spatial grid compensation tables are separate for the linear and the rotary axes. The 3D principle in generating 3D Error Compensation is assigning the correction values to each

grid point in the three-axis working volume. Once an axis position command set is entered to the controller, a trilinear interpolation on the table data entries is computed and added to the corresponding correction values to the entered command. This approach is commercially available e.g. as Fanuc's "3D Error Compensation" for linear axes ("Fanuc Controller," Series 30i/Model A). Based on the rigid body model, M. Esmaeili and Mayer generated 3D error compensation grid from ISO 230-1 error parameters. They used SAMBA indirect calibration method for producing the tables and validated the compensation by a ball-bar spherical test (Esmaeili & Mayer, 2020). Compensation grid structure function is also available in a Siemens controller ("Siemens Controller," SINUMERIK 840D/840Di/810D Extended Functions) as grid compensation capability. Alternatively, based on tables containing axes geometric errors, position and orientation errors can be compensated using a rigid body kinematic model. The aforementioned compensation functionality is also available in multiple machine control systems such as Fagor as "Volumetric Compensation" ("Fagor Controller, 8070 / 8065 CNC "), Heidenhain as "KinematicsComp" ("Heidenhain Controller: iTNC 530 "), Fidia as "Extended Screw Compensation" ("Fidia Controller: C10 - C20 - C20 Vision,") and Siemens as "Volumetric Compensation System" (AG, 2010) which compensate for the three linear axis 21 machine error parameters. Another compensation feature provided by Fidia controller is called "Volumetric Axes Compensation" (VAC) to compensate the linear axes errors. The system can reach maximum accuracy for all linear as well as rotary axes errors by combining VAC and rotary axes error compensation. To calculate the rotary axes errors, this controller offers a head measuring system (HMS) calibration system ("Fidia Controller: C10 - C20 - C20 Vision,"). ISO/TR 16907 does not mention the capability of combinatory tables and their associated table functions (ISO/TR16907, 2015). However, the Siemens controller 840D is equipped with such complex tables enabling the users to combine tables with summation and multiplication functionalities ("Siemens Controller," SINUMERIK 840D/840Di/810D Extended Functions). Based on ISO/TR 16907 (ISO/TR16907, 2015), common compensation table files contain the identification of the nominal position, the direction to be compensated, the input and the output axis.

Although the capability of building the complex tables has been available in some controllers for many years, little scientific research is done in this field. Creamer et al. (Jennifer Creamer et al., 2016) presented a volumetric error compensation scheme using 25 lookup tables (LUTs) generated from either of two models, a six degree-of-freedom model and an axis perturbation model and

concluded that the first model provided an effectiveness of 93.1% and the second model had an effectiveness of 92.2%. They used summation functionalities and considered univariate polynomials as the table functions. Later, Creamer et al. (J. Creamer et al., 2017) presented complementary research results regarding selecting the limited and constrained compensation tables applicable for machine tools having less available compensation tables in their controllers.

The current study investigates the limitations of 25 summation tables based on cubic polynomials in compensating the effect of inter-axis errors and relative linear axis positioning errors. It also proposes and evaluates, both theoretically and experimentally, the use of multiplication and summation functionalities of tables with trigonometric table functions inspired by the machine tool kinematics. The five-axis machine tool geometric error parameters of its kinematic model are obtained using probings of a reconfigurable uncalibrated master ball artefact (RUMBA) as an indirect method. The criteria for evaluating the compensation effectiveness are the reduction of the volumetric error and the effective geometric error parameters after compensation. Section 6.3 presents the machine tool error modeling. In section 6.4, the kinematic-based error compensation is explained. In section 6.5, the two table-based error compensation models are presented. Section 6.6 uses simulation to analyse the performance of the kinematic-based and two table-based compensation schemes. The experimental validation is explained in section 6.7 followed by the experimental results and the associate discussions in section 6.8. Section 6.9 presents the summary and conclusion.

6.3 Volumetric and geometric error modeling and calibration

The target machine topology is wCAYfXZSt containing two rotary axes (A- and C-axis) and three linear axes (X-, Y- and Z-axis). The nominal foundation frame is at the intersection of the A- and C-axis. *S*, *w* and *t* are the spindle, workpiece and tool, respectively (Figure 6.1).

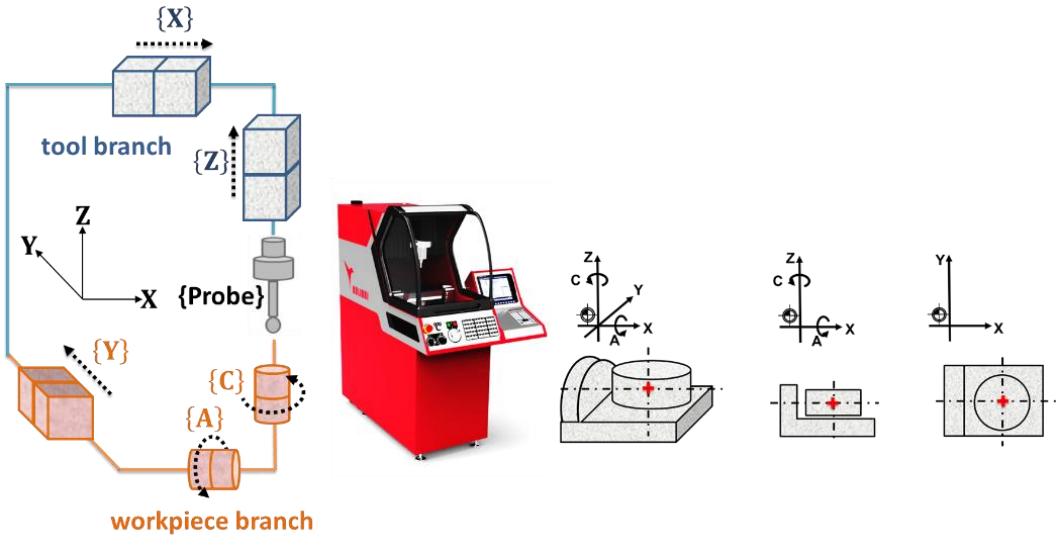

Figure 6.1. Target five-axis Kolibri machine tool, photo and topology.

Assuming the machine without any error, the homogeneous transformation matrix (HTM) of the nominal tooltip position and orientation with respect to the nominal workpiece position and orientation is,

$$ {}^{w_n}\boldsymbol{T}_{t_n} = ({}^{f}\boldsymbol{T}_{w_n})^{-1}({}^{f}\boldsymbol{T}_{t_n}) \tag{34} $$

where the first parenthesis contains the HTM of the workpiece position and orientation relative to the foundation frame and the second one is the HTM of the tooltip position and orientation relative to the foundation frame. The *n* subscript stands for nominal. The real machine has errors categorized either as inter-axis (axis location) errors or as intra-axis (error motion) (Soichi Ibaraki & Knapp, 2012). The inter-axis errors (axis location) are the position and orientation errors between two adjacent axes. The intra-axis errors (error motion) are the errors within one axis (Soichi Ibaraki & Knapp, 2012). These two types of errors are called machine error parameters in this paper. The intra- and inter-axis errors lead to linear and angular displacement error of the tool tip relative to the workpiece namely volumetric errors. Assuming rigid body elements with six degrees of freedom, the kinematic model of the actual, and so erroneous, machine tool including intra-axis and inter-axis errors is,

$$ {}^{w_a}\boldsymbol{T}_{t_a} = ({}^{f}\boldsymbol{T}_{w_a})^{-1}({}^{f}\boldsymbol{T}_{t_a}) \tag{35} $$

where the *a* subscript stands for actual. To calibrate the machine tool with an indirect method, error models are used (Abbaszadeh-Mir et al., 2002; Mayer, 2012; McHichi & Mayer, 2014; Md Mizanur & Mayer, 2015; Mohamed Slamani et al., 2010). The error model used here is a 10-error model (Table 6-1) containing 8 inter-axis machine error parameters and two scale mismatches (relative gains only) (Mayer, 2012).

Table 6-1. The studied machine error parameters symbol and their definitions.

Error symbol	Error definition
$E_{B(0X)A}$	Out-of-parallelism angle around Y of the A-axis relative to the X-axis
$E_{C(0Y)A}$	Out-of-squareness angle of the A-axis relative to the Y-axis
$E_{Y(0A)C}$	Y offset between the C and A axes
$E_{A(0Y)C}$	Out-of-squareness of the C-axis relative to the Y-axis
$E_{B(0A)C}$	Out-of-squareness of the C-axis relative to the A-axis
$E_{C(0Y)X}$	Out-of-squareness of the X-axis relative to the Y-axis
$E_{A(0Y)Z}$	Out-of-squareness of the Z-axis relative to the Y-axis
$E_{B(0X)Z}$	Out-of-squareness of the Z-axis relative to the X-axis
E_{YY1}- E_{XX1}	Positioning error gain mismatch of the Y-axis relative to the X-axis
E_{ZZ1}- E_{XX1}	Positioning error gain mismatch of the Z-axis relative to the X-axis

The machine error parameters are indirectly estimated from on-machine touch trigger probings of a reconfigurable uncalibrated master balls artefact (RUMBA) for various angular position combinations of the two machine tool rotary axes (Erkan, Mayer, & Dupont, 2011). The RUMBA artefact is assembled on the machine table. Because the artefact contains no calibrated length, only relative scale gains of the linear axes are estimated. The use of a single ball in the probing procedure instead of multiple balls constitutes a chase-the-ball process (Bringmann & Knapp, 2006). To calculate the machine error parameters indirectly, a system of linear equations is obtained considering the simplifications of small errors, i.e. sin(*error*)=*error* and cos(*error*)=1 and products of errors are neglected. So, the raw volumetric error (E_{RV}) and the machine error parameters and setup errors (E_P) are related to each other by the generated Jacobian of error parameters, J_P , as

$$E_{RV} = (J_P)(E_P) \tag{36}$$

Eq. (6) is solved to estimate E_P .

6.4 Kinematic-based (K-B) error compensation

K-B volumetric error compensation is achieved by reverse kinematics where the errors of the machine are compensated by small corrections of the axis commands. Based on the work of Givi and Mayer (Givi & Mayer, 2014), to bring the tool tip to the desired location, the required tool tip volumetric error compensation is minus the tool tip volumetric error, assuming small volumetric errors. Knowing the required volumetric error compensation for a set of commands $(q_X, q_Y, q_Z, q_A, q_C)$, the required axis command correction, $[\Delta q_X \ \Delta q_Y \ \Delta q_Z \ \Delta q_A \ \Delta q_C]^T$, is calculated by solving

$$[E_{XCV} \ E_{YCV} \ E_{ZCV} \ E_{ACV} \ E_{BCV} \ E_{CCV}]^T = J_q[\Delta q_X \ \Delta q_Y \ \Delta q_Z \ \Delta q_A \ \Delta q_C]^T \quad (37)$$

where J_q, the control Jacobian, is a 6×5 matrix of the first partial derivatives of the volumetric error compensation to the axis command corrections. E_{XCV}, E_{YCV}, E_{ZCV}, E_{ACV}, E_{BCV} and E_{CCV} are the required volumetric error compensation in the X, Y, Z, A, B and C directions, respectively. Eq. (37) is solved iteratively to obtain a numerically accurate solution for the axis command corrections. The process of evaluating the compensation capability of the K-B error compensation is illustrated in Figure 6.2. The compensation effectiveness compares the machine error parameters before and after applying the compensation as,

$$\text{Compensability} = \frac{\left|E_{p(Before\ \text{comp.})}\right| - \left|E_{p(After\ \text{comp.})}\right|}{\left|E_{p(Before\ \text{comp.})}\right|} \quad (38)$$

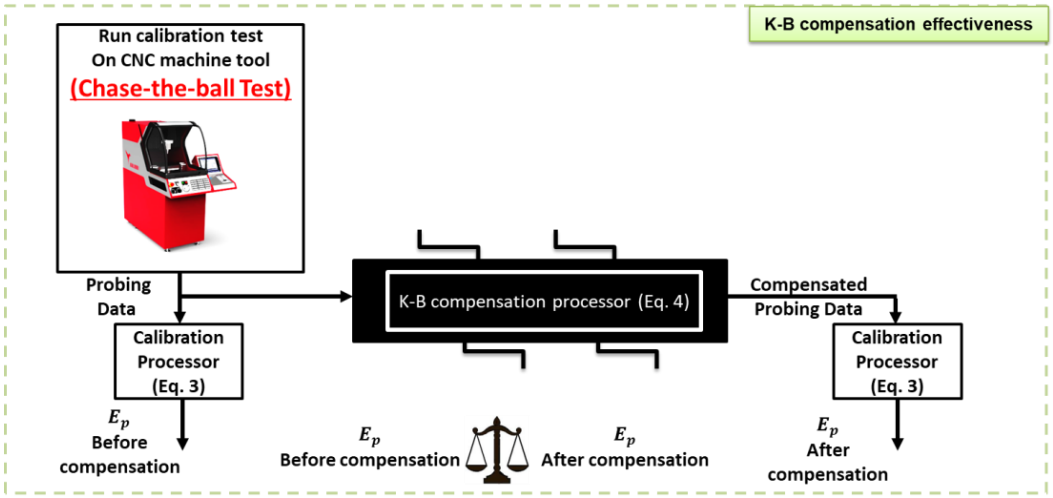

Figure 6.2. The process of evaluating the compensation capability of the K-B error compensation.

6.5 Table-based error compensation

The LUTs are the tables generated in the controllers to improve the machine tool accuracy. In the following sections, two LUT models are studied in order to assess their capability in compensating the volumetric error and the machine error parameters. Because the target machine tool does not have the necessary lookup table functionalities, pseudo lookup tables are generated and used offline.

6.5.1 Lookup tables preliminary model, 25 table-based error compensation (25Poly-T)

In this model, 25 lookup tables, five tables per axis are combined together by summation functionality to correct the associated axis command. Each table function is simulated by a univariate cubic polynomial function of one of the five axes' coordinate. So, each axis command correction is the sum of five univariate third degree polynomial functions, one for each basic axis (Jennifer Creamer et al., 2016).

$$\begin{bmatrix}\Delta q_X\\ \Delta q_Y\\ \Delta q_Z\\ \Delta q_A\\ \Delta q_C\end{bmatrix}=\begin{bmatrix} f_{Xx}(q_X)+f_{Xy}(q_y)+f_{Xz}(q_z)+f_{Xa}(q_a)+f_{Xc}(q_c)\\ f_{Yx}(q_x)+f_{Yy}(q_Y)+f_{Yz}(q_z)+f_{Ya}(q_a)+f_{Yc}(q_c)\\ f_{Zx}(q_x)+f_{Zy}(q_y)+f_{Zz}(q_Z)+f_{Za}(q_a)+f_{Zc}(q_c)\\ f_{Ax}(q_x)+f_{Ay}(q_y)+f_{Az}(q_z)+f_{Aa}(q_A)+f_{Ac}(q_c)\\ f_{Cx}(q_x)+f_{Cy}(q_y)+f_{Cz}(q_z)+f_{Ca}(q_a)+f_{Cc}(q_C)\end{bmatrix}=\begin{bmatrix} LUT_{Xx}+LUT_{Xy}+LUT_{Xz}+LUT_{Xa}+LUT_{Xc}\\ LUT_{Yx}+LUT_{Yy}+LUT_{Yz}+LUT_{Ya}+LUT_{Yc}\\ LUT_{Zx}+LUT_{Zy}+LUT_{Zz}+LUT_{Za}+LUT_{Zc}\\ LUT_{Ax}+LUT_{Ay}+LUT_{Az}+LUT_{Aa}+LUT_{Ac}\\ LUT_{Cx}+LUT_{Cy}+LUT_{Cz}+LUT_{Ca}+LUT_{Cc}\end{bmatrix} \quad (39)$$

Each command correction function is then discretized to fill one LUT. Figure 6.3 shows the LUTs per axis and the relationship between the basic axis commands (the initial commands) and a particular corrected axis. The corrected axis can be X, Y, Z, A or C. The weights are set to one in this model.

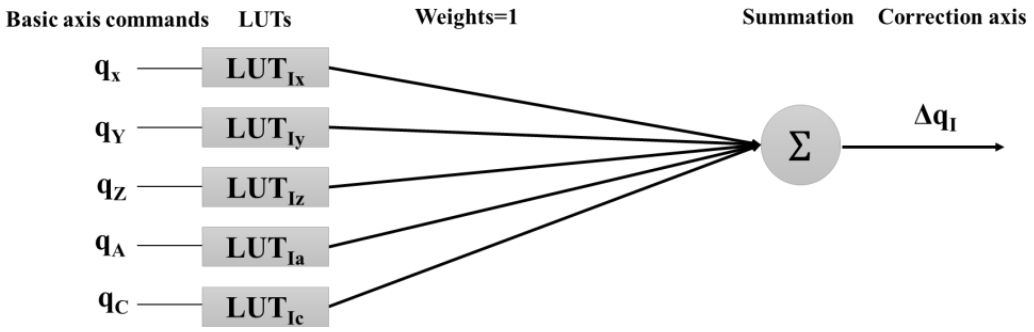

Figure 6.3. A correction axis, here represented as I, is the sum of five basic axis LUTs (25 Poly-T compensation scheme).

Since the numbers of entries for the LUTs are limited, a linear interpolation is applied for commands located between the commands available in the LUTs. To estimate the unknown coefficients of the basic axes' polynomials, Eq. (13) is developed by introducing the polynomials functions as,

$$\begin{bmatrix} \Delta q_X \\ \Delta q_Y \\ \Delta q_Z \\ \Delta q_A \\ \Delta q_C \end{bmatrix} = \begin{bmatrix} a_{Xx0} + a_{Xx1}q_X + a_{Xx2}q_X{}^2 + a_{Xx3}q_X{}^3 + \ldots + a_{Xc0} + a_{Xc1}q_c + a_{Xc2}q_c{}^2 + a_{Xc3}q_c{}^3 \\ a_{Yx0} + a_{Yx1}q_x + a_{Yx2}q_x{}^2 + a_{Yx3}q_x{}^3 + \ldots + a_{Yc0} + a_{Yc1}q_c + a_{Yc2}q_c{}^2 + a_{Yc3}q_c{}^3 \\ a_{Zx0} + a_{Zx1}q_x + a_{Zx2}q_x{}^2 + a_{Zx3}q_x{}^3 + \ldots + a_{Zc0} + a_{Zc1}q_c + a_{Zc2}q_c{}^2 + a_{Zc3}q_c{}^3 \\ a_{Ax0} + a_{Ax1}q_x + a_{Ax2}q_x{}^2 + a_{Ax3}q_x{}^3 + \ldots + a_{Ac0} + a_{Ac1}q_c + a_{Ac2}q_c{}^2 + a_{Ac3}q_c{}^3 \\ a_{Cx0} + a_{Cx1}q_x + a_{Cx2}q_x{}^2 + a_{Cx3}q_x{}^3 + \ldots + a_{Cc0} + a_{Cc1}q_C + a_{Cc2}q_C{}^2 + a_{Cc3}q_C{}^3 \end{bmatrix} \cdot \qquad (40)$$

The a_{Xx0}, a_{Xx1}, a_{Xx2}, …, a_{Cc0}, a_{Cc1}, a_{Cc2}, a_{Cc3} are the unknown polynomial coefficients used for generating the tables and from now on called table coefficients. They have three subscripts from left to right, the corrected axis, the basic axis and the degree of the basic axis command value. Constructing the extended control Jacobian in which the compensated volumetric errors are directly related to the table coefficients results in,

$$[E_{XCV} \quad E_{YCV} \quad E_{ZCV} \quad E_{ACV} \quad E_{BCV} \quad E_{CCV}]^T = J_{q\_extended} \left[a_{Xx0} \; a_{Xx1} \; a_{Xx2} \; \cdots \; a_{Cc1} \; a_{Cc2} \; a_{Cc3} \right]^T \qquad (41)$$

where $J_{q\_extended}$ is the extended control Jacobian containing the first partial derivatives of the volumetric error to the lookup table coefficients.

6.5.2 Error compensation lookup tables enriched model, 23 table-based error compensation (23Trigo-T)

The second lookup table model consists in using the summation and multiplication functionalities of the tables. This model is inspired by the nominal kinematics of the five-axis machine tools in which the control Jacobian matrix and its inverse also include some multiplications of the axes positions or axes positions functions. For instance, the nominal control Jacobian matrix for a five-axis machine tool with the topology of wCAYfXZt is,

$$J_{q(wCAYFXZt)} = \begin{bmatrix} 1 & 0 & 0 & 0 & \sin(q_A)q_Z - \cos(q_A)q_Y \\ 0 & -1 & 0 & q_Z & -\cos(q_A)q_X \\ 0 & 0 & 1 & q_Y & -\sin(q_A)q_X \\ 0 & 0 & 0 & -1 & 0 \\ 0 & 0 & 0 & 0 & \sin(q_A) \\ 0 & 0 & 0 & 0 & -\cos(q_A) \end{bmatrix} \tag{42}$$

and its pseudoinverse is,

$$J^{\dagger}_{q(wCAYFXZt)} = \begin{bmatrix} 1 & 0 & 0 & 0 & \sin(q_A)(\cos(q_A)q_Y - \sin(q_A)q_Z) & -\cos(q_A)(\cos(q_A)q_Y - \sin(q_A)q_Z) \\ 0 & -1 & 0 & -q_Z & \sin(q_A)(\cos(q_A)q_Y - \sin(q_A)q_Z) & \cos^2(q_A)q_X \\ 0 & 0 & 1 & q_Y & \sin^2(q_A)q_X & -\cos(q_A)\sin(q_A)q_X \\ 0 & 0 & 0 & -1 & 0 & 0 \\ 0 & 0 & 0 & 0 & \sin(q_A) & \cos(q_A) \end{bmatrix} \tag{43}$$

where q_X, q_Y, q_Z, q_A and q_C are the axis positions of the X, Y, Z, A and C axes, respectively. The columns in the control Jacobian associated with the rotary axes commands contain multiplication and trigonometric functions. Hence, it is hypothesized that the command corrections may perform better if it contains such terms.

Using the possible combinations of trigonometric terms in the compensation model, the command corrections functions are,

$$
\begin{aligned}
\Delta q_I = [&a_{I0} + \\
&q_X (a_{I1} + a_{I2}\cos(q_A) + a_{I3}\sin(q_A) + a_{I4}\cos(q_A)\sin(q_A) + a_{I5}\sin^2(q_A) + a_{I6}\cos^2(q_A)) + \\
&q_Y (a_{I7} + a_{I8}\cos(q_A) + a_{I9}\sin(q_A) + a_{I10}\cos(q_A)\sin(q_A) + a_{I11}\sin^2(q_A) + a_{I12}\cos^2(q_A)) + \\
&q_Z (a_{I13} + a_{I14}\cos(q_A) + a_{I15}\sin(q_A) + a_{I16}\cos(q_A)\sin(q_A) + a_{I17}\sin^2(q_A) + a_{I18}\cos^2(q_A))]
\end{aligned} \tag{44}
$$

$$
\Delta q_A = [a_{A0} + a_{A1}\cos(q_A) + a_{A2}\sin(q_A) + a_{A3}\cos(q_A)\sin(q_A) + a_{A4}\sin^2(q_A) + a_{A5}\cos^2(q_A))]
$$

$$
\Delta q_C = [a_{C0} + a_{C1}\cos(q_A) + a_{C2}\sin(q_A) + a_{C3}\cos(q_A)\sin(q_A) + a_{C4}\sin^2(q_A) + a_{C5}\cos^2(q_A))]
$$

where the *I* letter is substituted with *X*, *Y* or *Z*. The trigonometric terms are approximated by truncated Taylor series. This process is not part of table generation but part of the optimization and solution while using the Matlab® function Fitnlm to calculate the coefficients. In total, 69 table coefficients are estimated. The objective functions are the discrepancies between the axes corrections obtained by the 23Trigo-T model and those obtained with the K-B model. The input data base for the optimization is a 5D grid considering 10 nodes per axis for a total of 10^5 grid nodes (set of nominal commands). Generating the lookup tables follows the rules of the Siemens controller interpolatory compensation functions (Weikert, 2004) where just one weight can be assigned to each table and each table can have one base axis (input axis) and one compensation axis (output axis). Having calculated the coefficients, 23 tables (Figure 6.4) are generated.

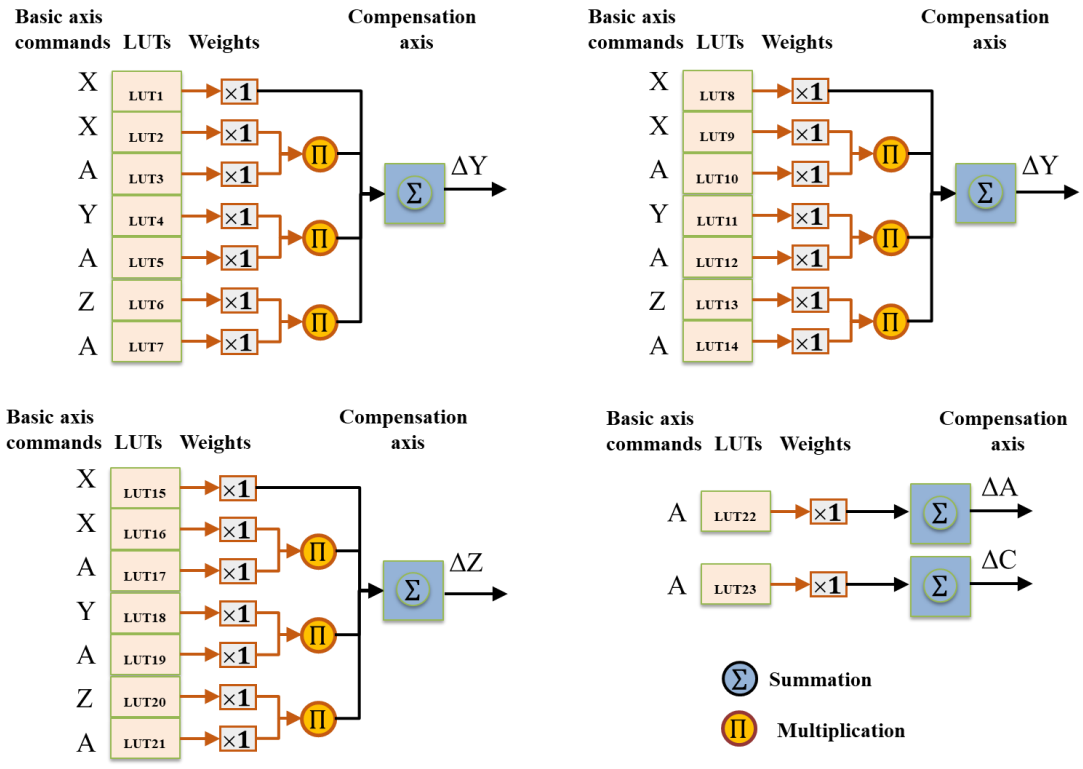

Figure 6.4. Schematic of the combinations of lookup tables outputs for a five-axis machine tool with topology of wCAYFXZt (23Trigo-T).

For a set of command, the linear interpolation is applied to each LUT's entry and the command corrections are calculated by,

$$\begin{aligned}
\Delta q_X &= [LUT_1 + LUT_2 LUT_3 + LUT_4 LUT_5 + LUT_6 LUT_7] \\
\Delta q_Y &= [LUT_8 + LUT_9 LUT_{10} + LUT_{11} LUT_{12} + LUT_{13} LUT_{14}] \\
\Delta q_Z &= [LUT_{15} + LUT_{16} LUT_{17} + LUT_{18} LUT_{19} + LUT_{20} LUT_{21}] \\
\Delta q_A &= [LUT_{22}] \\
\Delta q_C &= [LUT_{23}]
\end{aligned} \tag{45}$$

where LUT_1 to LUT_{23} are the interpolated outputs of the 23 lookup tables.

6.5.3 Evaluation of the proposed LUT schemes in compensating geometric machine error parameters

The evaluation process of the proposed LUT scheme is illustrated in Figure 6.5. The estimated machine error parameters (E_p) from the calibration RUMBA test are used to predict the volumetric errors (VE) at the grid nodes of nominal joint commands using the forward kinematic model of Eq.

(2). The grid node nominal joint commands and their associated K-B command corrections are used to generate the coefficients of the 25Poly-T and the 23Trigo-T table function coefficients from which 25 tables for 25Poly-T and 23 tables for 23Trigo-T are generated. The number of table entries for each table are 10. For validating the compensation procedure, a chase-the-ball calibration test is run on the machine tool. The probing data is processed to estimate the machine error parameters before compensation. The probing data is also compensated by applying linear interpolation on the 25 or 23 lookup table entries. The machine error parameters after compensation are obtained by re-estimating the compensated probing data. The compensation effectiveness is calculated by Eq. (7).

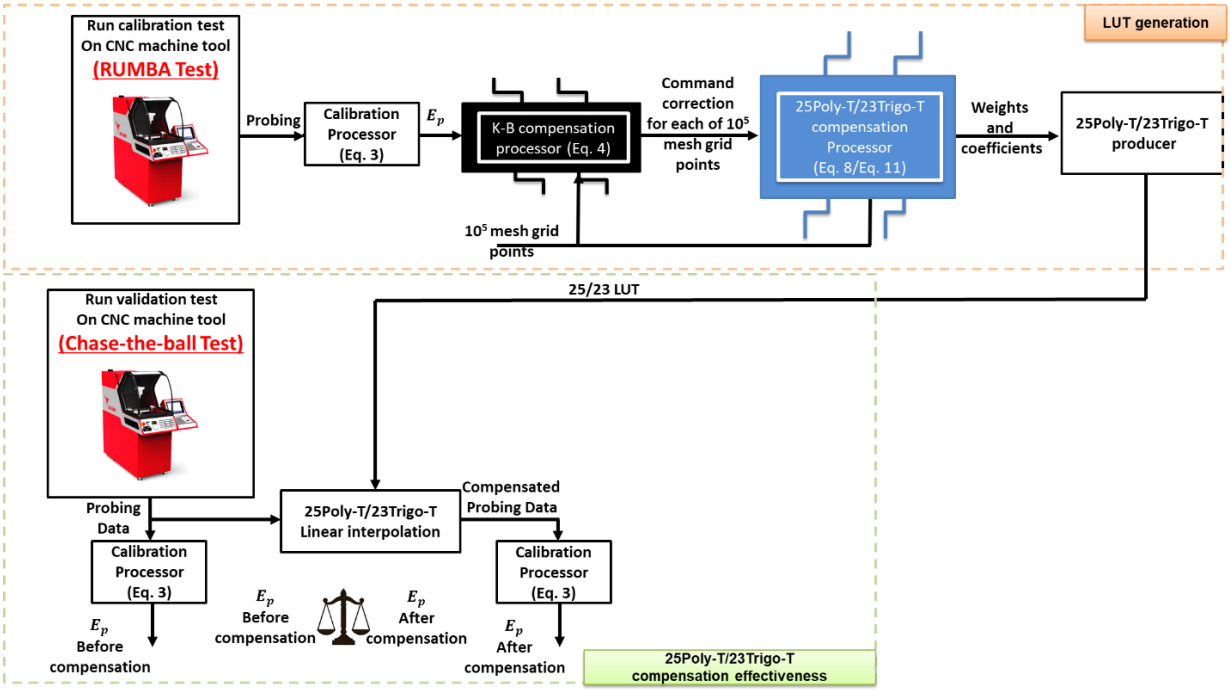

Figure 6.5. The process of generating the 25Poly-T and 23Trigo-T and verifying the effectiveness of the LUTs in correcting machine error parameters.

6.6 Mathematical model validation

Ten case studies are conducted, each simulating one non-zero machine error parameter as shown in Table 6-2. The processes shown in Figure 6.2 and Figure 6.5 are run but with simulated probing data without considering the RUMBA or Chase-the-ball calibration tests.

Table 6-2. The values of the simulated geometric error parameters for the ten case studies to explore the effectiveness of the table-based as well as the kinematic-based error compensation.

Error Parameter	**Case Studies (C. S.)**									
	C. S. 1	**C. S. 2**	**C. S. 3**	**C. S. 4**	**C. S. 5**	**C. S. 6**	**C. S. 7**	**C. S. 8**	**C. S. 9**	**C. S. 10**
$E_{B(0X)A\ [mrad]}$	0.4	0	0	0	0	0	0	0	0	0
$E_{C(0Y)A\ [mrad]}$	0	0.4	0	0	0	0	0	0	0	0
$E_{Y(0A)C\ [\mu m]}$	0	0	10	0	0	0	0	0	0	0
$E_{A(0Y)C\ [mrad]}$	0	0	0	0.4	0	0	0	0	0	0
$E_{B(0A)C\ [mrad]}$	0	0	0	0	0.4	0	0	0	0	0
$E_{C(0Y)X\ [mrad]}$	0	0	0	0	0	0.4	0	0	0	0
$E_{A(0Y)Z\ [mrad]}$	0	0	0	0	0	0	0.4	0	0	0
$E_{B(0X)Z\ [mrad]}$	0	0	0	0	0	0	0	0.4	0	0
E_{YY1}- $E_{XX1\ [\mu m/mm]}$	0	0	0	0	0	0	0	0	0.04	0
E_{ZZ1}- $E_{XX1\ [\mu m/mm]}$	0	0	0	0	0	0	0	0	0	0.04

Figure 6.6 shows the compensation effectiveness of individual machine error parameters using the K-B, 25Poly-T and 23Trigo-T compensation schemes. The maximum and the mean norm of the estimated volumetric error vectors (VE) before and after applying the three compensation models are shown in Figure 6.7. The largest simulated maximum and mean VE norms before compensation are 38 and 35 µm, respectively where the ranges are 260, 420 and 240 mm for X, Y and Z, respectively. As anticipated, all error parameters and the maximum and the mean norms of VEs are compensated using K-B error compensation since it is kinematically correct. As seen in Figure 6.6. 25Poly-T and 23Trigo-T error compensation models are able to compensate EA0C, EY0C, EA0Z, EYY1- EXX1 and EZZ1- EXX1. Their associated maximum and mean norms of VEs are likewise compensated (Figure 6.7). Some improvements are seen in EB0A (Figure 6.6, (C.S.1)) after using 25Poly-T. However, by applying 25Poly-T, the global minimizations of all simulated volumetric error vectors with a least square approach distributes EB0A between EB0A, EB0C and EY0C. Its maximum and mean norms of VEs are respectively reduced to about 23 µm and 13 µm (Figure 6.7). Similarly, EB0A, EC0A, EB0C, EC0X and EB0Z are partly reduced resulting in increasing the other errors in the model after applying the compensation, which is not desirable (Figure 6.6, (C.S.1), (C.S.2), (C.S.5), (C.S.6) and (C.S.8)). Values for the maximum and the mean norms of VEs for the aforementioned errors confirm that the compensation is partial (Figure 6.7). The trigonometric function based model 23Trigo-T overcomes the weaknesses of the 25Poly-T in correcting the EB0C, EB0A, EC0A, EC0X and EB0Z without significant increase in the other error parameters. The maximum and the mean norm of VE are reduced to less than 1 µm using the 23Trigo-T (Figure 6.7).

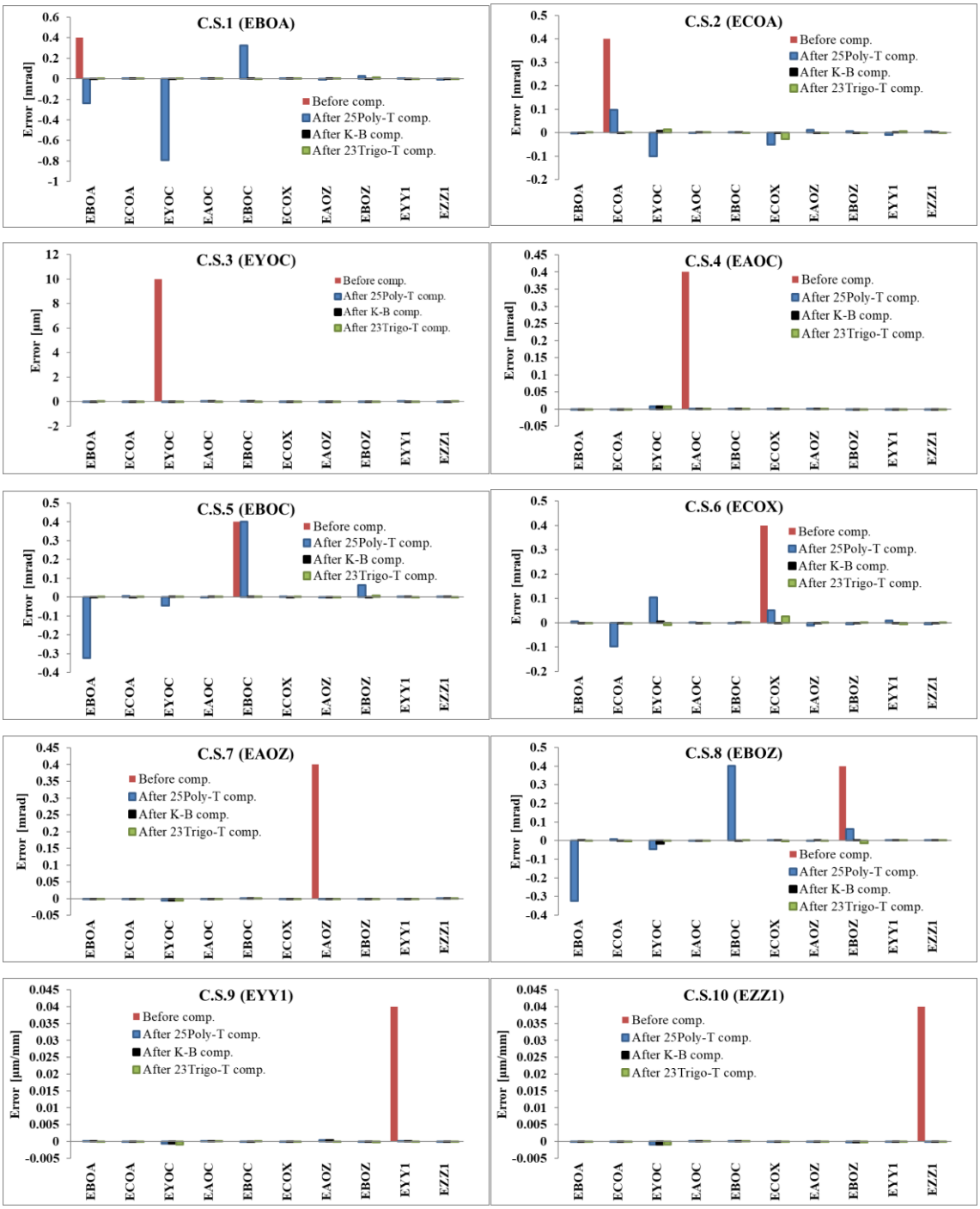

Figure 6.6. Error parameters before and after kinematic-based, 25Poly-T and 23Trigo-T compensation schemes for case studies (C.S.) 1 to 10 as defined in Table 6-2.

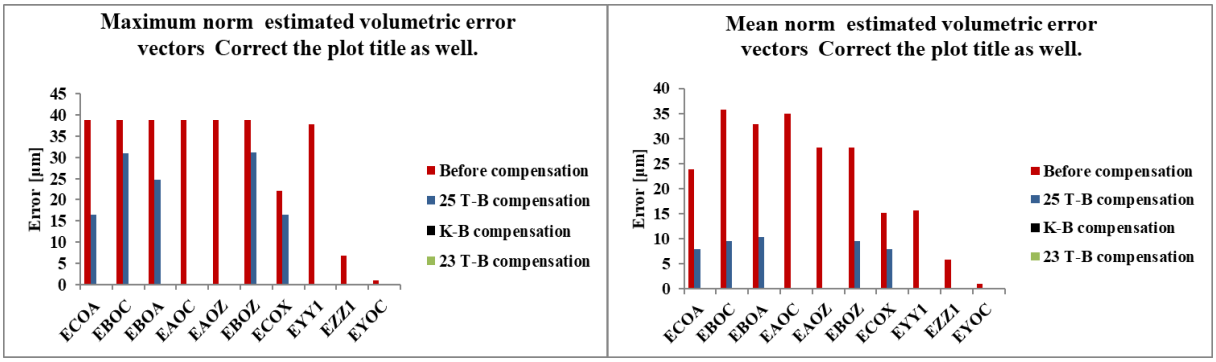

Figure 6.7. Maximum and mean norm estimated volumetric error vectors before and after kinematic-based (K-B), 25Poly-T and 23Trigo-T volumetric error compensation.

In order to gain some idea of the potential generality of the chosen terms and the compensation model, another simulation is run for a five-axis machine with the topology wCAYfXZt where the A rotary axis has an angle of 45˚ with the X-axis (Figure 6.8). The process shown in Figure 6.5 is used for generating the 23 lookup tables to compensate eight inter-axis, two spindle and three scale errors. The same table functions (Eq. (31)) and the same combinatory of the tables (Eq. (33)) are used to produce such lookup tables. The simulation results show that more than 99% of the maximum and the mean norm of the volumetric errors are compensated. The geometric errors are also significantly dropped by more than 99%. The simulation results support the efficacy of the proposed table-based compensation scheme (23Trigo-T) for compensating geometric and volumetric errors for another five-axis machine tool with nominally non-orthogonal axes.

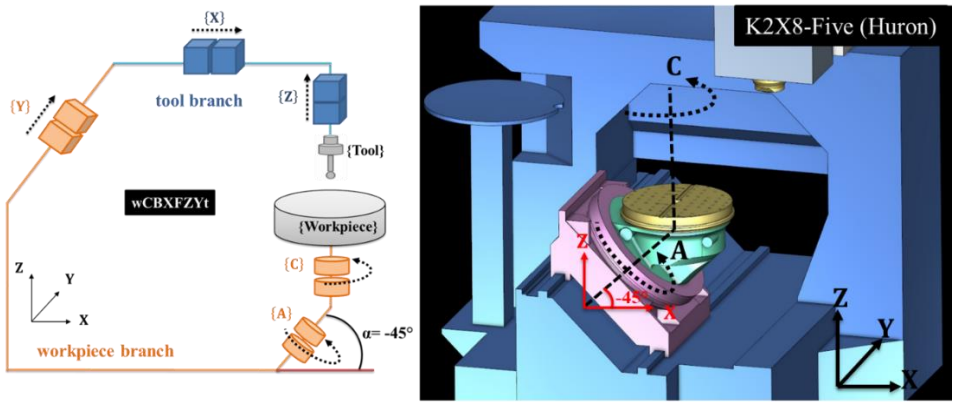

Figure 6.8. Schematic of the non-orthogonal five-axis machine tool (K2X8-Five, Huron)

6.7 Experimental test

The experimental test involves calibration, generating the LUTs and evaluating the compensation effectiveness. The stroke length of the machine tool axes are 260, 420 and 240 mm for the X-, Y- and Z-axis, respectively. The maximum rotations of the A- and C-axis are 240° and 360°, respectively but the accessible probing angles for indexing the rotary axes are from –55° to +55° and from 0° to 330° for the A- and C-axis, respectively. The error parameters are estimated using probing data from a RUMBA made of four master ball positions mounted and probed sequentially, in four separate setups named 1 to 4, which reduces the risks of collisions and obstruction during probing operations. The ball positions form a quadrilateral as shown in Figure 6.9. The master balls installed in setups 1 and 2 have a height of 37.5 mm from the base to the center of the ceramic balls, and the master balls installed in setups 3 and 4 have a height of 47.5 mm. Both balls have a diameter of 20 mm. For each setup, the master ball is measured with the measurement strategy detailed in Table 6-3. The two rotary axes are indexed in such a way as to cover as much of the total stroke of the rotary axes. Since no reference length is measured, it is not possible to distinguish the scale errors with respect to the international meter as was pointed out in (Erkan et al., 2011). However, the relative scale gain errors are estimated.

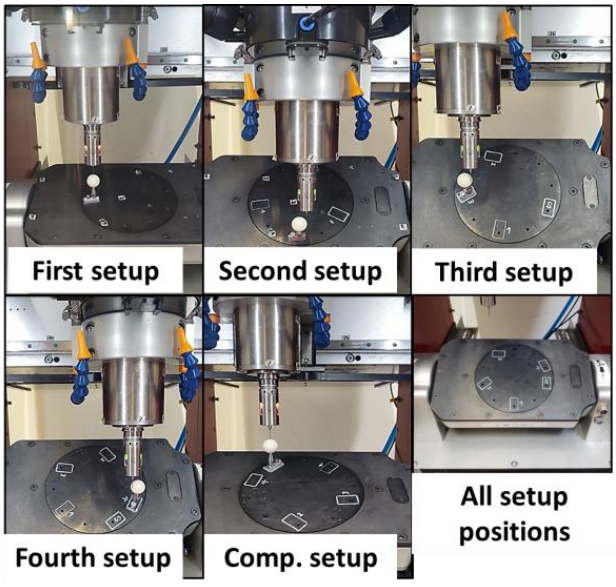

Figure 6.9. The setups for machine tool calibration and compensation validation.

The touch probe Hexagon IRP40.50 with a probe tip radius of 0.5 mm and a total length of 74 mm is used for both calibration and compensation effectiveness validation. The five setups and the touch probe are shown in Figure 6.9. Each ball is measured using five points, one at the pole in Z and four around the equator in an equidistant pattern that is rotated 45° relative to the machine Z axis to avoid potential collisions with the ball support. The measurement for one master ball is shown in Figure 6.10.

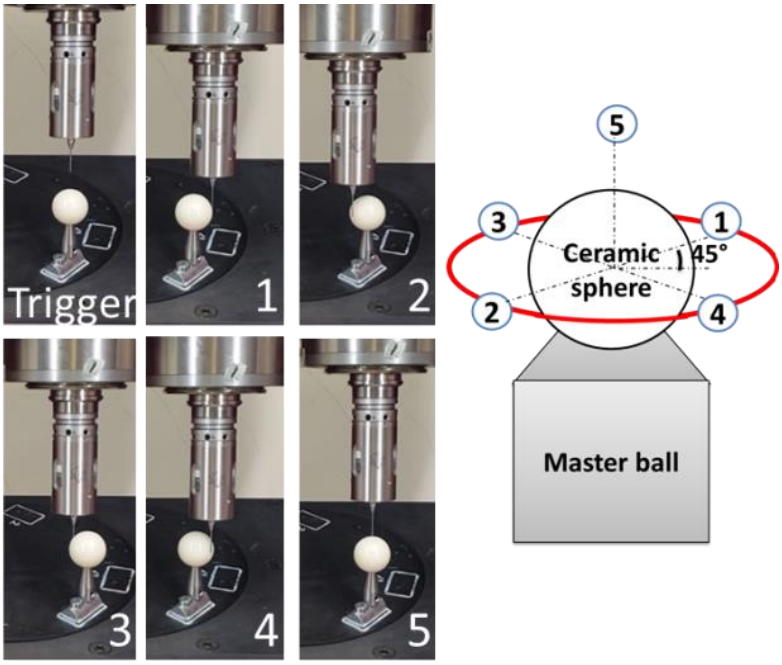

Figure 6.10. The measurement of the master ball (ball approach point, first, second, third, fourth and fifth probings).

The compensation validation setup, labeled "S", constitutes a "Chase-the-ball" procedure (Bringmann & Knapp, 2006) with a single master ball of diameter 10 mm and a height of 37.5 mm. The rotary axes indexations, shown in Table 6-3, allow estimating the machine error parameters. The setup is shown in Figure 6.9. The measurement process for calibration and compensation validation was repeated three times, once for each of three consecutive days, while the average temperature in the laboratory was between 21 and 22°C. Each ball probing lasted 1 min 50 s. The calibration test lasted 77 min for 42 A and C rotary axis indexation pairs while the compensation validation test lasted 110 min for 60 indexation pairs.

Table 6-3. The A and C indexations pairs for calibration and compensation validation tests.

Strategy for measurement	Rotary axes indexations (c° , a°)
Calibration test (setup 1,2,3,4)	(60, 15) (180, 30) (280, 45) (340, 50) (240, 40) (120, 20) (0, 0) (-100, -20) (250, -40) (350, -55) (-310, -55) (-40, -25) (180, 0) (280, 0) (360, 0) (320, 0) (210, 0) (-160, 0) (-300, 0) (-220, 0) (-50, 0) (0, 15) (0, 40) (0, 55) (0, 45) (0, 30) (0, -20) (0, -45) (0, -55) (0, -35) (-30, 44) (-208, 55) (-318, 36) (45, 30) (326, 21) (290, 9) (-12, -16) (-304, -54) (-10, -40) (100, -17) (197, -38) (345, -5)
Compensation test (setup "S")	(55, 8) (120, 16) (180, 40) (240, 38) (300, 55) (330, 50) (270, 45) (210, 36) (150, 23) (90, 12) (30, 4) (-30, -5) (-90, -12) (-150, -28) (-210, -31) (-270, -48) (-330, -52) (-300, -50) (-240, -43) (-180, -34) (-120, -23) (-55, -11) (140, 8) (190, 18) (250, 12) (290, 30) (310, 22) (10, 47) (50, 24) (100, 38) (160, 41) (200, 53) (-45, -34) (-140, -43) (-170, -50) (-220, -20) (-280, -15) (-310, -10) (-70, -5) (135, -16) (280, -50) (94, -36) (20, -10) (200, -26) (-40, 28) (-300, 50) (-280, 20) (-100, 37) (-280, 10) (0, 0) (90, 0) (240, 0) (300, 0) (180, 0) (45, 0) (-45, 0) (-180, 0) (-300, 0) (-240, 0) (-90, 0)

6.8 Results and discussions

The probing test data of the first to fourth calibration setups are used to estimate the ten machine tool error parameters by iteratively solving Eq. (3). The Jacobian of error parameters has a normalized condition number of 206. Table 6-4 lists the mean values and standard deviations of the estimated geometric machine error parameters of three test replicates. The mean of the volumetric error norms is 62.1 μm while the mean of the unexplained volumetric error norms of the tool tip relative to the master ball, which is the portion that the estimated parameters cannot predict, is 4.6 μm. EY(0A)C, EB(0X)A, EC(0Y)A, EA(0Y)Z, EY(0A)C and EYY1-EXX1 are amongst the largest errors.

Table 6-4. The calibration test results (RUMBA test).

Symbol Unit	EB0A [mrad]	EC0A [mrad]	EY0C [μm]	EA0C [mrad]	EB0C [mrad]	EC0X [mrad]	EA0Z [mrad]	EB0Z [mrad]	EYY1-EXX1 [μm/mm]	EZZ1-EXX1 [μm/mm]
Mean	1.09	-0.86	42.10	0.07	0.03	0.14	-0.44	0.11	-0.61	-0.22
σ	0.120	0.043	0.900	0.001	0.005	0.004	0.002	0.002	0.001	0.001

Table 6-5 lists the estimated mean values for the same ten error parameters and their associated standard deviations using the data from setup "S", which will be used for validation, gathered before table-based compensation. The condition number for the Jacobian is 216. They are close to

the calibration values. The estimated error parameters are similar to those obtain from the first four setups which suggests that the potential for calibration of the validation test is high.

Table 6-5. The validation results before compensation (Chase-the-ball).

Symbol Unit	EB0A [mrad]	EC0A [mrad]	EY0C [µm]	EA0C [mrad]	EB0C [mrad]	EC0X [mrad]	EA0Z [mrad]	EB0Z [mrad]	EYY1-EXX1 [µm/mm]	EZZ1-EXX1 [µm/mm]
Mean	1.29	-0.98	41.40	0.07	0.03	0.15	-0.48	0.15	-0.64	-0.25
σ	0.230	0.031	0.400	0.003	0.004	0.003	0.004	0.003	0.009	0.008

A grid having ten points per axis for a total of 10^5 grid nodes was built as the input data structure for generating the LUTs. The grid area covers the calibration range of the axes to avoid extrapolation. The error parameters listed in Table 6-4 are used to generate the LUTs for the 25Poly-T and 23Trigo-T models. The tables have 100 command entries with their associate corrections. The processes of generating the LUTs are programmed in Matlab®.

The capability of the generated compensation tables for the validation data, setup ”S”, is also evaluated by processing compensated probing data to estimate the effective, or apparent, geometry of the machine. The four sets of estimated error parameters, before compensation, after K-B compensation, after 25Poly-T compensation and after 23Trigo-T compensation are shown in Figure 6.11.

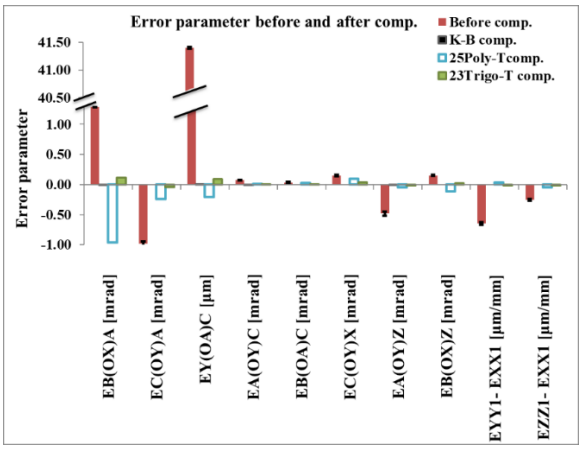

Figure 6.11. The effective geometric machine error parameters before and after pseudo compensation of the probing results for the validation test, “S” data, before compensation and after applying each of the three error compensation methods: K-B, 25Poly-T and 23Trigo-T.

The compensation effectiveness values are listed in Table 6-6. All compensation effectiveness values are above 88% for the 23Trigo-T. The compensation effectiveness of dominant error EB0A using the 25Poly-T is 26% whereas it is 89% with the 23Trigo-T. Another significant compensation

effectiveness improvement, although the parameter value is quite small, is seen in EB0C where the effectiveness is increased from 3% using 25Poly-T to 88% using 23Trigo-T. Significant improvements are also seen for EB0Z and EC0X. Significant relative improvements are seen both for large and small error parameters. In comparison with the 25Poly-T model, the 23Trigo-T appears to better mimics the K-B theoretical compensation model. The mean norm of the volumetric errors is 62.1 μm without any compensation. Using 25Poly-T yields a mean volumetric error norm of 23.3 μm. However, this value is further reduced to 4.1 μm for the 23Trigo-T, close to the 3.2 μm achieved by the theoretically exact kinematic model, K-B. The maximum volumetric errors norm before and after compensation using 25Poly-T and 23Trigo-T compensations are respectively 102.8, 38.2 and 7.2 μm (Table 6-7), whereas, K-B achieves 5.3 μm.

Table 6-6. The compensation effectiveness for all three error compensation methods: K-B, 25Poly-T and 23Trigo-T Eq. (7).

Error parameter	**Compensation effectiveness**		
	K-B error compensation	**25Poly-T error compensation**	**23Trigo-T error compensation**
EB0A	89%	26%	89%
EC0A	98%	76%	98%
EY0C	99%	98%	98%
EA0C	98%	98%	98%
EB0C	90%	3%	88%
EC0X	93%	38%	89%
EA0Z	98%	90%	94%
EB0Z	87%	27%	87%
EYY1- EXX1	94%	94%	94%
EZZ1- EXX1	93%	81%	91%

Table 6-7. The mean and maximum norm of the volumetric error vectors before compensation and after K-B, 25Poly-T and 23Trigo-T error compensation.

	Before compensation (μm)	K-B error compensation (μm)	25Poly-T error compensation (μm)	23Trigo-T error compensation (μm)
Mean volumetric error norm ($\overline{\|\|VE\|\|}$)	62.1	3.2	23.3	4.1
Maximum volumetric error norm ($\max\|\|VE\|\|$)	102.8	5.3	38.2	7.2

6.9 Conclusion

A trigonometrically enriched scheme using multiplication and summation functions is proposed in this paper to compensate the volumetric errors (VE) and the geometric error parameters. The enriched scheme finds its inspiration in the mathematical terms of the symbolically generated inverse of the control Jacobian. The 25Poly-T is generated using univariate polynomial functions of the five basic axes. The 23Trigo-T scheme uses trigonometric terms as can be found in the Jacobian of commands and its inverse. The new scheme performance is compared to the 25Poly-T scheme as well as to the theoretically exact inverse kinematics based (K-B) error compensation model. Each compensation model is used to offline correct the on-machine measurements of a Chase-the-ball type test for validation purposes. The test data is used, before and after correction, to estimate the effective machine error parameters of the machine as well as its volumetric errors. The compensation effectiveness of the three schemes is quantified by the reduction in the effective machine error parameters and also the volumetric errors.

Error parameters EB0A, EB0C, EC0X and EB0Z which were compensated by at most 38% by the 25Poly-T are compensated by at least 87% by the 23Trigo-T schemes, a result similar to that for the K-B error compensation. The maximum volumetric error norm for the non-compensated data and for the 25Poly-T, 23Trigo-T and K-B compensation schemes are respectively 102.8, 38.2, 7.2 and 5.3 µm, which represents a reduction by 92% for the proposed 23Trigo-T scheme which is a further reduction of 32% compared to the 25Poly-T scheme and is only 2% less than the performance of the K-B theoretically exact compensation scheme.

6.10 Acknowledgment

This research was supported by Natural Sciences and Engineering Research Council of Canada (NSERC) under the CANRIMT Strategic Research Network Grant NETGP 479639-15 and by the Deutsche Forschungsgemeinschaft (DFG, German Research Foundation) under Germany's Excellence Strategy – EXC 2023 Internet of Production – 390621612.

6.11 References

Abbaszadeh-Mir, Y., Mayer, J. R. R., Cloutier, G., & Fortin, C. (2002). Theory and simulation for the identification of the link geometric errors for a five-axis machine tool using a

telescoping magnetic ball-bar. *International Journal of Production Research, 40*(18), 4781-4797. doi:10.1080/00207540210164459

AG, S. (2010). Function description VCS (Volumetric Compensation System).

Bringmann, B., & Knapp, W. (2006). Model-based 'Chase-the-Ball' Calibration of a 5-Axes Machining Center. *CIRP Annals, 55*(1), 531-534. doi:10.1016/s0007-8506(07)60475-2

Castro, H. F. F., & Burdekin, M. (2005). Evaluation of the measurement uncertainty of a positional error calibrator based on a laser interferometer. *International Journal of Machine Tools and Manufacture, 45*(3), 285-291. doi:10.1016/j.ijmachtools.2004.08.012

Creamer, J., Bristow, D. A., & Landers, R. G. (2017). Selection of limited and constrained compensation tables for five-axis machine tools. *International Journal of Advanced Manufacturing Technology, 92*(1-4), 1315-1327. doi:10.1007/s00170-017-0230-4

Creamer, J., Sammons, P. M., Bristow, D. A., Landers, R. G., Freeman, P. L., & Easley, S. J. (2017). Table-Based Volumetric Error Compensation of Large Five-Axis Machine Tools. *Journal of Manufacturing Science and Engineering, 139*(2). doi:10.1115/1.4034399

Donmez, M. A., Bloquist, D. S., Hocken, R. J., & Liu, C. R. (1986). A general methodology for machine tool accuracy enhancement by error compensation. *Precision Engineering, 4*, 187–196.

Erkan, T., Mayer, J. R. R., & Dupont, Y. (2011). Volumetric distortion assessment of a five-axis machine by probing a 3D reconfigurable uncalibrated master ball artefact. *Precision Engineering, 35*(1), 116-125. doi:10.1016/j.precisioneng.2010.08.003

Esmaeili, S., & Mayer, J. R. R. (2020). An Integrated Geometric and Hysteretic Error Model of a Three Axis Machine Tool and Its Identification With a 3D Telescoping Ball-Bar. *Journal of Manufacturing and Materials Processing, 4*(1). doi:10.3390/jmmp4010024

Florussen, G. H. J., & Spaan, H. A. M. (2007). Static R-test: allocating the centreline of rotary axes of machine tools. *International Conference on Laser Metrology, CMM and Machine Tool Performance, LAMDAMAP*, 196-202.

Givi, M., & Mayer, J. R. R. (2014). Volumetric error formulation and mismatch test for five-axis CNC machine compensation using differential kinematics and ephemeral G-code. *International Journal of Advanced Manufacturing Technology, 77*(9-12), 1645-1653. doi:10.1007/s00170-014-6558-0

Givi, M., & Mayer, J. R. R. (2016). Optimized volumetric error compensation for five-axis machine tools considering relevance and compensability. *CIRP Annals, 12*, 44-55. doi:10.1016/j.cirpj.2015.09.002

Groos, L., Held, C., Keller, F., Wendt, K., Franke, M., & Gerwien, N. (2020). Mapping and compensation of geometric errors of a machine tool at different constant ambient temperatures. *Precision Engineering, 63*, 10-17. doi:https://doi.org/10.1016/j.precisioneng.2020.01.001

Schwenke, H., Franke, M., & Hannaford, J. (2005). Error Mapping of CMMs and Machine Tools by a Single Tracking Interferometer. CIRP Ann. Manuf. Technol., 54, 475–478.

Härtig, F., Keck, C., Kniel, K., Schwenke, H., Härtig, F., & Kniel, K. (2009). Selbstnachführendes Laserinterferometer für die Koordinatenmesstechnik (Tracking Laser Interferometer for Coordinate Metrology). *Technisches Messen, 71*, 227-232.

Hocken. (1993). Software Compensation of Precision Machines. *A Report from Precision Engineering Laboratory UNC Charlotte to National Institute of Standards and Technology*.

Ibaraki, S., Iritani, T., & Matsushita, T. (2010). Error Calibration on Fiveaxis Machine Tools by on-the-machine Measurement of Artifacts using a Touch-trigger Probe. *Proceeding of 4th CIRP International Conference on High Performance Cutting (CIRP HPC 2010)*.

Ibaraki, S., & Knapp, W. (2012). Indirect Measurement of Volumetric Accuracy for Three-Axis and Five-Axis Machine Tools: A Review. *International Journal of Automation Technology, 6*, 110-124. doi:10.3929/ethz-a-007593181

Lei, W. T., & Sung, M. P. (2008). NURBS-based fast geometric error compensation for CNC machine tools. *International Journal of Machine Tools and Manufacture, 48*(3-4), 307-319. doi:10.1016/j.ijmachtools.2007.10.007

Majda, P. (2012). Modeling of geometric errors of linear guideway and their influence on joint kinematic error in machine tools. *Precision Engineering, 36*(3), 369-378. doi:10.1016/j.precisioneng.2012.02.001

Mayer, J. R. R. (2012). Five-axis machine tool calibration by probing a scale enriched reconfigurable uncalibrated master balls artefact. *CIRP Annals, 61*(1), 515-518. doi:10.1016/j.cirp.2012.03.022

McHichi, N. A., & Mayer, J. R. R. (2014). Axis Location Errors and Error Motions Calibration for a Five-axis Machine Tool Using the SAMBA Method. *Procedia CIRP, 14*, 305-310. doi:10.1016/j.procir.2014.03.088

Md Mizanur, R., & Mayer, J. R. R. (2015). Five axis machine tool volumetric error prediction through an indirect estimation of intra- and inter-axis error parameters by probing facets on a scale enriched uncalibrated indigenous artefact. *Precision Engineering, 40*, 94-105. doi:10.1016/j.precisioneng.2014.10.010

Ramesh, R., Mannan, M. A., & Poo, A. N. (2000). Error compensation in machine tools — a review Part I: geometric, cutting-force induced and fixturedependent errors. *International Journal of Machine Tools and Manufacture, 40*, 1235-1256.

Sartori, S., & Zhang, G. X. (1995). Geometric Error Measurement and Compensation of Machines. *CIRP Annals, 44*(2), 599-609. doi:10.1016/s0007-8506(07)60507-1

Schwenke, H., Knapp, W., Haitjema, H., Weckenmann, A., Schmitt, R., & Delbressine, F. (2008). Geometric error measurement and compensation of machines—An update. *CIRP Annals, 57*(2), 660-675. doi:10.1016/j.cirp.2008.09.008

Schwenke, H., Schmitt, R., Jatzkowski, P., & Warmann, C. (2009). On-the-fly calibration of linear and rotary axes of machine tools and CMMs using a tracking interferometer. *CIRP Annals, 58*(1), 477-480. doi:10.1016/j.cirp.2009.03.007

Slamani, M., Mayer, R., Balazinski, M., Zargarbashi, S. H. H., Engin, S., & Lartigue, C. (2010). Dynamic and geometric error assessment of an XYC axis subset on five-axis high-speed machine tools using programmed end point constraint measurements. *International Journal*

of Advanced Manufacturing Technology, *50*(9-12), 1063-1073. doi:10.1007/s00170-010-2584-8

Weikert, S. (2004). R-Test, a New Device for Accuracy Measurements on Five Axis Machine Tools. *CIRP Annals, 53*(1), 429-432. doi:10.1016/s0007-8506(07)60732-x

Xiang, S., & Altintas, Y. (2016). Modeling and compensation of volumetric errors for five-axis machine tools. *International Journal of Machine Tools and Manufacture, 101*, 65-78. doi:https://doi.org/10.1016/j.ijmachtools.2015.11.006

Zha, J., Wang, T., Li, L., & Chen, Y. (2020). Volumetric error compensation of machine tool using laser tracer and machining verification. *The International Journal of Advanced Manufacturing Technology*, *108*(7-8), 2467-2481. doi:10.1007/s00170-020-05556-8

Zhang, H., Yang, J., Zhang, Y., Shen, J., & Wang, C. (2010). Measurement and compensation for volumetric positioning errors of CNC machine tools considering thermal effect. *International Journal of Advanced Manufacturing Technology*, *55*(1-4), 275-283. doi:10.1007/s00170-010-3024-5

Zhu, S., Ding, G., Qin, S., Lei, J., Zhuang, L., & Yan, K. (2012). Integrated geometric error modeling, identification and compensation of CNC machine tools. *International Journal of Machine Tools and Manufacture*, *52*(1), 24-29. doi:https://doi.org/10.1016/j.ijmachtools.2011.08.011

CHAPTER 7 ARTICLE 4: CNC TABLE BASED COMPENSATION OF INTER-AXIS AND LINEAR AXIS SCALE GAIN ERRORS FOR A FIVE-AXIS MACHINE TOOL FROM SYMBOLIC VARIATIONAL KINEMATICS

Sareh M. Esmaeili [a], J.R.R. Mayer [a] (2)

[a] *Department of Mechanical Q1 Engineering, École Polytechnique (Montréal), P.O. Box 6079, Station Downtown, Montréal, QC H3C3A7, Canada*

NOTE: Based on the paper resubmitted to the International Journal of CIRP Annals (2021)

7.1 Abstract

A compensation lookup tables (LUTs) scheme is programmed using a CNC's indigenous LUTs capability to virtually correct geometric error parameters of a five-axis machine tool. Using variational kinematics, the geometric errors are forward propagated to the tool tip and the required axis command corrections are obtained in closed form by inverse kinematics. 40 lookup tables and multiplication and summation functionalities compensate ten inter-axis errors and three linear positioning gain errors. Validation tests on a wCAYFXZt topology machine with a 45° angle between the C- and A-axis show significant reductions in dominant geometric errors and a 79% improvement in volumetric errors.

Keywords: Compensation, machine tool, lookup table

7.2 Introduction

Machine tool geometric error measurement and compensation help to produce good parts (Soichi Ibaraki & Knapp, 2012; Schwenke et al., 2008). Various compensation options are implemented within the CNC by original equipment manufacturers (OEMs). ISO/TR 16907 (ISO/TR16907, 2015) lists a number of potential options. However, most published research covers user implementation with means independent from the OEM. Modifying the G-code axis commands on the basis of forward and inverse kinematic models (R. M. D. Mahbubur, J. Heikkala, K. Lappalainen, & J. A. Karjalainen, 1997) (Givi & Mayer, 2014) does not directly improve the machine and create program traceability issues as the code must be changed for different machines and as a particular machine errors change. Forward and inverse machine kinematic models based

on screw theory (Xiang & Altintas, 2016) was implemented in an open CNC, as opposed to an OEM CNC, to predict the volumetric error and generate axis corrections. Some CNCs allow users to define lookup tables input and output with the option to combine them, such as summation and multiplication, through a specific language, but there are no guidelines on what scheme will effectively compensate specific geometric errors. A summation scheme was proposed (Jennifer Creamer et al., 2016), using 25 compensation lookup tables (LUTs), where each table is modelled as a univariate polynomial to compensate, in a least squares sense, the predicted volumetric errors due to estimated amalgamated inter- and intra-axis errors modelled as polynomials. Each axis correction is the sum of five LUTs outputs, one per axis. Alternatively, the LUT polynomials are directly generated to explain the measured volumetric errors. Validation is conducted using laser trackers on a large swivel head gantry. Cross LUTs multiplication was also used for a five axis gantry for amalgamated (J. Li et al., 2019) without distinguishing between inter- and intra-axis geometric error sources.

This paper proposes the concept of a variational forward inverse kinematics LUTs scheme (FIK-LUT), implementable using a CNC's indigenous LUT programming language, to compensate for the eight inter-axis errors defined in ISO 230-1 (ISO230-1, 2012), the two spindle translational offsets and three linear axes positioning gain errors. The CNC performs the compensation automatically as directed by the programmed scheme. A reduction in both the volumetric errors and in the effective geometric error sources is sought. In section 7.3, the linearized forward and inverse model is presented with its use to form the FIK-LUTs schemes using summation, multiplication and weights. The scheme is validated on a machine with a nominal 45 degree between its A- and C-axis in Section 7.4. Finally, the conclusion follows in section 7.5.

7.3 Look up table scheme construction

As an example, the FIK-LUTs scheme for the X-axis correction is shown in Figure 7.1.

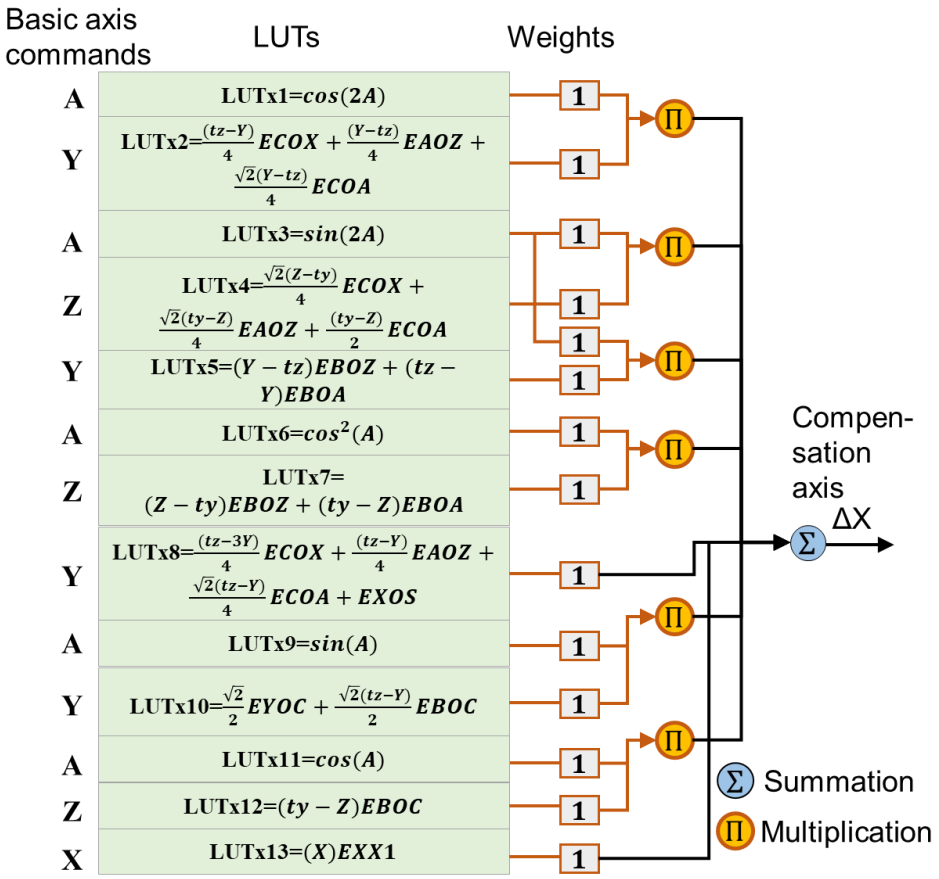

Figure 7.1. The 13 FIK-LUTs scheme for X-axis correction.

The FIK-LUTs scheme is designed for a particular machine topology and the geometric errors to be compensated. The target machine tool has the topology wCAYfXZt with its A-axis tilted by -45° around Y with w, f and t as the workpiece, foundation and tool frames, respectively.

The 13 geometric errors (Mayer, 2012) for compensation are listed in Table 7-1 and shown in Figure 7.2. The purpose of the compensation is to provide the CNC with the means to produce a set of corrected axis command, for the five mechanical axes, denoted by,

$$\boldsymbol{q}^c = \boldsymbol{q} + \Delta\boldsymbol{q} \tag{46}$$

where $\boldsymbol{q}$ and $\boldsymbol{q}^c$, are the nominal and compensated axis command sets, respectively and $\Delta\boldsymbol{q}$ is the axis command corrections set

$$\Delta\boldsymbol{q} = [\Delta X \quad \Delta Y \quad \Delta Z \quad \Delta A \quad \Delta C]^T . \tag{47}$$

Table 7-1. The error parameters in 13-error model.

Description	Symbol
Inter-axis errors	
Squareness error of the A-axis relative to the X-axis	*EBOA*
Squareness error of the A-axis relative to the Y-axis	*ECOA*
Y-offset between the C- and A-axis	*EYOC*
Squareness error of the C-axis relative to the Y-axis	*EAOC*
Squareness error of the C-axis relative to the A-axis	*EBOC*
Squareness error of the X-axis relative to the Y-axis	*ECOX*
Squareness error of the Z-axis relative to the Y-axis	*EAOZ*
Squareness error of the Z-axis relative to the X-axis	*EBOZ*
Offset of the spindle in X	*EXOS*
Offset of the spindle in Z	*EZOS*
Intra-axis errors	
Positioning linear errors of the X axis	*EXX1*
Positioning linear errors of the Y axis	*EYY1*
Positioning linear errors of the Y axis	*EZZ1*

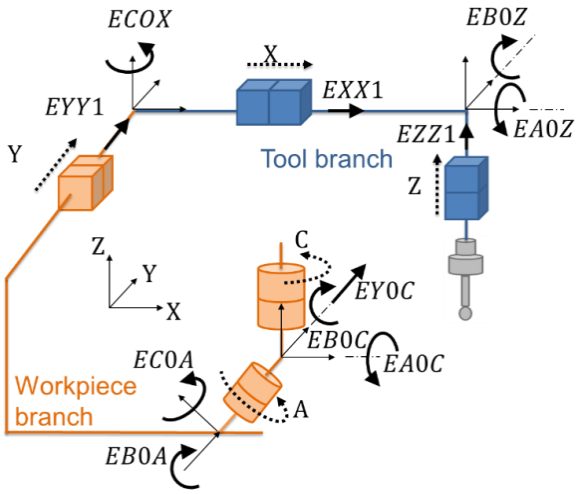

Figure 7.2. Kinematic diagram of the target machine tool with the 13 geometric error parameters. The spindle is modelled as a B-axis (not otherwise present on this machine)

The FIK-LUT scheme uses equations of the required $\Delta\boldsymbol{q}$ as functions of $\boldsymbol{q}$ and the geometric error parameters, $\boldsymbol{E}_{\mathbf{P}}$, in order to compensate for the volumetric errors that they induce. $\boldsymbol{E}_{\mathbf{P}}$ is forward propagated to the tool tip to yield the complete volumetric error twist (position and orientation), $\boldsymbol{E}_{\mathbf{V}}$, using the Jacobian of geometric errors under small error assumption,

$$\boldsymbol{E}_{\mathrm{V}} = \boldsymbol{J}_{\text{13-error}} \boldsymbol{E}_{\mathrm{P}} \tag{48}$$

where

$$\boldsymbol{E}_{\mathrm{V}} = [E_{\mathrm{XV}} \quad E_{\mathrm{YV}} \quad E_{\mathrm{ZV}} \quad E_{\mathrm{AV}} \quad E_{\mathrm{BV}} \quad E_{\mathrm{CV}}]^T \tag{49}$$

and $\boldsymbol{J}_{\text{13-error}}$ contains inter- and intra-axis parts,

$$\boldsymbol{J}_{\text{13-error}} = \left[\boldsymbol{J}_{\text{inter-axis}} \quad \boldsymbol{J}_{\text{intra-axis}}\right]. \tag{50}$$

The inverse of the Jacobian of commands produces the required $\Delta\boldsymbol{q}$ for a given $\boldsymbol{E}$v (Lei & Hsu, 2003b)

$$\Delta\boldsymbol{q} = \boldsymbol{J}^{+}_{\text{command}} \boldsymbol{E}_{\mathrm{V}} \tag{51}$$

Symbolic forms of those equations forms the basis for building the FIK-LUT.

7.3.1 Forward kinematic model

The nominal forward kinematics is modelled as a product of homogenous transformation matrices (HTMs), $\boldsymbol{T}$, for each pair of adjacent components from the workpiece to the tool through each machine axes

$$\begin{aligned} {}^{w_n}\boldsymbol{T}_{t_n} = {} & [({}^{F}\boldsymbol{T}_{Y_0}\,{}^{Y_0}\boldsymbol{T}_{Y})({}^{Y}\boldsymbol{T}_{A_0}\,{}^{A_0}\boldsymbol{T}_{A})({}^{A}\boldsymbol{T}_{C_0}\,{}^{C_0}\boldsymbol{T}_{C})({}^{C}\boldsymbol{T}_{w_n})]^{-1} \\ & [({}^{F}\boldsymbol{T}_{X_0}\,{}^{X_0}\boldsymbol{T}_{X})({}^{X}\boldsymbol{T}_{Z_0}\,{}^{Z_0}\boldsymbol{T}_{Z})({}^{Z'}\boldsymbol{T}_{t_n})] \end{aligned} \tag{52}$$

where w_n and t_n are the nominal locations of the workpiece and tool and for example Y_0 and Y are the nominal axis locations before motion and its nominal after motion.

7.3.2 Jacobian of geometric error parameter

The Jacobian matrix is obtained symbolically using transport matrices considering the frame of action of each inter- and intra-axis errors and its effect at the tool (Abbaszadeh-Mir et al., 2002; Y A. Mir et al., 2002). A transport matrix, ${}^{2}\boldsymbol{C}_{1}$, is a 6×6 matrix used to propagate the effect of a small rotation and translation occurring at a location 1 of a rigid body to another location 2 rigidly

attached to the former. The transport matrix (or velocity transformation) is obtained as (Craig, 1974),

$$ {}^{2}C_{1} = \begin{bmatrix} {}^{1}_{2}R_{3\times3}{}^{\mathrm{T}} & {}^{1}_{2}R^{\mathrm{T}}[{}^{1}P_{\mathrm{o}2,3\times1}\times]^{\mathrm{T}} \\ 0_{3\times3} & {}^{1}_{2}R_{3\times3}{}^{\mathrm{T}} \end{bmatrix} \tag{53} $$

where ${}^{1}_{2}R_{3\times3}$ and ${}^{1}P_{\mathrm{o}2,3\times1}$ are the rotation matrix and the origin vector between frames 1 and 2, respectively. ${}^{1}P_{\mathrm{o}2,3\times1}\times$ is

$$ {}^{1}P_{\mathrm{o}2,3\times1}\times = \begin{bmatrix} 0 & -{}^{1}p_{\mathrm{o}2,z} & {}^{1}p_{\mathrm{o}2,y} \\ {}^{1}p_{\mathrm{o}2,z} & 0 & -{}^{1}p_{\mathrm{o}2,x} \\ -{}^{1}p_{\mathrm{o}2,y} & {}^{1}p_{\mathrm{o}2,x} & 0 \end{bmatrix}. \tag{54} $$

The Jacobian of inter-axis geometric errors for the target machine tool is defined as,

$$ \boldsymbol{J}_{\text{inter-axis}} = \begin{bmatrix} {}^{\mathrm{t}}C_{\mathrm{X}_0} & {}^{\mathrm{t}}C_{\mathrm{Y}_0} & {}^{\mathrm{t}}C_{\mathrm{Z}_0} & {}^{\mathrm{t}}C_{\mathrm{A}_0} & {}^{\mathrm{t}}C_{\mathrm{C}_0} & {}^{\mathrm{t}}C_{\mathrm{t}} & {}^{\mathrm{t}}C_{\mathrm{w}} \end{bmatrix} \tag{55} $$

where, for example, ${}^{\mathrm{t}}C_{\mathrm{A}_0}$ expresses the sensitivity of the volumetric error to geometric error parameters occurring at A_0, the reference frame of the A-axis before motion. The inter-axis errors correspond to columns 6, 16, 17, 23, 24, 26, 28, 29, 31 and 33 for *ECOX*, *EAOZ*, *EBOZ*, *EBOA*, *ECOA*, *EYOC*, *EAOC*, *EBOC*, *EXOS* and *EZOS*, respectively.

The Jacobian of the intra-axis errors for the positioning errors of the X-, Y- and Z-axis contains these transport matrices projected in the tool frame,

$$ \boldsymbol{J}_{\text{intra-axis}} = \begin{bmatrix} {}^{t}C_{X} & {}^{t}C_{Y} & {}^{t}C_{Z} & {}^{t}C_{A} & {}^{t}C_{C} \end{bmatrix} \tag{56} $$

Columns 1, 8 and 15 of the intra-axis Jacobian, $\boldsymbol{J}_{13\text{-error}}$, cater for *EXX1*, *EYY1* and *EZZ1*, respectively, as

$$\begin{aligned} \boldsymbol{J}_{EXX1} &= \begin{bmatrix} X & 0 & 0 & 0 & 0 & 0 \end{bmatrix}^{\mathrm{T}} \\ \boldsymbol{J}_{EYY1} &= \begin{bmatrix} 0 & 0 & -Y & 0 & 0 & 0 \end{bmatrix}^{\mathrm{T}} \\ \boldsymbol{J}_{EZZ1} &= \begin{bmatrix} 0 & -Z & 0 & 0 & 0 & 0 \end{bmatrix}^{\mathrm{T}}. \end{aligned} \tag{57}$$

The complete Jacobian, $J_{13\text{-}error}$, for the 13-error model is,

$$\begin{aligned} \boldsymbol{J}_{\text{13-error}} = [&\boldsymbol{J}_{\text{ECOX}} \quad \boldsymbol{J}_{\text{EAOZ}} \quad \boldsymbol{J}_{\text{EBOZ}} \quad \boldsymbol{J}_{\text{EBOA}} \quad \boldsymbol{J}_{\text{ECOA}} \quad \boldsymbol{J}_{\text{EYOC}} \quad \boldsymbol{J}_{\text{EAOC}} \\ &\boldsymbol{J}_{\text{EBOC}} \quad \boldsymbol{J}_{\text{EXOS}} \quad \boldsymbol{J}_{\text{EZOS}} \quad \boldsymbol{J}_{\text{EXX1}} \quad \boldsymbol{J}_{\text{EYY1}} \quad \boldsymbol{J}_{\text{EZZ1}}] \end{aligned} \tag{58}$$

7.3.3 Jacobian of command

The Jacobian of commands, $\boldsymbol{J}_{\text{command}}$, propagates the effect of axis command corrections, applied at the nominal location of the axis after its nominal motion, to the tool location. Columns 1, 8, 15, 22 and 36 of $\boldsymbol{J}_{\text{intra-error}}$ are selected for the X-, Y-, Z-, A- and C-axis command corrections respectively.

Substituting the Jacobians in Eq. (3) and (6) yields a set of five axis command corrections for each of the 13 geometric errors as follows, where S and C stand for sin and cos functions, respectively,

$$\Delta q_{\mathrm{ECOX}} = ECOX[\frac{Y(\mathrm{C}(2A)-3)+\sqrt{2}\mathrm{S}(2A)(Z-t_y)}{4} \quad \frac{(\mathrm{C}^2(A)-1)(t_y-Z-X)}{2}$$
$$\frac{Y(1-\mathrm{C}(2A))-\sqrt{2}X\mathrm{S}(2A)}{4} \quad \frac{\sqrt{2}}{2}(\mathrm{C}(A)-1) \quad -\mathrm{C}(A)]$$

$$\Delta q_{\mathrm{EAOZ}} = EAOZ[\frac{Y(\mathrm{C}(2A)-1)+\sqrt{2}\mathrm{S}(2A)(t_y-Z)}{4} \quad \frac{(1-\mathrm{C}^2(A))(X+Z-t_y)}{2}$$
$$\frac{Y(3+\mathrm{C}(2A))+\sqrt{2}X\mathrm{S}(2A)}{4} \quad -\frac{\sqrt{2}}{2}(\mathrm{C}(A)+1) \quad \mathrm{C}(A)]$$

$$\Delta q_{\mathrm{EBOZ}} = EBOZ[\frac{-2\mathrm{C}(A)(t_y-Z)-\sqrt{2}Y\mathrm{S}(A)}{4} \quad \frac{\mathrm{S}(2A)(t_y-X-Z)}{2}$$
$$\frac{\sqrt{2}\mathrm{S}(A)(Y\mathrm{C}(A)+\sqrt{2}X\mathrm{S}(2A))}{2} \quad -\mathrm{S}(A) \quad \sqrt{2}\mathrm{S}(A)]$$

$$\Delta q_{\mathrm{EBOA}} = EBOA[\frac{\mathrm{C}(A)(\mathrm{C}(A)(t_y-Z)-\sqrt{2}Y\mathrm{S}(A))}{2} \quad \frac{\sqrt{2}\mathrm{S}(2A)(X+Z-t_y)}{4}$$
$$\frac{\mathrm{C}(A)(2X\mathrm{C}(A)-\sqrt{2}Y\mathrm{S}(A))}{2} \quad \mathrm{S}(A) \quad -\sqrt{2}\mathrm{S}(A)] \qquad . (59)$$

$$\Delta q_{\mathrm{ECOA}} = ECOA[\frac{-\sqrt{2}Y(\mathrm{C}(2A)-1)+2\mathrm{S}(2A)(t_y-Z)}{4} \quad \frac{-\sqrt{2}\mathrm{S}^2(A)(X+Z-t_y)}{2}$$
$$\frac{\sqrt{2}Y\mathrm{C}^2(A)+X\mathrm{S}(2A)}{2} \quad -\mathrm{C}(A) \quad \sqrt{2}\mathrm{C}(A)]$$

$$\Delta q_{\mathrm{EYOC}} = EYOC[\frac{\sqrt{2}}{2}\mathrm{S}(A) \quad \mathrm{C}(A) \quad -\frac{\sqrt{2}}{2}\mathrm{S}(A) \quad 0 \quad 0]$$

$$\Delta q_{\mathrm{EAOC}} = EAOC[0 \quad 0 \quad 0 \quad \sqrt{2} \quad -1]$$

$$\Delta q_{\mathrm{EBOC}} = EBOC[\mathrm{C}(A)(t_y-Z)-\frac{\sqrt{2}}{2}Y\mathrm{S}(A) \quad \frac{\sqrt{2}}{2}\mathrm{S}(A)(X+Z-t_y) \quad X\mathrm{C}(A) \quad 0 \quad 0]$$

$$\Delta q_{\mathrm{EXOS}} = EXOS[1 \quad 0 \quad 0 \quad 0 \quad 0]$$

$$\Delta q_{\mathrm{EZOS}} = EZOS[0 \quad -1 \quad 0 \quad 0 \quad 0]$$

$$\Delta q_{\mathrm{EXX1}} = EXX1[X \quad 0 \quad 0 \quad 0 \quad 0]$$

$$\Delta q_{\mathrm{EYY1}} = EYY1[0 \quad Y \quad 0 \quad 0 \quad 0]$$

$$\Delta q_{\mathrm{EZZ1}} = EZZ1[0 \quad 0 \quad Z \quad 0 \quad 0]$$

7.3.4 Generation of FIK-LUTs

The CNC FIK-LUTs scheme implements the axis command corrections by combining a minimum number of simple tables each having as input an axis command, the basic axis, and as output an associated correction to the output axis, the compensation axis.

An NC code generates the tables, their entries and instructs the CNC on how to combine their interpolated outputs. A sample code is shown in Figure 7.3 where table 1 is multiplied by table 2

and the result added to Table 3. The number of table entries for the first, second and third tables are 10, 15 and 15, respectively. The input axes for the first, second and third tables are Z-, Y- and X-axis, respectively and their output axis is the X-axis. By entering any axis command for X, Y and Z, the output of the two first tables are multiplied together and are added to the third table.

The tables' functions explicitly include the geometric error parameters. The functions are discretized to produce a limited number of table entries that the controller linearly interpolates for the required axis commands. The proposed LUTs can be implemented by a machine user if the CNCs offer a compensation facility by which users can combine the compensation tables by summation and multiplication functionalities.

7.4 Experimental validation

7.4.1 Measurement before and after applying compensation

The tables are loaded in the Siemens Sinumerik 840D controller of the K2X8-Five machine tool from Huron Graffenstaden.

The machine geometric errors and volumetric accuracy, without and with compensation, is evaluated by probing the Scale and Master Ball Artefact (SAMBA) (Mayer, 2012) shown in Figure 7.5. Two test strategies are used. The Calibration test, is used for the preparation of lookup tables and the other called Validation test is used to evaluate the compensation performance. Each ball probing takes 1 min 50 s. The Calibration test strategies use 26 A-, Spindle and C- axis position sets for a total of 28 ball probings whereas the Validation test uses 10 sets for 26 ball probings. For tests before compensation, all tables are off. For compensation, only the new 40 FIK-LUTs are activated.

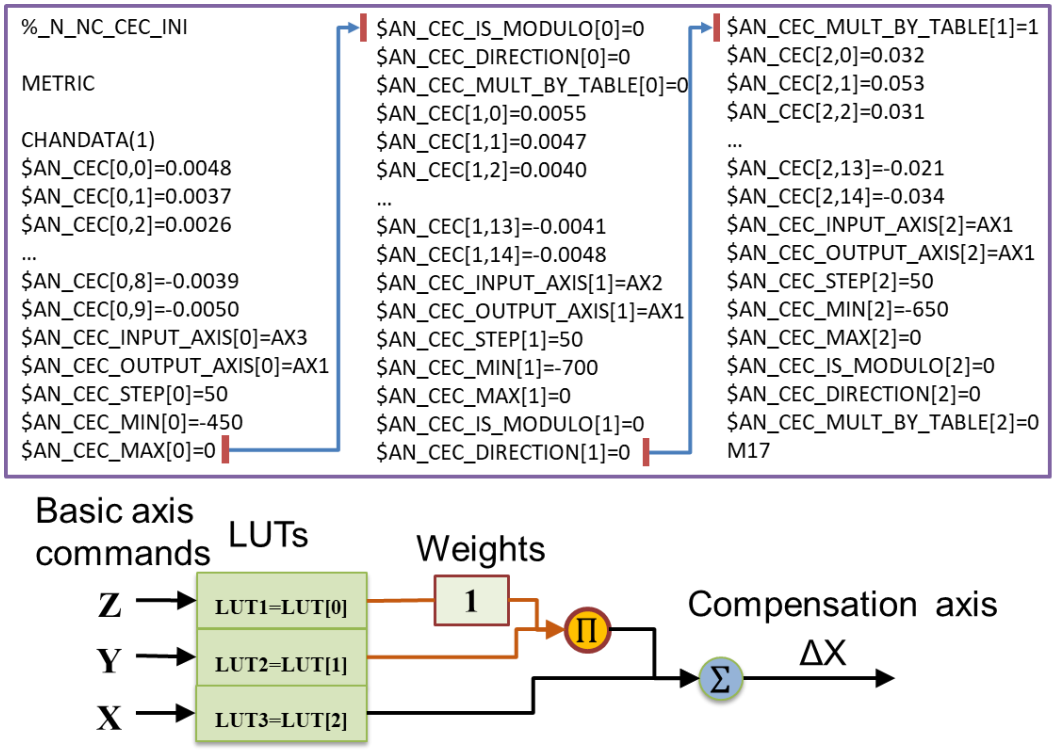

Figure 7.3. NC code for a sample of table multiplication (Siemens 840D controller) ("Siemens Controller," SINUMERIK 840D/840Di/810D Extended Functions). Note: $AN_CEC_MULT_BY_TABLE=0 means the table is added to the other tables by default.

40 LUTs are used to compensate the 13 error parameters consisting of 13, 11, 14, 1 and 1 tables for the X-, Y-, Z-, A- and C-axis, respectively. The A- and C-axis corrections are shown in Figure 7.4.

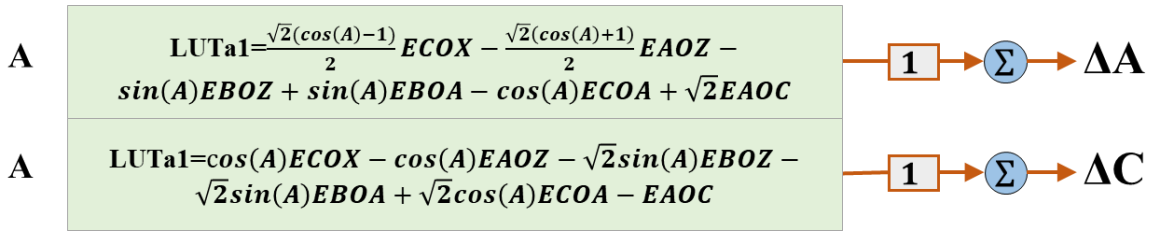

Figure 7.4. The 2 FIK-LUTs scheme for A- and C-axis correction.

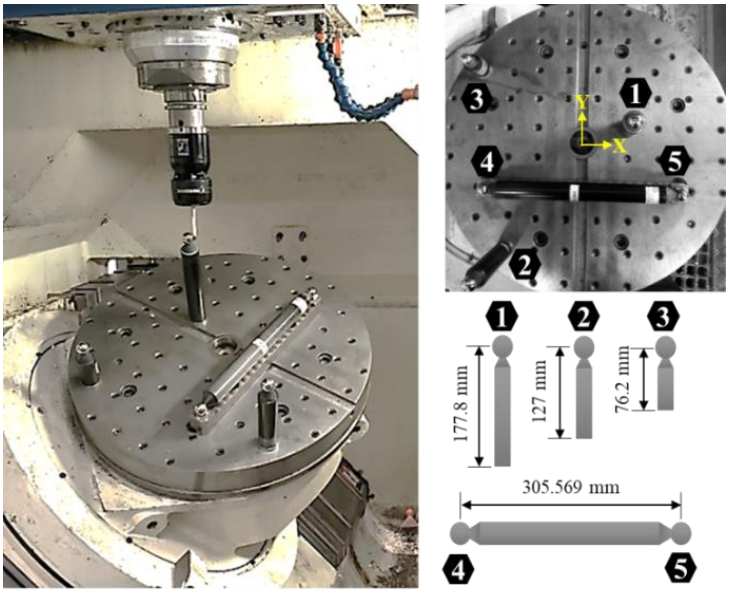

Figure 7.5. SAMBA artefact. All balls are 19.05 mm diameter.

First, the Calibration test is run once and the Validation test is run twice, with tables off, to assess the uncompensated state of the machine. Then the FIK-LUTS are generated from the Calibration test results and the sequence is repeated with the compensation tables activated. This completes a cycle which is executed four times. The room temperature varies between 20° and 21°C.

7.4.2 Measurement results and lookup table generation

The Validation test results before compensation are listed in Table 7-2. The mean volumetric error is 44 µm and the estimated error parameters cannot explain a mean VE norm of 4.1 µm. After compensation, the mean VE norm is reduced to 9.1 µm for a 79% reduction. The compensation ratios of the error parameters sorted from the biggest to the smallest magnitude of the mean VE norm caused by each error exhibit a significant reduction for the dominant errors as *EZOS*, *EAOZ*, *EZZ1*, *EBOA*, *EAOC* and *ECOX*, However, for small error parameters, no reliable trend can be observed. Figure 7.6 illustrates the mean of volumetric error norm before and after compensation and their relative standard deviation for the validation test.

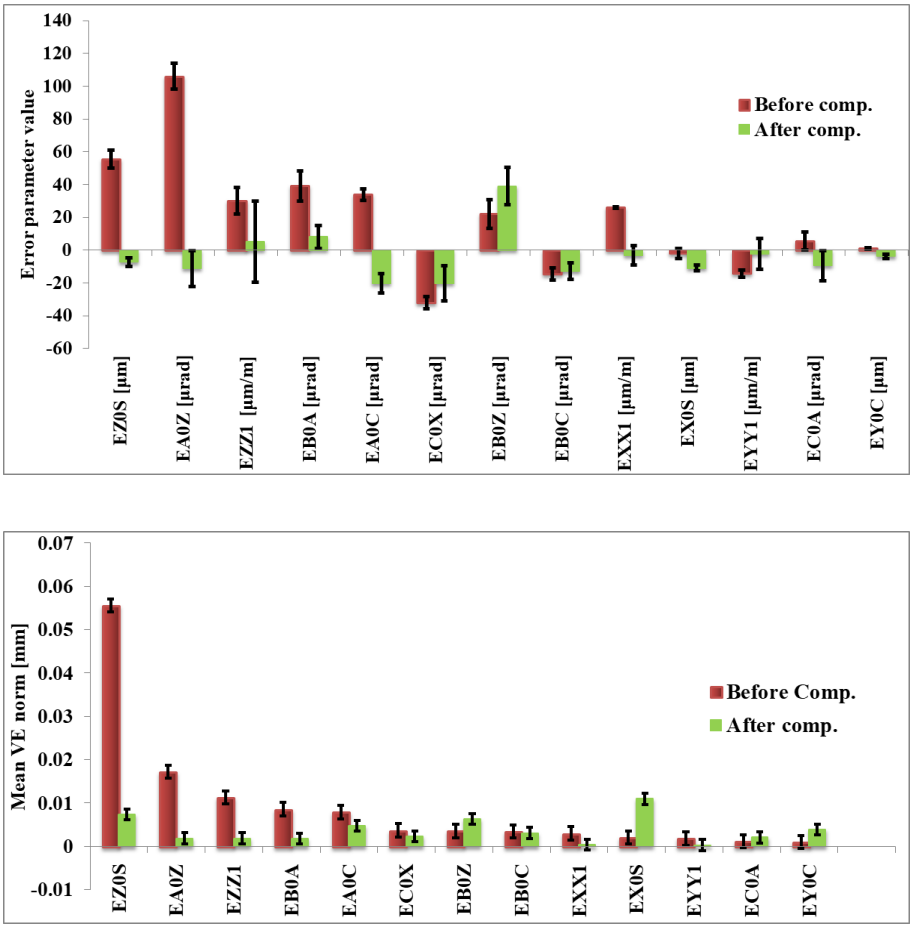

Figure 7.6. top) The mean error parameters before and after compensation with +/- two pooled SD errors bands; bottom) The mean of volumetric error norm before and after compensation for the validation test.

Table 7-2. The estimation results for the validation test before and after generating and activating lookup tables.

	Error parameter ($\overline{Ep} \pm U$) values[1]		$\overline{\|VE\|}$ due to each E_p [μm]		
Error parameters	Before comp.	After comp.	Before comp.	After comp.	After/Before $\overline{Ep}$ Comp. ratio
EZOS [μm]	55.6±6.8	-7.4	55.6	7.3	-0.13
EAOZ [μrad]	106.0±14.5	-11.3	17.2	1.8	-0.11
EZZ1 [μm/m]	30.0±13.8	5.0	11.3	1.8	0.17
EBOA [μrad]	39.1±10.6	8.1	8.6	1.7	0.21
EAOC [μrad]	33.8±8.3	-20.3	7.9	4.7	-0.60
ECOX [μrad]	-32.0±10.8	-20.3	3.7	2.3	0.63
EBOZ [μrad]	22.0±8.0	39.0	3.6	6.3	1.77
EBOC [μrad]	-14.6±3.3	-12.9	3.5	3.0	0.88
EXX1 [μm/m]	25.9±8.1	-3.2	3.0	0.3	-0.12
EXOS [μm]	-2.1±4.9	-11.0	2.1	11.0	5.29
EYY1 [μm/m]	-14.3±12.8	-2.3	1.8	0.3	0.16
ECOA [μrad]	5.5±13.7	-9.5	1.2	2.0	-1.72
EYOC [μm]	1.0±1.4	-3.9	1.0	3.9	-3.97
$\overline{\|VE\|}$ [μm]	44	-	9.1	0.21	
$\overline{\|VE\|}$ unexplained by the model [μm]	4.1	-	4.8	1.19	

[1] U of Ep from eight runs over two non-consecutive days (Sepahi-Boroujeni, Mayer, & Khameneifar, 2021).

7.5 Conclusion

Combinatory lookup tables are generated from symbolic variational forward and inverse kinematics functions (FIK-LUTs) relating the required axis command corrections to the eight inter-axis errors, two spindle lateral offsets and the three linear axis scale gain errors of a 5-axis machine tool. The machine geometric errors are calibrated, using one set of positions, and the FIK-LUTs are generated. The compensation effectiveness is evaluated using a new validation set of positions shows significant reduction in the dominant error parameters as well as a reduction by 79% of the mean volumetric error norm.

7.6 Acknowledgments

This research is supported by NSERC CANRIMT2 Network and partners. Thanks are due to technicians Guy Gironne and Vincent Mayer and to industrial partner's manufacturing technology specialist Rachid Guiassa.

7.7 References

Abbaszadeh-Mir, Y., Mayer, J. R. R., Cloutier, G., & Fortin, C. (2002). Theory and simulation for the identification of the link geometric errors for a five-axis machine tool using a telescoping magnetic ball-bar. *International Journal of Production Research, 40*(18), 4781-4797. doi:10.1080/00207540210164459

Controller, S. SINUMERIK 840D/840Di/810D Extended Functions.

Craig, J. J. (1974). Introductionto Robotics, Mechanics andControls, 2nd edition, (Addison-Wesley, Reading, Massachusetts).

Creamer, J., Sammons, P. M., Bristow, D. A., Landers, R. G., Freeman, P. L., & Easley, S. J. (2016). Table-Based Volumetric Error Compensation of Large Five-Axis Machine Tools. Journal of Manufacturing Science and Engineering, 139(2). doi:10.1115/1.4034399

Givi, M., & Mayer, J. R. R. (2014). Volumetric error formulation and mismatch test for five-axis CNC machine compensation using differential kinematics and ephemeral G-code. *The International Journal of Advanced Manufacturing Technology*, *77*(9-12), 1645-1653. doi:10.1007/s00170-014-6558-0

Ibaraki, S., & Knapp, W. (2012). Indirect Measurement of Volumetric Accuracy for Three-Axis and Five-Axis Machine Tools: A Review. *Int. J. of Automation Technology*, *6*(2), 15.

ISO230-1. (2012). Test code for machine tools – Part 1: geometric accuracy of machines operating under no-load or quasi-static conditions.

ISO/TR16907:2015(E), Technical Report, Machine tools — Numerical compensation of geometric errors.

Lei, W. T., & Hsu, Y. Y. (2003). Accuracy enhancement of five-axis CNC machines through realtime error compensation. *International Journal of Machine Tools & Manufacture, 43*(9), 871-877.

Li, J., Mei, B., Shuai, C., Liu, X.-j., & Liu, D. (2019). A volumetric positioning error compensation method for five-axis machine tools. *The International Journal of Advanced Manufacturing Technology, 103*(9), 3979-3989. doi:10.1007/s00170-019-03745-8

Mahbubur, R. M. D., Heikkala, J., Lappalainen, K., & Karjalainen, J. A. (1997). Positioning accuracy improvement in five-axis milling by post processing. *International Journal of Machine Tools and Manufacture, 37*(2), 223-236. doi:https://doi.org/10.1016/0890-6955(95)00091-7

Mayer, J. R. R. (2012). Five-axis machine tool calibration by probing a scale enriched reconfigurable uncalibrated master balls artefact. *CIRP Annals, 61*(1), 515-518. doi:10.1016/j.cirp.2012.03.022

Mir, Y. A., Mayer, J. R. R., & Fortin, C. (2002). Tool path error prediction of a five-axis machine tool with geometric errors. *Proceedings of the Institution of Mechanical Engineers, 216*, 697-712.

Schwenke, H., Knapp, W., Haitjema, H., Weckenmann, A., Schmitt, R., & Delbressine, F. (2008). Geometric error measurement and compensation of machines-An update. *CIRP Annals - Manufacturing Technology, 57*(2), 660-675.

Sepahi-Boroujeni, S., Mayer, J. R. R., & Khameneifar, F. (2021). Efficient uncertainty estimation of indirectly measured geometric errors of five-axis machine tools via Monte-Carlo validated GUM framework. *Precision Engineering, 67*, 160-171. doi:https://doi.org/10.1016/j.precisioneng.2020.09.027

Xiang, S., & Altintas, Y. (2016). Modeling and compensation of volumetric errors for five-axis machine tools. *International Journal of Machine Tools and Manufacture, 101*, 65-78. doi:https://doi.org/10.1016/j.ijmachtools.2015.11.006

CHAPTER 8 GENERAL DISCUSSION

To achieve the objective of the project, two general table-based error compensation methods have been studied, one for Cartesian volumetric error compensation and the other for volumetric error compensation. This chapter presents the general discussion of this research study. The main methods and important outcomes are explained in the context of machine tool table-based volumetric error compensation.

A three-dimensional lookup table is a Control parameter modification capability embedded in Fanuc controller. For generating such a lookup table, a three-dimensional mesh grid is required to be built on the joint space. This thesis proposes generating an optimized 3D mesh grid to compensate Cartesian volumetric errors. The optimized table was obtained by the iterative method. The objective was to minimize the norm of the RMS of the volumetric error. Two error models, including 13 and 84 error parameters and coefficients, were used while indirectly calibrating the five-axis machine tool. The two pseudo three-dimensional error compensation tables were developed for the two error models with the optimized number of the 3D mesh grid elements. A 3D ball-bar test was designed for validation purposes. Firstly, the ball-bar test was run before applying for any compensation. Afterwards, the positions located on the meridians and an equator were corrected using the trilinear interpolation applied on the two pseudo lookup tables, and the ball-bar tests were run with the updated values. The size and form errors show a good improvement in terms of error compensation. The volumetric Cartesian error projected on the ball-bar axis direction was compensated using the pseudo optimized lookup tables. Noted that, this kind of table is not useful to compensate the angular errors of the tool tip volumetric errors.

Interpolatroy compensation lookup table is a type of complex compensation table that existed in some controllers such as Siemens controller, which let the users make combinatory tables based on their need. The controller applies linear interpolation on the table entries when the G-code is entered. The user can define whether the tables to be added together or to be multiplied by each other. Three research works have been proposed for generating such interpolatory compensation lookup tables.

The straightforward combination of the tables is using the summation functionalities. Since a five-axis machine tool has five axes, five tables per axis, 25 tables in total, are the maximum numbers of the tables useful for correcting five axes. In this work, the Jacobian of commands was built to

calculate the command correction. Then, the command corrections were simulated by univariate polynomials of degree three, and the Jacobian of table coefficients was made, presenting the relationship between the table coefficients and the command corrections. Two error models containing 12 and 81 error parameters and coefficients were used. Having calculated the table coefficients, the two-pseudo combinatory tables were generated for the two error models.

The very fact that the tables' configurations are dependent on Jacobian of commands and the inverse Jacobian of command was approved in the third work. This model was used for compensating the inter-axis and three gain errors. To compensate such errors combination, not only the summation functionalities of the tables but also the multiplication functionalities are necessary while table generation, and this has been proven through simulation and experimental tests by comparing different table-based models with the kinematic-based compensation. The kinematic-based error compensation showed a better agreement with the model, including summation and multiplication functionalities rather than just summation functionalities. The enriched model included 23 tables (23Trigo-T). The table coefficients in the enriched model were calculated through classic optimization wherein the objective function was minimizing the discrepancies between the command corrections and the table functions.

The enriched model was improved in the last work, in which the number of the tables increased to 40. This model was obtained by the exact linearized kinematic equations for the target five-axis machine tool. The similarity of the last table-based error compensation model to the kinematic-based error compensation is more than the former models. This model used the advantage of summation and multiplication functionalities while generating the tables. This model was evaluated for compensating 13 error parameters and volumetric errors. The real tables were built, enabled, and used in Siemens controller. Noted that the number of the tables depends on the topology of the machine and the error parameters to be compensated.

CHAPTER 9 CONCLUSION (AND RECOMMANDATIONS)

9.1 Conclusion and contributions of the work

This thesis proposed a methodology for integrating five-axis machine tools calibration, lookup table compensations generation as well as the whole procedure validation.

- The 3D compensation table presented in the first work can compensate Cartesian volumetric errors in a five-axis machine tool working on three-axis mode operation. By studying the effect of different error models on the mesh grid dimension, it has been concluded that a minimized mesh grid dimension depends on the error parameters that existed in the error model or the error parameters that the machine tool under the test exhibits. For example, eight nodes are adequate when the machine tool has linear inter-axis errors in the 13-error model. However, the table's optimum dimension depends on the actual error parameter values for the 84-error model. For instance, for the tested machine, a 19x19x19 for 6859 nodes was required to gain a 0.1 micrometer threshold in an 84-error error model.
- A 3D ball-bar test consisting of several meridians and an equator was designed to validate the 3D compensation table. The path best fit sphere radius deviation from the nominal sphere was the criteria for the size error, and the standard deviations of the residuals were the criteria for the form error. Those criteria were compared before and after applying 3D compensation tables, which revealed that the average effectiveness of the 3D grid error compensation table was over 82%.
- The second, third and fourth articles focus on volumetric error and geometric error compensation in a five-axis machine by generating and enabling combinatory lookup tables in the controller. Combinatory lookup tables consist of one to several simple tables combined by summation or multiplication functionalities.
- In the second paper, the lookup tables were combined by summation functions to compensate volumetric error and geometric error parameters. Two error models were developed to calibrate the machine tool, followed by generating 5 tables per axis, 25 tables in total, for each error model. Comparing validation test results before and after generating pseudo compensation tables showed the compensation lookup tables produced by the

enriched error model (81-error model) could not more compensate the errors but just by 2% in comparison with the 12-error model. However, the two tables were incapable of compensating some inter-axis errors.

- In the third paper, the compensation model functions were achieved from the trigonometric terms in the Jacobian and the inverse Jacobian of commands for the tested five-axis machine tool. 23 lookup tables were generated to compensate 10 error parameters and the volumetric errors. The enriched proposed compensation model (23Trigo-T) was compared with 25 polynomial lookup tables (25Poly-T) and the kinematic-based error compensation was considered as the reference of comparison. 23Trigo-T model was more effective over 32% rather than 25 polynomial lookup tables for mean volumetric error compensation. The simulation results of the 23Trigo-T model for compensating the volumetric errors of two different five-axis machine tools reveal the potential generality of this model.
- In the fourth paper, the exact table-based compensation model (forward inverse kinematic lookup table, FIK-LUT) was produced for a five-axis machine tool wherein a 13-error model was used to calibrate the machine tool errors. 40 tables were combined by the functions achieved from the symbolic equations to compensate 8 inter-axes, 2 spindle, and 3 gain errors. The FIK-LUT was generated in Siemens controller 840D of a non-perpendicular five-axis machine tool. The validation and calibration tests differed in the measurement strategy. The model was able to compensate over 79% of the mean estimated volumetric error norm. The dominant error was also reduced by 87%.

9.2 Future works

Generating complex tables for volumetric error compensation is somehow a new field of research recently highly demanded. The following are some subjects for future works;

- There are three table-based compensation models provided in this thesis for volumetric error compensations. As a future work, it is suggested to launch all these models on some other five-axis machine tools to verify the effectiveness of the models for a different machine tool.

- The last model (FIK-LUT) provided in this thesis is a comprehensive compensation model introduced for five-axis machine tools. It is useful to do research and to expand the last model for six-axis machine tools.
- Table-based volumetric error compensation can be verified for each inter- and intra-axis error to see the effectiveness of the tables. The research will provide numbers of the tables required for each error to be compensated.
- Since not all the controllers are equipped with the same number of compensation tables, it is important to build such combinatory tables by which the volumetric errors of the target machine tool are minimized. Hence, automatically choosing the optimized number of the complex tables can be another subject of research. This research allows the users to have optimized tables based on the magnitude of the inter- and intra-axis errors of the target machine tool.
- Volumetric error compensation is applicable when the machine is in machining mode. As a research topic, it is suggested to validate the compensation procedure by machining a part before and after compensation and measuring the dimensions by a CMM.
- Proposing a general table-based compensation scheme to be practical for different five-axis machines can be a highly demanding research topic. In paper 3, the potential model is introduced. However, more experimental tests are required to validate the proposed model.
- As thermal errors have a significant effect on the tool tip errors, a combination of thermal error compensation and geometric error compensation will improve the accuracy of the machine tools. Some controllers like Siemens allow the users to build such combinatory tables. It is suggested to simultaneously investigate the effect of those compensations on tool tip errors.

REFERENCES

Abbaszadeh-Mir, Y., Mayer, J. R. R., Cloutier, G., & Fortin, C. (2002). Theory and simulation for the identification of the link geometric errors for a five-axis machine tool using a telescoping magnetic ball-bar. *International Journal of Production Research, 40*(18), 4781-4797. doi:10.1080/00207540210164459

AG, S. (2010). Function description VCS (Volumetric Compensation System).

Attia, M. H., & Kops, L. (1979). Nonlinear Thermoelastic Behavior of Structural Joints—Solution to a Missing Link for Prediction of Thermal Deformation of Machine Tools. *Journal of Manufacturing Science and Engineering, 101*, 348-354.

Bi, Q., Huang, N., Sun, C., Wang, Y., Zhu, L., & Ding, H. (2015). Identification and compensation of geometric errors of rotary axes on five-axis machine by on-machine measurement. *International Journal of Machine Tools and Manufacture, 89*, 182-191. doi:10.1016/j.ijmachtools.2014.11.008

Bourke, P. (1999). Nearest neighbour weighted interpolation.

Bringmann, B., & Knapp, W. (2006). Model-based 'Chase-the-Ball' Calibration of a 5-Axes Machining Center. *CIRP Annals, 55*(1), 531-534. doi:10.1016/s0007-8506(07)60475-2

Bringmann, B., Küng, A., & Knapp, W. (2005). A Measuring Artefact for true 3D Machine Testing and Calibration. *CIRP Annals - Manufacturing Technology, 54*(1), 471-474. doi:10.1016/s0007-8506(07)60147-4

Bryan J, C. R., Holland E (1967). Spindle Accuracy. *American Machinist,Special Report No. 612 (December 4).*

Bryan, J. B. (1982a). A simple method for testing measuring machines and machine tools Part 1: Principles and applications. *Precis Eng, 4*, 61-69.

Bryan, J. B. (1982b). A simple method for testing measuring machines and machine tools. Part 2: Construction details. *4*, 125-138. doi:10.1016/0141-6359(82)90075-7

Castro, H. F. F. (2008). Uncertainty analysis of a laser calibration system for evaluating the positioning accuracy of a numerically controlled axis of coordinate measuring machines and machine tools. *Precision Engineering, 32*(2), 106-113. doi:10.1016/j.precisioneng.2007.05.001

Castro, H. F. F., & Burdekin, M. (2005). Evaluation of the measurement uncertainty of a positional error calibrator based on a laser interferometer. *International Journal of Machine Tools and Manufacture, 45*(3), 285-291. doi:10.1016/j.ijmachtools.2004.08.012

Chen, T.-C., Chang, C.-J., Hung, J.-P., Lee, R.-M., & Wang, C.-C. (2016). Real-Time Compensation for Thermal Errors of the Milling Machine. *Applied Sciences, 6*(4), 101. doi:10.3390/app6040101

Cho, M.-W., Seo, T.-i., & Kwon, H.-D. (2003). Integrated error compensation method using OMM system for profile milling operation. *Journal of Materials Processing Technology, 136*(1-3), 88-99. doi:10.1016/s0924-0136(02)00943-3

Cho, M. W., & Seo, T. I. (2002). Machining error compensation using radial basis function network based on CAD/CAM/CAI integration concept. *International Journal of Production Research, 40*(9), 2159-2174. doi:10.1080/00207540210124057

Craig, J. J. (1974). Introductionto Robotics, Mechanics andControls, 2nd edition, (Addison-Wesley, Reading, Massachusetts).

Creamer, J., Bristow, D. A., & Landers, R. G. (2017). Selection of limited and constrained compensation tables for five-axis machine tools. *International Journal of Advanced Manufacturing Technology, 92*(1-4), 1315-1327. doi:10.1007/s00170-017-0230-4

Creamer, J., Sammons, P. M., Bristow, D. A., Landers, R. G., Freeman, P. L., & Easley, S. J. (2016). Table-Based Volumetric Error Compensation of Large Five-Axis Machine Tools. *Journal of Manufacturing Science and Engineering, 139*(2). doi:10.1115/1.4034399

Creamer, J., Sammons, P. M., Bristow, D. A., Landers, R. G., Freeman, P. L., & Easley, S. J. (November 15-21, 2013, San Diego, California, USA). Table-Based Compensation for 5-Axis Machine Tools. *Proceedings of the ASME 2013 International Mechanical Engineering Congress and Exposition IMECE2013*.

Cui, G., Lu, Y., Li, J., Gao, D., & Yao, Y. (2012). Geometric error compensation software system for CNC machine tools based on NC program reconstructing. *The International Journal of Advanced Manufacturing Technology, 63*(1-4), 169-180. doi:10.1007/s00170-011-3895-0

Donmez, M. A., Bloquist, D. S., Hocken, R. J., & Liu, C. R. (1986). A general methodology for machine tool accuracy enhancement by error compensation. *Precision Engineering, 4*, 187–196.

Erkan, T., Mayer, J. R. R., & Dupont, Y. (2011). Volumetric distortion assessment of a five-axis machine by probing a 3D reconfigurable uncalibrated master ball artefact. *Precision Engineering, 35*(1), 116-125. doi:10.1016/j.precisioneng.2010.08.003

Esmaeili, S., & Mayer, J. R. R. (2020). An Integrated Geometric and Hysteretic Error Model of a Three Axis Machine Tool and Its Identification With a 3D Telescoping Ball-Bar. *Journal of Manufacturing and Materials Processing, 4*(1). doi:10.3390/jmmp4010024

Eung-Suk, L., Suk-Hwan, S., & Jin-Wook, S. (1998). A Comprehensive Method for Calibration of Volumetric Positioning Accuracy of CNC-Machines. *Advanced Manufacturing Technology, 14*, 43-49.

Everett, L. J., A. H. Suryohadiprojo. (1988). A study of kinematic models for forward calibration of manipulators". *1988 IEEE International Conference*.

Fagor Controller, 8070 / 8065 CNC

Fanuc Controller. (Series 30i/Model A).

Fidia Controller: C10 - C20 - C20 Vision.

Florussen, G. H. J., & Spaan, H. A. M. (2007). Static R-test: allocating the centreline of rotary axes of machine tools. *International Conference on Laser Metrology, CMM and Machine Tool Performance, LAMDAMAP*, 196-202.

Freeman, P. (2016). A Novel Means of Software Compensation for Robots and Machine Tools. *Aerospace Manufacturing and Automated Fastening Conference & Exhibition*.

Givi, M., & Mayer, J. R. R. (2014). Volumetric error formulation and mismatch test for five-axis CNC machine compensation using differential kinematics and ephemeral G-code. *International Journal of Advanced Manufacturing Technology, 77*(9-12), 1645-1653. doi:10.1007/s00170-014-6558-0

Givi, M., & Mayer, J. R. R. (2016). Optimized volumetric error compensation for five-axis machine tools considering relevance and compensability. *CIRP Annals, 12*, 44-55. doi:10.1016/j.cirpj.2015.09.002

Groos, L., Held, C., Keller, F., Wendt, K., Franke, M., & Gerwien, N. (2020). Mapping and compensation of geometric errors of a machine tool at different constant ambient temperatures. *Precision Engineering, 63*, 10-17. doi:10.1016/j.precisioneng.2020.01.001

Haitao, Z., Jianguo, Y., & Jinhua, S. (2007). Simulation of thermal behavior of a CNC machine tool spindle. *International Journal of Machine Tools and Manufacture, 47*(6), 1003-1010. doi:10.1016/j.ijmachtools.2006.06.018

Härtig, F., Keck, C., Kniel, K., Schwenke, H., Härtig, F., & Kniel, K. (2009). Selbstnachführendes Laserinterferometer für die Koordinatenmesstechnik (Tracking Laser Interferometer for Coordinate Metrology). *Technisches Messen, 71*, 227-232.

Heidenhain Controller: iTNC 530

Hocken. (1993). Software Compensation of Precision Machines. *A Report from Precision Engineering Laboratory UNC Charlotte to National Institute of Standards and Technology*.

Hocken, R. J. (1980). Machine tool accuracy. *Technology of Machine Tools. California, Lawrence Livermore Laboratory 5*.

Hong, C., Ibaraki, S., & Oyama, C. (2012). Graphical presentation of error motions of rotary axes on a five-axis machine tool by static R-test with separating the influence of squareness errors of linear axes. *International Journal of Machine Tools and Manufacture, 59*, 24-33. doi:10.1016/j.ijmachtools.2012.03.004

Ibaraki, S., Iritani, T., & Matsushita, T. (2010). Error Calibration on Fiveaxis Machine Tools by on-the-machine Measurement of Artifacts using a Touch-trigger Probe. *Proceeding of 4th CIRP International Conference on High Performance Cutting (CIRP HPC 2010)*.

Ibaraki, S., & Knapp, W. (2012). Indirect Measurement of Volumetric Accuracy for Three-Axis and Five-Axis Machine Tools: A Review. *International Journal of Automation Technology, 6*, 110-124. doi:10.3929/ethz-a-007593181

ISO230-1. (2012). Test code for machine tools – Part 1: geometric accuracy of machines operating under no-load or quasi-static conditions.

ISO/TR16907. (2015). Machine tools-Numerical compensation of geometric errors.

ISO/TR 16907. Technical report: Machine tools - Numerical compensation of geometric errors, 2015.

J., B. (1990). International Status of Thermal Error Research (1990) *CIRP Annals - Manufacturing Technology, 39*, 645-656.

J.P. Allen, S. R. P., D.G. Ford. (1997). Practical application of thermal error correction- 4 case studies. *WIT Transactions on Engineering Sciences, 16*.

Jingxia Yuan, J. N. (1998). The real-time error compensation technique for CNC machining systems. *Mechatronics 8*, 359-380.

Jung, J.-H., Choi, J.-P., & Lee, S.-J. (2006). Machining accuracy enhancement by compensating for volumetric errors of a machine tool and on-machine measurement. *Journal of Materials Processing Technology, 174*(1-3), 56-66. doi:10.1016/j.jmatprotec.2004.12.014

Kang, Y., Chang, C.-W., Huang, Y., Hsu, C.-L., & Nieh, I. F. (2007). Modification of a neural network utilizing hybrid filters for the compensation of thermal deformation in machine tools. *International Journal of Machine Tools and Manufacture, 47*(2), 376-387. doi:10.1016/j.ijmachtools.2006.03.007

Kato, N., Masaomi., T., & Sato, R. (2013). Analysis of circular trajectory equivalent to cone-frustum milling in five-axis machining centers using motion simulator. *Int. J. Mach. Tools Manuf, 64*, 1-11.

Khan, A. W., & Chen, W. (2010). A methodology for systematic geometric error compensation in five-axis machine tools. *The International Journal of Advanced Manufacturing Technology, 53*(5-8), 615-628. doi:10.1007/s00170-010-2848-3

Koliskor, A. (1971). Compensating for automatic-cycle machining errors. *Machines and Tooling, 41*, 1-14.

Lavernhe, S., Tournier, C., & Lartigue, C. (2007). Kinematical performance prediction in multi-axis machining for process planning optimization. *The International Journal of Advanced Manufacturing Technology, 37*(5-6), 534-544. doi:10.1007/s00170-007-1001-4

Lei, W. T., & Hsu, Y. Y. (2003a). Accuracy enhancement of five-axis CNC machines through real-time error compensation. *International Journal of Machine Tools and Manufacture, 43*(9), 871-877. doi:10.1016/s0890-6955(03)00089-0

Lei, W. T., & Hsu, Y. Y. (2003b). Accuracy enhancement of five-axis CNC machines through realtime error compensation. *International Journal of Machine Tools & Manufacture, 43*(9), 871-877.

Lei, W. T., & Sung, M. P. (2008). NURBS-based fast geometric error compensation for CNC machine tools. *International Journal of Machine Tools and Manufacture, 48*(3-4), 307-319. doi:10.1016/j.ijmachtools.2007.10.007

Li, J., Mei, B., Shuai, C., Liu, X.-j., & Liu, D. (2019). A volumetric positioning error compensation method for five-axis machine tools. *The International Journal of Advanced Manufacturing Technology, 103*(9-12), 3979-3989. doi:10.1007/s00170-019-03745-8

Li, J. G., Zhao, H., Yao, Y. X., & Liu, C. Q. (2007). Off-line optimization on NC machining based on virtual machining. *The International Journal of Advanced Manufacturing Technology, 36*(9-10), 908-917. doi:10.1007/s00170-006-0915-6

Li, Z., Yang, J., Fan, K., & Zhang, Y. (2014). Integrated geometric and thermal error modeling and compensation for vertical machining centers. *The International Journal of Advanced Manufacturing Technology, 76*(5-8), 1139-1150. doi:10.1007/s00170-014-6336-z

Liotto, G., & C.P., C. (1997). Laser Doppler displacement meter (LDDM) allows new diagonal measurement for large aspect ratio machine tool easily and accurately. *Transactions on Engineering Sciences, 16*, 187-194.

LO, C.-C., & HSIAO, C.-Y. (1998). A method of tool path compensation for repeated machining process. *International Journal of Machine Tools and Manufacture, 38,* 205-213.

Loughridge, R., & Abramovitch, D. Y. (2013). A tutorial on laser interferometry for precision measurements. 3686-3703. doi:10.1109/acc.2013.6580402

M. Esmaeili, S., & Mayer, J. R. R. (2020). Generation of a 3D error compensation grid from ISO 230-1 error parameters obtained by a SAMBA indirect calibration and validated by a ball-bar spherical test. *The International Journal of Advanced Manufacturing Technology, 106*(11-12), 4649-4662. doi:10.1007/s00170-020-04928-4

Mahbubur, R. M., Heikkala, J., Lappalainen, K., & Karjalainen, J. A. (1997). Positioning Accuracy improvement in five-axis milling by post processing. *International Journal of Machine Tools and Manufacture, 37,* 223-236.

Mahbubur, R. M. D., Heikkala, J., Lappalainen, K., & Karjalainen, J. A. (1997). Positioning accuracy improvement in five-axis milling by post processing. *International Journal of Machine Tools and Manufacture, 37*(2), 223-236. doi:https://doi.org/10.1016/0890-6955(95)00091-7

Majda, P. (2012). Modeling of geometric errors of linear guideway and their influence on joint kinematic error in machine tools. *Precision Engineering, 36*(3), 369-378. doi:10.1016/j.precisioneng.2012.02.001

Mayer, J. R. R. (2012). Five-axis machine tool calibration by probing a scale enriched reconfigurable uncalibrated master balls artefact. *CIRP Annals, 61*(1), 515-518. doi:10.1016/j.cirp.2012.03.022

McHichi, N. A., & Mayer, J. R. R. (2014). Axis Location Errors and Error Motions Calibration for a Five-axis Machine Tool Using the SAMBA Method. *Procedia CIRP, 14,* 305-310. doi:10.1016/j.procir.2014.03.088

McHichi, N. A., & Mayer, J. R. R. (2019). Optimal calibration strategy for a five-axis machine tool accuracy improvement using the D-optimal approach. *The International Journal of Advanced Manufacturing Technology, 103*(1-4), 251-265. doi:10.1007/s00170-019-03454-2

Md Mizanur, R., & Mayer, J. R. R. (2015). Five axis machine tool volumetric error prediction through an indirect estimation of intra- and inter-axis error parameters by probing facets on a scale enriched uncalibrated indigenous artefact. *Precision Engineering, 40,* 94-105. doi:10.1016/j.precisioneng.2014.10.010

Mir, Y. A., Mayer, J. R. R., & Fortin, C. (2002). Tool path error prediction of a five-axis machine tool with geometric errors. *Proceedings of the Institution of Mechanical Engineers, 216,* 697-712.

Mir, Y. A., Mayer, J. R. R., & Fortin, C. (2005). Tool path error prediction of a five-axis machine tool with geometric errors. *Proceedings of the Institution of Mechanical Engineers, Part B: Journal of Engineering Manufacture, 216*(5), 697-712. doi:10.1243/0954405021520391

Montavon, B., Dahlem, P., & Schmitt, R. H. (March 2019). Fast machine tool calibration using a single Laser Tracker. *Laser Metrology and Machine Performance XIII*.

Mooring, B. W. (1991). Fundamentals of manipulator calibration.

Prakash Vinoda, N. R. T., Sajin S, Shashi Kumar P V, Narendranath S. (2014). Real-time positioning error compensation for a turning machine using neural network. *Advances in Manufacturing and Materials Engineering*.

R. Ramesh, M. A. M., A.N. Poo. (2000). Error compensation in machine tools — a review Part II: thermal errors. *International Journal of Machine Tools and Manufacture, 40*, 1257-1284.

Rahman, M., Heikkala, J., & Lappalainen, K. (2000). Modeling, measurement and error compensation of multi-axis machine tools. Part I: theory. *International Journal of Machine Tools and Manufacture, 40*, 1535–1546.

Rahman, M. M., & Mayer, J. R. R. (2015). Five axis machine tool volumetric error prediction through an indirect estimation of intra- and inter-axis error parameters by probing facets on a scale enriched uncalibrated indigenous artefact. *Precision Engineering, 40*, 94-105. doi:10.1016/j.precisioneng.2014.10.010

Ramesh, R., Mannan, M. A., & Poo, A. N. (2000a). Error compensation in machine tools — a review Part I: geometric, cutting-force induced and fixturedependent errors. *International Journal of Machine Tools and Manufacture, 40*, 1235-1256.

Ramesh, R., Mannan, M. A., & Poo, A. N. (2000b). Error compensation in machine tools — a review Part II: thermal errors. *International Journal of Machine Tools and Manufacture, 40*, 1257–1284.

Ratchev, S., Liu, S., Huang, W., & Becker, A. A. (2006). An advanced FEA based force induced error compensation strategy in milling. *International Journal of Machine Tools and Manufacture, 46*(5), 542-551. doi:10.1016/j.ijmachtools.2005.06.003

S.M. Wang, K. F. E. (1992). Volumetric error compensation for multi-axis machines. *1992 IEEE International Conference on Systems, Man and Cybernetics, 183-188*.

Sartori, S., & Zhang, G. X. (1995). Geometric Error Measurement and Compensation of Machines. *CIRP Annals, 44*(2), 599-609. doi:10.1016/s0007-8506(07)60507-1

Schmitz, T. L., Ziegert, J. C., Canning, J. S., & Zapata, R. (2008). Case study: A comparison of error sources in high-speed milling. *Precision Engineering, 32*(2), 126-133. doi:10.1016/j.precisioneng.2007.06.001

Schultschik, R. (1977). The Components of the Volumetric Accuracy. *CIRP Annals, 25*, 223-228.

Schwenke, H., Franke, M., & Hannaford, J. (2005). Error Mapping of CMMs and Machine Tools by a Single Tracking Interferometer. *CIRP Ann. Manuf. Technol., 54*, 475–478.

Schwenke, H., Knapp, W., Haitjema, H., Weckenmann, A., Schmitt, R., & Delbressine, F. (2008). Geometric error measurement and compensation of machines—An update. *CIRP Annals - Manufacturing Technology, 57*(2), 660-675. doi:10.1016/j.cirp.2008.09.008

Schwenke, H., Schmitt, R., Jatzkowski, P., & Warmann, C. (2009). On-the-fly calibration of linear and rotary axes of machine tools and CMMs using a tracking interferometer. *CIRP Annals, 58*(1), 477-480. doi:10.1016/j.cirp.2009.03.007

Sepahi-Boroujeni, S., Mayer, J. R. R., & Khameneifar, F. (2021). Efficient uncertainty estimation of indirectly measured geometric errors of five-axis machine tools via Monte-Carlo validated GUM framework. *Precision Engineering, 67*, 160-171. doi:https://doi.org/10.1016/j.precisioneng.2020.09.027

Siemens Controller. (SINUMERIK 840D/840Di/810D Extended Functions).

Slamani, M., Mayer, J. R. R., & Cloutier, G. M. (2011). Modeling and Experimental Validation of Machine Tool Motion Errors Using Degree Optimized Polynomial Including Motion Hysteresis. *Experimental Techniques, 35*(1), 37-44. doi:10.1111/j.1747-1567.2009.00576.x

Slamani, M., Mayer, R., Balazinski, M., Zargarbashi, S. H. H., Engin, S., & Lartigue, C. (2010). Dynamic and geometric error assessment of an XYC axis subset on five-axis high-speed machine tools using programmed end point constraint measurements. *International Journal of Advanced Manufacturing Technology, 50*(9-12), 1063-1073. doi:10.1007/s00170-010-2584-8

Slocum, A. H. (1992). Precision machine design. *Society of Manufacturing Engineers , Michigan.*

Srivastava, A. K., Veldhuis, S. C., & Elbestawlt, M. A. (1995). Modeling geometric and thermal errors in five-axis CNC machine tool *International Journal of Machine Tools and Manufacture, 35*, 1321-1337.

Suh, S.-H., Lee, E.-S., & Sohn, J.-W. (1999). Enhancement of Geometric Accuracy via an Intermediate Geometrical Feedback Scheme. *Journal of Manufacturing Systems, 18*, 12-21.

Vahebi Nojedeh, M., Habibi, M., & Arezoo, B. (2011). Tool path accuracy enhancement through geometrical error compensation. *International Journal of Machine Tools and Manufacture, 51*(6), 471-482. doi:10.1016/j.ijmachtools.2011.02.005

Wang, C. (2000). Laser vector measurement technique for the determination and compensation of volumetric positioning errors. Part I: Basic theory. *Review of Scientific Instruments, 71*(10), 3933. doi:10.1063/1.1290504

Wang, S.-M., Liu, Y.-L., & Kang, Y. (2002). An efficient error compensation system for CNC multi-axis machines. *International Journal of Machine Tools and Manufacture, 42*, 1235–1245.

Wang, S.-M., Yu, H.-J., & Liao, H.-W. (2005). A new high-efficiency error compensation system for CNC multi-axis machine tools. *The International Journal of Advanced Manufacturing Technology, 28*(5-6), 518-526. doi:10.1007/s00170-004-2389-8

Weckenmann A, P. N. (2005). Comparison of CMM Length Measurement Tests Conducted with Different 1D, 2D and 3D Standards *Proceedings of 2nd International Scientific Conference Metrology in Production Engineering, Poland,*, 113–117.

Weikert, S. (2004). R-Test, a New Device for Accuracy Measurements on Five Axis Machine Tools. *CIRP Annals, 53*(1), 429-432. doi:10.1016/s0007-8506(07)60732-x

Xi, X.-C., Poo, A.-N., Hong, G.-S., & Huo, F. (2010). Experimental implementation of Taylor series expansion error compensation on a bi-axial CNC machine. *The International Journal of Advanced Manufacturing Technology, 53*(1-4), 285-299. doi:10.1007/s00170-010-2843-8

Xiang, S., & Altintas, Y. (2016). Modeling and compensation of volumetric errors for five-axis machine tools. *International Journal of Machine Tools and Manufacture, 101*, 65-78. doi:10.1016/j.ijmachtools.2015.11.006

Y A Mir, J. R. R. M., C Fortin. (2002). Tool path error prediction of a ®ve-axis machine tool with geometric errors. *Proceedings of the Institution of Mechanical Engineers, Part B: Journal of Engineering Manufacture, 216*, 697-712.

Yang, J., & Ding, H. (2016). A new position independent geometric errors identification model of five-axis serial machine tools based on differential motion matrices. *International Journal of Machine Tools and Manufacture, 104*, 68-77. doi:10.1016/j.ijmachtools.2016.02.001

Yuan, J., & Ni, J. (1998). The real-time error compensation technique for CNC machining systems. *Mechatronics, 8*, 359-380.

Zargarbashi, S. H. H., & Mayer, J. R. R. (2009). Single setup estimation of a five-axis machine tool eight link errors by programmed end point constraint and on the fly measurement with Capball sensor. *International Journal of Machine Tools and Manufacture, 49*(10), 759-766. doi:10.1016/j.ijmachtools.2009.05.001

Zha, J., Wang, T., Li, L., & Chen, Y. (2020). Volumetric error compensation of machine tool using laser tracer and machining verification. *The International Journal of Advanced Manufacturing Technology, 108*(7-8), 2467-2481. doi:10.1007/s00170-020-05556-8

Zhan-Qiang, L., Venuvinod, P. K., & Ostafiev, V. A. (1998). On-machine measurement of workpieces with the cutting tool. *Integrated Manufacturing Systems, 9*(3), 168-172. doi:10.1108/09576069810210448

Zhang, G. X., & Zang, Y. F. (1991). A Method for Machine Geometry Calibration Using 1-D Ball Array. *CIRP Annals, 40*(1), 519-522. doi:https://doi.org/10.1016/S0007-8506(07)62044-7

Zhang, H., Yang, J., Zhang, Y., Shen, J., & Wang, C. (2010). Measurement and compensation for volumetric positioning errors of CNC machine tools considering thermal effect. *The International Journal of Advanced Manufacturing Technology, 55*(1-4), 275-283. doi:10.1007/s00170-010-3024-5

Zhu, S., Ding, G., Qin, S., Lei, J., Zhuang, L., & Yan, K. (2012). Integrated geometric error modeling, identification and compensation of CNC machine tools. *International Journal of Machine Tools and Manufacture, 52*(1), 24-29. doi:10.1016/j.ijmachtools.2011.08.011